General Disclaimer

One or more of the Following Statements may affect this Document

- This document has been reproduced from the best copy furnished by the organizational source. It is being released in the interest of making available as much information as possible.

- This document may contain data, which exceeds the sheet parameters. It was furnished in this condition by the organizational source and is the best copy available.

- This document may contain tone-on-tone or color graphs, charts and/or pictures, which have been reproduced in black and white.

- This document is paginated as submitted by the original source.

- Portions of this document are not fully legible due to the historical nature of some of the material. However, it is the best reproduction available from the original submission.

(NASA-CR-173924) THEORETICAL RESEARCH PROGRAM TO PREDICT THE PROPERTIES OF MOLECULES AND CLUSTERS CONTAINING TRANSITION METAL ATOMS Final Report, Jul. 1981 - Jul. 1984 (Polyatomics Research, Inc.) 97 p

N84-32502

G3/26

Unclas
01066

Theoretical Research Program to Predict the Properties of Molecules and Clusters containing Transition Metal Atoms

Final Report Covering Period July 1981 - July 1984

Supported under NASA Cooperative Agreement NCC2-148

NASA Technical Officer: Dr. David Cooper

NASA Ames Research Center
STC 230-3
Moffett Field, CA 94035

Principal Investigator: Dr. Stephen Walch

Polyatomics Research Institute
1101 San Antonio Road, Suite 420
Mountain View, CA 94043

The enclosed document is the final technical report on work performed under NASA Cooperative Agreement NCC2-148. This report covers the work of Dr. Stephen Walch who acted as principal investigator. The information contained herein is complete and was submitted in July, 1984.

TABLE OF CONTENTS

I. INTRODUCTION

The primary focus of this research has been the theoretical study of transition metal (TM) chemistry. A major goal of this work is to provide reliable information about the interaction of H atoms with iron metal. This information is needed to understand the effect of H atoms on the processes of embrittlement and crack propagation in iron. The method employed in the iron hydrogen studies is the cluster method in which the bulk metal is modelled by a finite number of iron atoms. There are several difficulties in the application of this approach to the hydrogen iron system. First the nature of TM-TM and TM-H bonding for even diatomic molecules was not well understood when these studies were started. Secondly relatively large iron clusters are needed to provide reasonable results. Therefore it is not possible to include all of the valence electrons on each iron atom. In the present calculations only the 4s electron of each iron atom was included directly in the calculation while the Ar core and 3d electrons are incorporated into the effective core potential (ECP) based on the $4s^1 3d^7$ state of the Fe atom. In order to understand the effects of removing the 3d electrons from the valence space, it is necessary to have detailed information about the nature of TM-TM and TM-H bonding. For these reasons we have carried out in parallel two levels of calculation: i) highly accurate studies of TM dimers and hydrides. (These studies are carried out with large basis sets and include extensive electron correlation). ii) studies of large clusters of Fe atoms with and without H adatoms. [These studies are carried out at the SCF level and make the approximation of incorporating the TM core and 3d electrons into the core (ECP approximation).] The studies of diatomic species provide benchmark calculations which are used to test the approximations in the cluster studies, while the cluster studies on Fe_nH are designed to provide potential function input for studies of hydrogen embrittlement.

Since much of the work to be discussed here has been described in manuscripts, relevant manuscripts have been included in the appendices and the reader is referred to these papers and to the publications list for further details. This report concentrates on the TM hydrides, TM

dimers, and Fe_nH cluster results. The Fe_nH cluster results are described in detail in a manuscript included as Appendix A. The results for the TM hydrides and dimers are summarized in Sections II and III, respectively; while, Appendix B contains copies of publications on these topics. During the course of this work several other projects were undertaken. These include all-electron calculations on the CsH and Cs_2 molecules, calculations on the alkali dimers, an ab-initio study of core-valence correlation, and studies of atomic correlation and basis sets. References to this work are given in the publications list.

II. TRANSITION METAL HYDRIDES

Fig. 1 shows the relative ordering of the $4s^2 3d^n$ and $4s^1 3d^{n+1}$ states of the TM atoms. The important features of Fig. 1 are: i) a monatonic decrease in excitation energy from Sc to Cr with $4s^1 3d^{n+1}$ an excitated state for Sc through V but the ground state for Cr. ii) a sharp reversal in the ordering of the states for Mn with $4s^2 3d^n$ again lower, and iii) a monatonic decrease in excitation energy from Mn to Cu with $4s^1 3d^{10}$ the ground state of Cu. The character of the ground states of the TM hydrides is strongly correlated with the ordering of atomic states. For example, for CrH the ground state is $^6\Sigma^+$ arising from $4s^1 3d^5$ while for MnH the ground state is $^7\Sigma^+$ arising from $4s^2 3d^5$. For elements where the $4s^2 3d^n$ and $4s^1 3d^{n+1}$ states are closer in energy a strong admixture of states occurs, e.g. for VH the ground state is $^5\Delta$ arising from a mixture of $4s^2 3d\pi^2 3d\delta^1$ and $4s^1 3d\sigma^1 3d\pi^2 3d\delta^1$ atomic character with a 3d population of $\sim$3.4.

The ratio of sizes of 4s and 3d orbitals increases monatonically from 2.364 to 3.239 going from Sc to Cu. Because the 4s orbital is so much larger than the 3d orbital we find the bonding in the TM hydrides involves primarily the 4s electrons (with some admixture of 4p character) while the 3d electrons remain essentially atomic like. The one exception is ScH which shows a Sc(3d)-H(1s) bond in the lowest $^1\Sigma^+$ state. Note that Sc is most likely to show 3d bonding since the 4s and 3d orbital sizes are more nearly comparable.

CASSCF/CI studies have been carried out for TiH, VH, CrH, MnH, FeH, and NiH. These calculations show good agreement with experiment for the R_e, ω_e, and D_e; thus confirming the theoretical model.

Studies have also been carried out for the $^5\Delta$ state of FeH^-. These calculations show that photodetachment from FeH^- leads to a large change in R_e for the $^4\Delta$ state but little change in R_e for the $^6\Delta$ state. These results confirm the assignment of Stevens, Fiegerle, and Lineberger (SFL) of the vertical photodetachment transition with a long vibrational progression to $^4\Delta$, and hence that the ground state of FeH is $^4\Delta$. However the calculations show that the simple theoretical model used by SFL to assign the above transitions is not correct in that the $^4\Delta$ state of FeH

and the $^5\Delta$ state of FeH^- have 3d populations of 6.26 and 6.50 respectively, whereas SFL assumed 7.0 for both of these states. Thus the theoretical calculations in conjunction with the experiment by SFL establish that the ground state of FeH is $^4\Delta$.

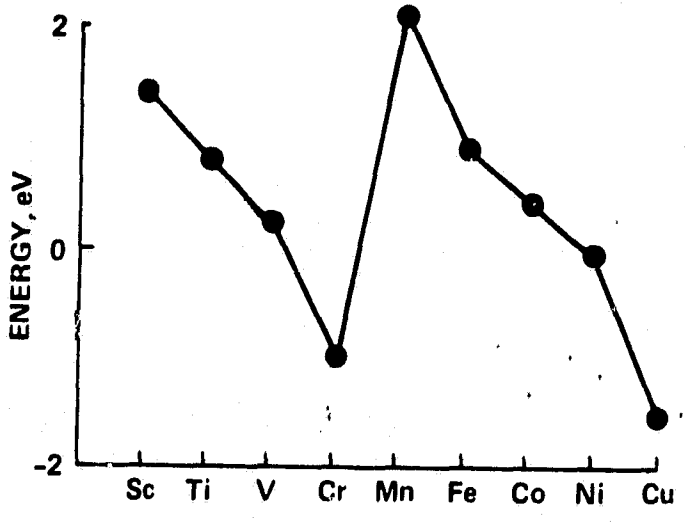

FIG. 1. $4s^1 3d^{n+1} - 4s^2 3d^n$ excitation energies of scandium to copper $[E(sd^{n+1}) - E(s^2 d^n)]$. All units are in eV.

III. TRANSITION METAL DIMERS.

For the TM dimers molecular states may arise from three different atomic asymptotes: $4s^2 3d^n + 4s^2 3d^n$, $4s^2 3d^n + 4s^1 3d^{n+1}$, and $4s^1 3d^{n+1} + 4s^1 3d^{n+1}$. The accessibility of these asymptotes of course depends on the $4s^1 3d^{n+1} - 4s^2 3d^n$ excitation energies (see Fig.1). Thus for Sc_2 we find that the low-lying states arise from the first two asymptotes with $4s^1 3d^{n+1} + 4s^1 3d^{n+1}$ too high in energy to lead to the ground state while for Ti_2, V_2, and Cr_2 the ground states arise from the $4s^1 3d^{n+1} + 4s^1 3d^{n+1}$ atomic asymptote.

Because the 4s orbital is significantly larger than the 3d orbital the predominant interaction in the TM dimers at large internuclear distance (R) is between the 4s electrons with very little 3d interaction. For states arising from the $4s^2 3d^n + 4s^2 3d^n$ atomic asymptote this interaction is basically repulsive and only a shallow well at large R_e ($\sim 8.0 a_o$) arising from the 4s→4p near degeneracy effect is observed. For states arising from the $4s^2 3d^n + 4s^1 3d^{n+1}$ atomic asymptote the 4s interaction is weakly bonding at intermediate R but is repulsive at small R leading to intermediate R_e values ($\sim 5.0 a_o$). At these R_e values the 3d-3d overlaps (S) are small which favors one-electron 3d bonds whose bonding terms vary with distance like S over two-electron 3d bonds whose bonding terms vary with distance like S^2. Finally for states arising from the $4s^1 3d^{n+1} + 4s^1 3d^{n+1}$ atomic asymptote the 4s-4s interaction is attractive and also appears to be relatively flat well inside the optional 4s-4s bonding radius. Thus, states arising from this atomic asymptote are able to move into short R_e regions where the 3d-3d overlaps are large enough to favor two-electron 3d bonding.

For the TM elements with more than half filled 3d shells, the formation of 3d bonds becomes much less favorable for two reasons. First the 4s to 3d orbital sizes are larger for the right half of the first transition row. Secondly the presence of doubly occupied 3d orbitals leads to repulsive interactions which effectively cancel any bonding interactions from the 3d shell. Thus the bonding here is dominated by the 4s electrons. An example is Cu_2 where the Cu atom has a $4s^1 3d^{10}$

ground state and the bonding is predominantly a 4s-4s bond with the 3d electrons remaining atomic like.

The dominant configurations for important states of those TM dimers which have been studied are:

Sc_2 $^3\Sigma_g^-$ $4s\sigma_g^2$ $4s\sigma_u^2$ $3d\pi_{xu}^1$ $3d\pi_{yu}^1$

$^5\Sigma_u^-$ $4s\sigma_g^2$ $3d\sigma_g^1$ $4s\sigma_u^1$ $3d\pi_{xu}^1$ $3d\pi_{yu}^1$

Ti_2 $^7\Sigma_u^+$ $4s\sigma_g^2$ $3d\sigma_g^1$ $4s\sigma_u^1$ $3d\pi_{xu}^1$ $3d\pi_{yu}^1$ $3d\delta_{xyg}^1$ $3d\delta_{x^2-y^2g}^1$

$^1\Sigma_g^+$ $4s\sigma_g^2$ $3d\sigma_g^2$ $3d\pi_{xu}^2$ $3d\pi_{yu}^2$

V_2 $^3\Sigma_g^-$ $4s\sigma_g^2$ $3d\sigma_g^2$ $3d\pi_{xu}^2$ $3d\pi_{yu}^2$ $3d\delta_{xyg}^1$ $3d\delta_{x^2-y^2g}^1$

Cr_2 $^1\Sigma_g^+$ $4s\sigma_g^2$ $3d\sigma_g^2$ $3d\pi_{xu}^2$ $3d\pi_{yu}^2$ $3d\delta_{xyg}^2$ $3d\delta_{x^2-y^2g}^2$

Cu_2 $^1\Sigma_g^+$ $4s\sigma_g^2$ $3d\sigma_g^2$ $3d\pi_{xu}^2$ $3d\pi_{yu}^2$ $3d\delta_{xyg}^2$ $3d\delta_{x^2-y^2g}^2$

$3d\sigma_u^2$ $3d\pi_{xg}^2$ $3d\pi_{yg}^2$ $3d\delta_{xyu}^2$ $3d\delta_{x^2-y^2u}^2$

Fig. 2 shows calculated potential curves for low-lying states of Sc_2. The initial study of Sc_2 by Walch and Bauschlicher found only weakly bound states arising out of the $^2D + {}^2D$ asymptote in contrast to mass spectrometric experiments which indicated strong bonding (D_e = 26± 5kcal/mole). A $^5\Sigma_u$ state was found which was bound by ∿0.8eV with respect to $^2D + {}^4F(4s^14p^13d^1)$ atomic limit, but unbound with respect to $^2D + {}^2D$. However at about the same time that this work was published, matrix isolation studies by Knight, VanZee and Weltner indicated a bound $^5\Sigma$ state of Sc_2. From the ESR studies it appeared that this state arose from the $^2D + {}^4F$ $(4s^13d^2)$ atomic asymptote which had not been studied in detail in the previous theoretical studies. A re-examination of this system revealed a new $^5\Sigma_u^-$ state which had been missed

in the previous study because its R_e ($\sim 5.0a_o$) is much shorter than the R_e values for the states studied previously ($\sim 7.0a_o$). The $^5\Sigma_u^-$ state turned out to be of considerable theoretical interest because it exhibited multiple 3d bonding (three one-electron bonds) and constituted the first theoretical evidence of multiple 3d bonding in a first row transition metal dimer.

The studies on Sc_2 were extended to Ti_2, V_2 and Cr_2. Initially the high spin $^7\Sigma_u^+$ state of Ti_2 was studied. The Sc_2 $^5\Sigma_u^-$ and Ti_2 $^7\Sigma_u^+$ states come from the mixed ($4s^2 3d^n + 4s^1 3d^{n+1}$) asymptote and exhibit multiple one-electron 3d bonding. These states have long bond lengths ($R_e \gtrsim 5.0a_o$) and small vibrational frequencies ($\omega_e \sim 200cm^{-1}$). The $^5\Sigma_u^-$ state of Sc_2 is consistent with the $^5\Sigma$ state which has been observed in matrix studies by Knight, Van Zee, and Weltner. The bond length here is not known but the calculated vibrational frequency of $184cm^{-1}$ is reasonably close to the experimental value of $238.9cm^{-1}$.

For Ti_2 from reference to Fig 1 one sees that the excitation energy to the $4s^1 3d^{n+1} + 4s^1 3d^{n+1}$ atomic asymptote is about half as large as for Sc_2. Thus the $^1\Sigma_g^+$ state which arises from the $4s^1 3d^3 + 4s^1 3d^3$ atomic asymptote becomes a competitor for the gound state of Ti_2. The bonding here is a triple two-electron 3d bond ($3d\sigma$, $3d\pi_x$, $3d\pi_y$). This leads to a short R state, $R_e = 3.73a_o$ and $\omega_e = 438cm^{-1}$. The bond length is not known experimentally but the experimental vibrational frequency is $407.9cm^{-1}$ which is consistent with the $^1\Sigma_g^+$ state of Ti_2, but inconsistent with the $^7\Sigma_u^+$ state. Based on this we tentatively assign the ground state of Ti_2 as $^1\Sigma_g^+$.

Fig. 3 shows calculated potential curves for the $^3\Sigma_g^-$ state of V_2. The $^3\Sigma_g^-$ state of V_2 has the same triple two-electron 3d bond as in Ti_2 with the remaining two electrons in the $3d\delta$ orbitals. Because the $3d\delta$ orbitals still have small overlaps in the region near R_e ($\sim 3.5a_o$), the lowest state is a triplet state arising by forming two one-electron $3d\delta$ bonds. The R_e and ω_e values obtained from the CASSCF curves are in good agreement with the recent results of Langridge-Smith, Morse, Hansen, Smalley and Merer for the $^3\Sigma$ ground state of V_2. An important feature of Fig. 3 is the large effect of 4f functions, an effect which is also evident in the Cr_2 curves

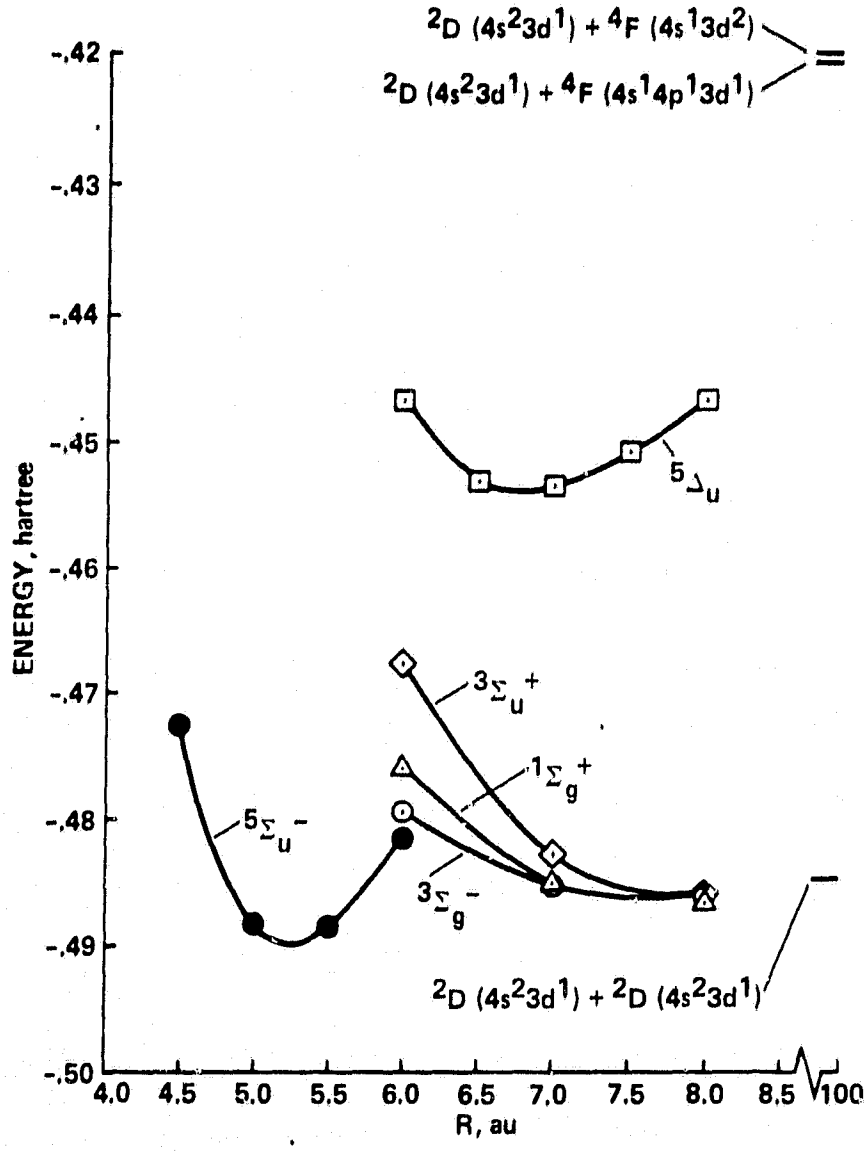

FIG. 2. Potential energy curves for the low-lying states of Sc_2 from CASSCF CI(SD) calculations. The locations of the $^2D + {}^2D$, $^2D + {}^4F(4s^14p^13d^1)$, and $^2D + {}^4F(4s^13d^2)$ asymptotes are indicated.

in Fig. 4. Since these states exhibit strong 3d bonding, the large effect (∿1.0ev) for 4f as a polarization function is not surprising. This large effect is not observed for the one-electron 3d bonds in the $Sc_2\ ^5\Sigma_u^-$ or $Ti_2\ ^7\Sigma_u^+$ states. However, this is expected given the strong R dependence of this effect. For example from Fig. 4 one sees that for Cr_2 near R_e the effect of 4f is large but is near zero by $3.75a_o$.

Fig. 4 shows the calculated potential curves for Cr_2. Here the 3dδ orbitals are doubly occupied which is expected to be unfavorable based on the V_2 result that the 3dδ orbitals were preferentially singly occupied. This is consistent with the weaker bonding in Cr_2, D_e ∿1.0eV as compared to V_2, D_e ∿2.5eV. Because of the weaker bonding in Cr_2 the CASSCF potential curve is not bound. However the potential curve does exhibit a shoulder near the experimental R_e which is suggestive of an inner well.

A major problem with the CASSCF studies for V_2 and Cr_2 is that only a small percentage of the binding energy is obtained for V_2 and no well is obtained for Cr_2. This result is not unexpected for CASSCF. Normally these problems would be corrected by configuration interaction (CI). However, the CI expansions required for V_2 and Cr_2 exceed current computational capabilities. Several different attempts have been made to include the missing correlation in other ways. One approach due to Goodgame and Goddard assumes that the missing correlation serves mainly to correct the location of the ionic atomic asymptotes. These authors attempt to include these effects by empirical modification of the integrals to correct the atomic ionization potentials and electron affinities to agree with experiment. This method does lead to a reasonable potential curve for Cr_2 although the bond length is somewhat too short which suggests that this method over corrects. Another approach by Walch attempts to include extra correlation effects by expanding the valence space in the CASSCF calculation. Here atomic 4p and 3d′ terms are added (where 3d′ is a tight diffuse correlating orbital for the 3d). This approach should include the principle correlation effects needed to describe charge transfer within the 4s and 3d shell. Unfortunately, it is not possible to add all these extra valence orbitals at

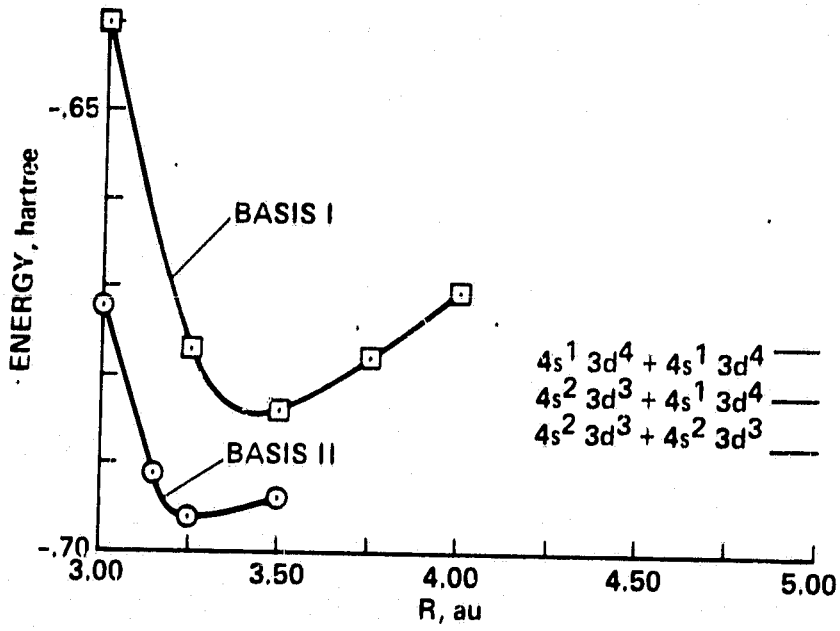

FIG. 3. Calculated CAS SCF potential curves for the $^3\Sigma_g^-$ state of V_2. Basis I is the [8s6p4d] basis while basis II is the [8s6p4d2f] basis.

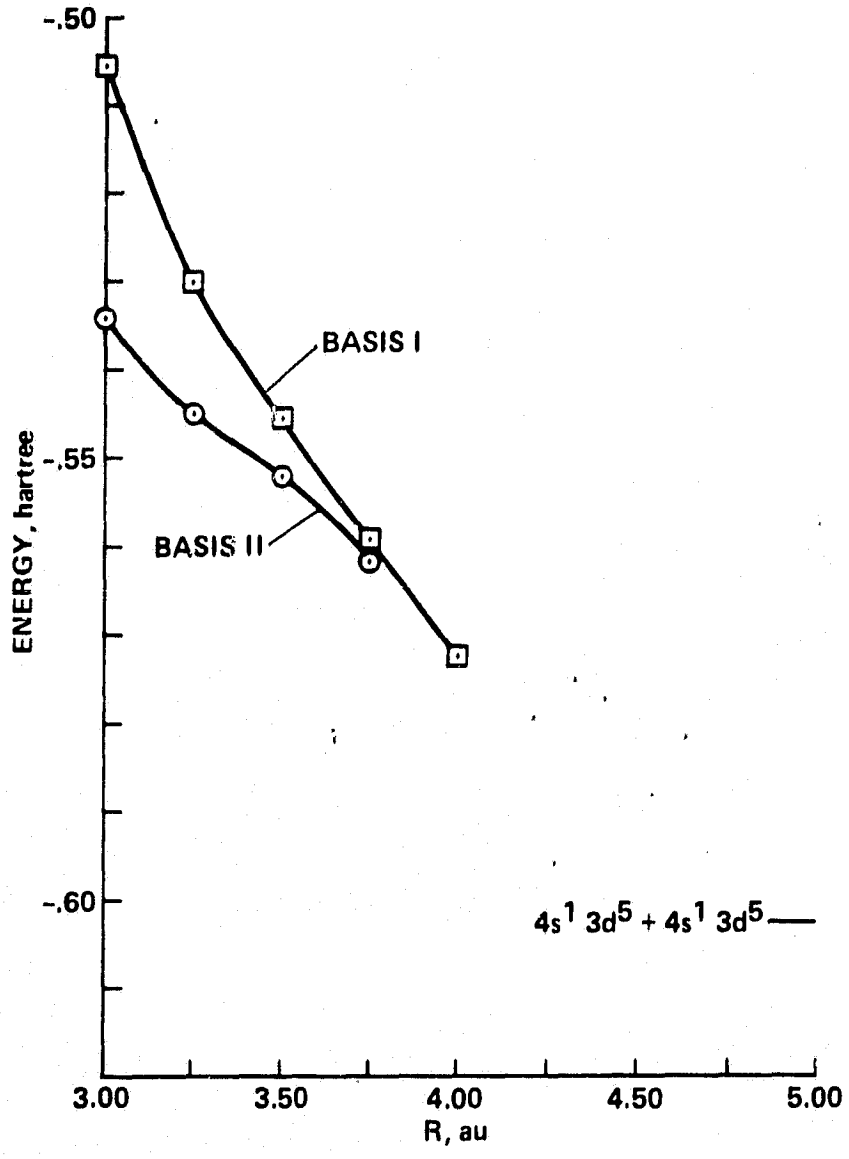

FIG. 4. Calculated CAS SCF potential curves for the $^1\Sigma_g^+$ state of Cr_2. Basis I and Basis II are the same size as in fig. 1.

once (due to computational limitations) and the extra orbitals are added separately by symmetry blocks. From checks on H_2 it appears that there is no real problem with additivity due to this approach. However, checks on N_2 and Ti_2 indicate that because the method dissociates to SCF atoms certain atomic correlation terms are not included and these terms are more important in the large R region than they are near R_e. Thus, the method does overestimate the binding energy that would be obtained in a more complete MCSCF calculation. In spite of these difficulties the method does nearly reproduce the CI potential curves for H_2, N_2 and Ti_2 and therefore we reproduce the estimated potential curve for Cr_2 in Fig. 5. Analysis of this potential curve gives (experimental values in parenthesis) $R_e = 1.78A^o(1.68A^o)$, $\omega_e = 383cm^{-1}(480cm^{-1})$ and $D_e = 0.71eV)$. Note that the long bond length and small ω_e are consistent with underestimating the binding energy.

A significant feature of the studies of the TM dimers is the presence of outer wells associated with 4s-4s bonding and one-electron 3d bonding in some cases (e.g. the $^7\Sigma_u^+$ state of Ti_2 and analogous states in V_2), and inner wells associated with two-electron 3d bonding (e.g. the $^1\Sigma^+$ state of Ti_2 and the $^3\Sigma_g^-$ state of V_2). These types of effects have been observed experimentally for small Fe clusters where the dimer exhibits a bond length of $\sim 3.8a_o$ which presumably involves some 3d bonding but larger clusters exhibit longer bond lengths approaching the nearest neighbor distance in BCC Fe ($\sim 4.7a_o$).

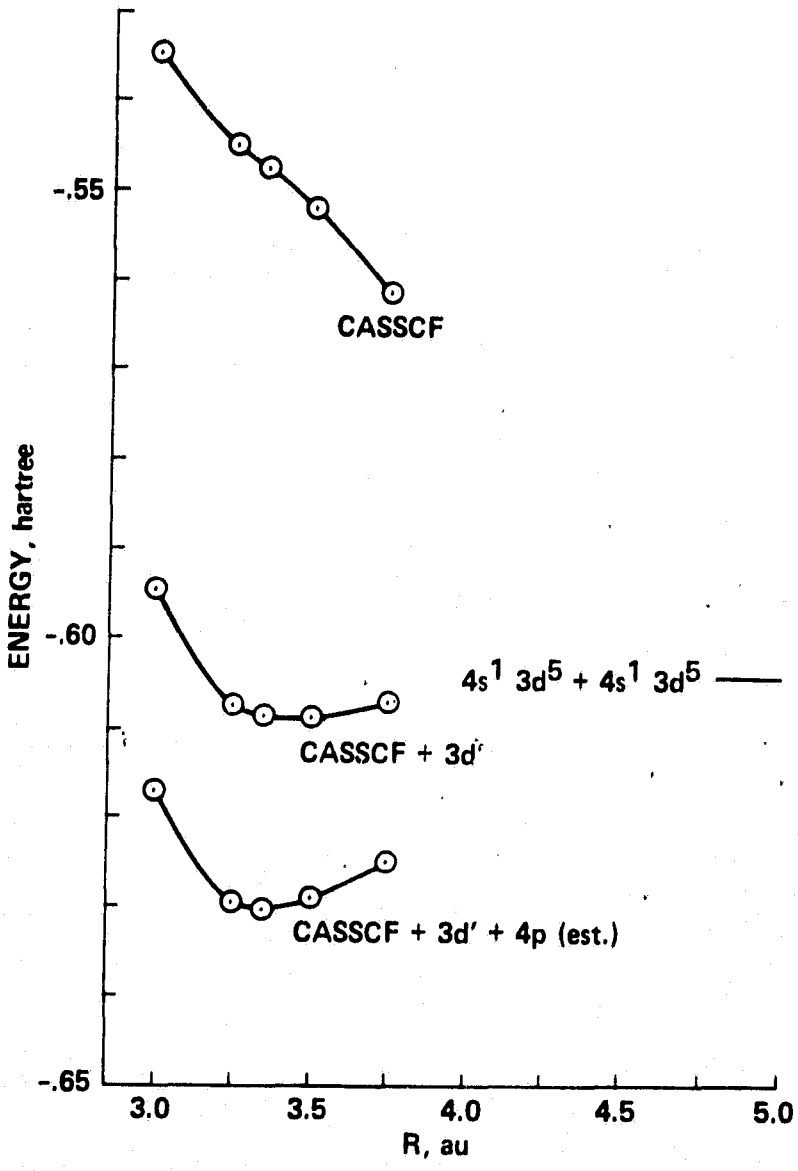

FIG. 5. Estimated potential curves for Cr_2 based on extended valence space CASSCF calculations. The effect of 4p is estimated based on calculations on Ti_2.

IV. Fe_nH CLUSTER CALCULATIONS

The Fe_nH cluster calculations are described in detail in a manuscript contained in Appendix A. For a summary of the main results, the reader is referred to the introduction of the above paper.

V. PUBLICATIONS

A. Transition Metal Hydrides

1. On the d-Bond in ScH
   C.W. Bauschlicher, Jr. and S.P. Walch
   J. Chem. Phys., 76, 4560 (1982)

2. CASSCF/CI Calculations for First Row Transition Metal Hydrides: The TiH($^4\Phi$), VH($^5\Delta$), CrH($^6\Sigma^+$), MnH($^7\Sigma^+$), FeH($^{4,6}\Delta$) and NiH($^2\Delta$) States
   S.P. Walch and C.W. Bauschlicher, Jr.
   J. Chem. Phys., 78, 4597 (1983)

3. On Incorporation of Atomic Correlation in Transition Metal Molecular Calculations: NiH
   S.P. Walch and C.W. Bauschlicher, Jr.
   Chem. Phys. Lett., 86, 66 (1982)

4. Theoretical Evidence Supporting the $^4\Delta$ Ground State Assignment for FeH
   S.P. Walch, Chem. Phys. Lett., 105, 54 (1984)

B. Transition Metal Dimers

5. CASSCF/CI Calculations for the $^3\Sigma_g^-$, $^1\Sigma_g^+$, $^3\Sigma_u^+$ and $^5\Delta_u$ States of Sc_2
   S.P. Walch and C.W. Bauschlicher, Jr.
   Chem. Phys. Lett., 94, 290 (1983)

6. Theoretical Evidence for Multiple One-Electron 3d Bonding in a First Row Transition Metal Dimer: The $^5\Sigma_u^-$ State of Sc_2
   S.P. Walch and C.W. Bauschlicher, Jr.
   J. Chem. Phys., 79, 3590 (1983).

7. Theoretical Evidence for Multiple 3d Bonding in the V_2 and Cr_2 Molecules
   S.P. Walch, C.W. Bauschlicher, Jr., B.O. Roos, and C.J. Nelin
   Chem. Phys. Lett., 103, 175 (1984)

8. Extended CASSCF Calculations for Transition Metal Dimers: the Ti_2 $^1\Sigma_g^+$ V_2 $^3\Sigma_g^-$, and Cr_2 $^1\Sigma_g^+$ states
   S.P. Walch, Chem. Phys. Lett., submitted

9. On the Nature of the Bonding in Cu_2
   C.W. Bauschlicher, Jr., S.P. Walch, and P.E.M. Siegbahn
   J. Chem. Phys., 76, 6015 (1982)

10. On the Nature of Bonding in Cu_2 - An Ab Initio Viewpoint
    C.W. Bauschlicher, Jr., S.P. Walch and P.E.M. Siegbahn
    J. Chem. Phys., 78, 3347 (1983)

C. Iron Clusters

11. Model Studies of the Interaction of H Atoms with BCC Iron
S.P. Walch
Surface Science, in press

D. Alkali Metals and Core-Valence Correlation

12. Ab Initio Calculation of the X $^1\Sigma^+$ State of CsH
B.C. Laskowski, S.P. Walch, and P.A. Christianson
J. Chem. Phys., 78, 6824 (1983)

13. All Electron GVB/CI Potential Curves for the X $^1\Sigma_g^+$ State of Cs_2
S.P. Walch, C.W. Bauschlicher, Jr., P.E.M. Siegbahn, and H. Partridge
Chem. Phys. Lett., 92, 54 (1982)

14. Electron Affinities of the Alkali Dimers: Na_2, K_2 and Rb_2
H. Partridge, D.A. Dixon, S.P. Walch, C.W. Bauschlicher, Jr., and J.L. Gole
J. Chem. Phys., 79, 1859 (1983)

15. An Ab Initio Study of Core Valence Correlation
H. Partridge, C.W. Bauschlicher, Jr., S.P. Walch, and Bowen Liu
J. Chem. Phys., 79, 1866 (1983)

E. Atomic Calculations and Basis Sets

16. On Correlation in the First Row Transition Metal Atoms
C.W. Bauschlicher, Jr., S.P. Walch, and H. Partridge
J. Chem. Phys., 76, 1033 (1982)

17. On the Electron Affinity of Cu Atom
C.W. Bauschlicher, Jr., S.P. Walch and H. Partridge
Chem. Phys. Lett., 103, 291 (1984)

18. On the Choice of Gaussian 4f Functions for Use in Calculations on Transition Metal Atoms
S.P. Walch and C.W. Bauschlicher, Jr.
Chem. Phys. Lett., 105, 171 (1984)

19. Supplemental Basis Functions for the Second Transition Row Elements
S.P. Walch, C.W. Bauschlicher, Jr. and C.J. Nelin
J. Chem. Phys., 79, 3600 (1983)

F. Oxygen on Nickel

20. Comment on "Evidence for Two States of Chemisorbed O on Ni (100)"
C.W. Bauschlicher, Jr., S.P. Walch, P.S. Bagus, and C.R. Brundle
Phys. Rev. Lett., 50, 864 (1983)

APPENDIX A

The following paper discusses the Fe_nH cluster calculations.

Model Studies of the Interaction of H Atoms with BCC Iron

Stephen P. Walch*

Polyatomics Research Institute†
Mountain View, CA 94043

Abstract

Ab Initio/Effective Core Potential cluster studies are reported for the interaction of H atoms with BCC iron. The calculations use a one-electron ECP based on the $4s^1 3d^7$ state of the Fe atom. Two-fold and four-fold sites on the (100) surface as well as octahedral, tetrahedral, and trigonal interior sites were studied. Four-fold surface sites are found to be bound by $\sim$1.5eV with the H atom $\sim 0.5a_o$ above the surface. Penetration of the surface at a four-fold site involves movement toward a second layer atom and is expected to be unfavorable. Two-fold surface sites have small binding energies $\sim$0.25eV. Penetration of the surface at this site involves movement toward a tetrahedral interior site and is downhill in energy. Tetrahedral interior sites are found to be bound by $\sim$1.3eV and are a minimum on the potential energy surface. Octahedral sites are a maximum on the potential energy surface and are estimated to be $\sim$0.2eV higher (including lattice relaxation effects). Trigonal sites are found to be a saddle point connecting adjacent tetrahedral sites and this pathway leads to an estimated barrier to diffusion of $\sim$0.1eV (including lattice relaxation effects). The volume expansion for a H atom in a tetrahedral site is calculated to be 21%.

* Supported by NASA grant #NCC2-148

† Mailing address: 1101 San Antonio Road, Suite 420

dimers, and Fe_nH cluster results. The Fe_nH cluster results are described in detail in a manuscript included as Appendix A. The results for the TM hydrides and dimers are summarized in Sections II and III, respectively; while, Appendix B contains copies of publications on these topics. During the course of this work several other projects were undertaken. These include all-electron calculations on the CsH and Cs_2 molecules, calculations on the alkali dimers, an ab-initio study of core-valence correlation, and studies of atomic correlation and basis sets. References to this work are given in the publications list.

I. Introduction

Hydrogen embrittlement of metals is an important technological problem [1]. As part of a program to understand the effect of H atoms on crack propagation in iron we have undertaken a theoretical study of the interaction of H atoms with clusters of iron atoms in the BCC structure (α-Iron). In the studies reported here we first fixed the Fe atoms at the lattice positions of the perfect crystal and studied the interaction with a H atom at two-fold and four-fold sites on the (001) surface and at a series of octahedral, tetrahedral, and trigonal sites interior to the solid. These studies determine the geometry and binding energy at surface chemisorption sites and provide information on the barriers to diffusion within the metal and to penetration of the surface at two-fold and four-fold sites. We then relaxed the geometry of the nearest neighbor Fe atoms for the octahedral, tetrahedral and trigonal interior sites. These studies are important because they further refine the energetics for the diffusion process and because significant expansion of the lattice is found for tetrahedral sites. This expansion could induce stress in the metal leading to fracture.

The computational method employed here is the ab initio SCF method using a one-electron (4s valence) iron effective core potential (ECP) [2] based on the $4s^1 3d^7$ state of the Fe atom. Here the Ar core and the $3d^7$ configuration are incorporated into the ECP leaving only a single 4s valence electron. The justification for including only the 4s electrons in the valence space comes from all-electron studies of diatomic molecules involving transition metal (TM) atoms. Here is is found that for elements on the right hand side of the first transition row, the bonding in the hydrides [3] and dimers at the nearest neighbor distances in the metal [4-6] involves the 4s,4p electrons with the 3d electrons remaining essentially atomic like. The selection of the $4s^1 3d^7$ atomic configuration of the Fe atom is based on experimental bulk magnetic information [7] and on calculations [8] which show that although the $4s^2 3d^6$ state is the ground state of the free Fe atom with the $4s^1 3d^7$ state 0.88eV higher, in an environment appropriate to Fe metal the $4s^1 3d^7$ state becomes the lowest state.

The present calculations involve Fe clusters of up to 66 Fe atoms and show slow convergence with respect to cluster size; cluster edge effects still introduce significant uncertainties even for the largest clusters studied. Important qualitative features of the H-Fe_n interaction include: i) H atoms are most stable at surface four-fold sites (binding energy $\sim$1.5eV) with a barrier to movement into the bulk (toward an Fe atom in the second layer). ii) Two-fold sites are only weakly bound but it is downhill from this location to move into the bulk (toward an interior tetrahedral site). iii) Interior octahedral and tetrahedral sites are less stable than four-fold surface sites (binding energy $\sim$1.3eV) with tetrahedral sites lower in energy ($\sim$0.23eV separation for the unrelaxed lattice and $\sim$0.18eV separation for the relaxed lattice based on $Fe_{66}H$). The tetrahedral site is a minimum on the potential energy surface while the octahedral site is a maximum. iv) Tetrahedral interior sites show a large volume expansion $\sim$21%. v) The lowest pathway for T$\leftrightarrow$T diffusion involves a trigonal site which is a saddle point on the potential energy surface (Calculated barrier $\sim$0.17eV for the unrelaxed lattice and $\sim$0.10eV for the relaxed lattice based on $Fe_{66}H$).

Section II discusses some features of the electronic structure of Fe clusters. Section III discusses the cluster calculations. Section IV discusses the features of the calculated potential, while Section V compares the computed energetics to experiment.

II. Electronic Structure of the Fe Clusters

For the TM atoms of the first transition row the 4s orbital is significantly larger than the 3d orbital. As one moves from left to right in the first transition row the ratio $\langle r_{4s} \rangle / \langle r_{3d} \rangle$ increases monatonically from 2.36 to 3.24 with a value of 2.95 for Fe [9]. Thus, for large bond distances one expects bonding to the 4s orbital to be more favorable than bonding to the 3d orbital with the 4s becoming increasingly favorable on the right side of the row.

For the TM hydrides only ScH [10] shows a short R state involving 3d bonding; whereas the other hydrides including FeH show predominately 4s bonding character with the 3d orbitals remaining quite atomic like [3]. The situation for the dimers is similar with the possiblity for elements on the left half of the row of 4s-4s bonding at large R and 3d-3d bonding at small R. Examples of the latter are V_2 [11] and Cr_2 [11,12]. With more than half filled 3d shells the favorability of 3d bonding decreases since the repulsion between doubly occupied 3d orbitals cancels 3d bonding interactions arising out of the singly occupied 3d orbitals. For Cu_2 [4] with a closed 3d shell (for the $4s^1 3d^{10}$ state) the bonding is described as predominately 4s-4s bonding with the 3d orbitals essentially atomic like. Given this, one expects the dominant bonding interactions for Fe-Fe and Fe-H bonds to involve the 4s,4p electrons of the Fe atom with the Fe 3d electrons remaining essentially atomic like.

Fig. 1 shows the results of all-electron calculations for the Fe_2 molecule. The electronic state considered here arises from the $4s^2 3d^6 + 4s^1 3d^7$ atomic limit. The significant feature of Fig. 1 is that there is weak 3d bonding in the small R region as evidenced by the low-spin state (maximum 3d bonding) being lower, but in the large R region the high spin state (no 3d bonding) is lower thus indicating negligible 3d bonding. Similar conclusions have been reached by Shim and Gingerich [6] for states derived from the $4s^1 3d^7 + 4s^1 3d^7$ atomic limit. Thus we conclude that at the Fe-Fe distances involved in BCC Fe metal-metal 3d bonding is of negligible importance. (The nearest neighbor distance is $4.68a_o$ in BCC Fe [13]). For these reasons we believe it is a reasonable though extreme approximation to include only 4s electrons in the valence shell with the 3d electrons incorporated into the ECP.

The ECP is based on the $4s^1 3d^7$ Fe atomic configuration. The choice of this configuration is supported by experimental magnetic date [7] which show 2.22 effective Bohr magnetons per Fe atom. Assuming that this magnetic moment arises only from the 3d electrons and that the 3d electrons are completely high spin coupled, this magnetic data is co sistent with a mixture of $4s^1 3d^7$ and $3d^8$. However this data could also be consistent with $4s^1 3d^7$ and some low-spin coupling. The choice of $4s^1 3d^7$ is also supported by calculations in which one Fe atom is placed in the center of a cubic arrangement of eight one-electron $4s^1 3d^7$ like Fe atoms (BCC unit cell). The result is that the $4s^1 3d^7$ configuration is 0.25eV below the $4s^2 3d^6$ configuration in this environment, although for the free atom $4s^1 3d^7$ is 0.88eV above $4s^2 3d^6$. Given this choice of atomic configuration with the 3d electrons incorporated into the ECP leaves only one valence electron per iron atom. This approach is very similar to the one-electron Ni cluster studies based on the $4s^1 3d^9$ Ni atomic configuration [14].

Comparison between ECP and all-electron results can be made for FeH. Here the ECP calculation leads to R_e = 2.96 a_o and D_e = 1.85eV whereas the all-electron calculation leads to R_e = 3.02 a_o and D_e = 3.20eV for the $^4\Delta$ state of FeH [5]. However, a direct comparison here is not appropriate since the ECP calculation corresponds to pure $4s^1 3d^7$ atomic character whereas the FeH molecule in the $^4\Delta$ state is a strong mixture of $4s^1 3d^7$ and $4s^2 3d^6$. The latter configuration mixing, which occurs in the all-electron calculations, is expected to lengthen R_e (due to more $4s^2 3d^6$ character) and increase D_e as compared to the ECP calculation; these expectations are borne out by the results quoted above. Based on these results, to the extent that mixing of $4s^1 3d^7$ and $4s^2 3d^6$ is important for the cluster, we expect the calculations with the ECP to slightly underestimate FeH bond lengths and to significantly underestimate H atom binding energies. Relative energetics for a given cluster would still be expected to be accurate and the emphasis here is therefore on comparisons of relative energies for different H atom locations within a given cluster.

III. The Cluster Calculations

The basis set for Fe is a (4s3p)/[2s1p] basis. The 4s functions are a (31) contraction of the outer four Wachters' 4s functions [15]. The contraction here is based on an atomic SCF calculation for the ^2S state arising from the $4s^1$ configuration. Note that this contraction is different from the all electron contraction because the ECP 4s orbital does not have a nodal structure. The 4p function was obtained by optimization of a 3 term GTO fit to a 2p STO [16] for the ^2P atomic state arising out of the $4s^1$ configuration. The resulting exponents were multiplied by 1.5 to make them more suitable for describing 4s → 4p correlation [17]. The H basis set is a (5s1p)/[3s1p] basis. The s basis is a (311) contraction of Huzinaga's 5s set [18], while the 2p functions are a single set of gaussian primitives with exponent 1.0. The one-electron ECP is given in Table I.

As has been well documented [19] 4p functions are very important for describing the bonding in Ni clusters and these effects are also found to be important for Fe clusters. Omission of the 4p functions leads to a loss of most of the metal metal bonding energy and leads to overestimation of metal-H binding energies due to i) poor description of the metal metal bonds and ii) basis set superposition effects (i.e. the H basis functions mimic the effect of the missing 4p functions and thus lower the cluster energy even without the H atom electron and associated nuclear charge). Thus, unlike Upton and Goddard [14] who omitted the important 4p functions, we have included the 4p functions for those Fe atoms which are within bonding distance of the H atom in any site considered in the cluster. These Fe atoms are denoted as primary (P). To reduce edge effects we have also added the nearest neighbors of the primary atoms. These we denote as secondary (S) atoms. Because these atoms are more distant from the H adatom, the omission of the 4p functions is less serious and we chose to include only the 4s functions on these atoms in order to keep the calculations of more reasonable size. For example, the Fe_{66} cluster involves 330 basis functions with 4p functions on all centers, but only 198 functions if 22 atoms are primary and the remainder are secondary.

Fig. 2 shows the Fe_{36} cluster which is a representative cluster for interior sites. The primary atoms here consist of eight atoms in an arrangement consisting of two fused tetrahedra. Each primary atom has the full complement of eight nearest neighbors which are included at the secondary level. The locations of the H atoms are also indicated in Fig. 2. The Fe_{36} cluster contains i) octahedral sites which have six nearest neighbor Fe atoms and ii) tetrahedral sites which have four nearest neighbors. (Note that these are not regular octahedra or tetrahedra since they are compressed in one direction.) Moving from left to right along the H atom positions indicated by open circles one passes alternately through octahedral and tetrahedral sites at separations of d/4 where d is the lattice constant. Thus the potential should exhibit a periodicity in the direction indicated with $\lambda = d/2$, i.e. all octahedral sites should be equivalent and all tetrahedral sites should be equivalent. This periodicity is not necessarily present in the clusters due to cluster edge effects and we have used periodicity as a criterion for judging the size of cluster edge effects. Two other clusters were studied which are related to the Fe_{36} cluster. These were the smaller Fe_{30} cluster which is related to the Fe_{36} cluster by deleting two primary atoms and associated secondary atoms from one end of the cluster and a larger Fe_{48} cluster which extends the Fe_{36} cluster by addition of an additional tetrahedron of primary atoms and associated secondary atoms at one end.

The BCC metal also exhibits periodicity in a direction perpendicular to the path discussed above for the Fe_{36} cluster. This path is indicated by the solid circles in Fig. 2. Also illustrated in Fig. 2, by the triangle, is a trigonal site which is found to be a saddle point connecting the two adjacent tetrahedral sites. In order to study the T↔T diffusion via the trigonal site we considered additional clusters which are equivalent in the two periodicity directions. The primary cluster here is a 22 atom cluster consisting of four fused BCC unit cells centered about the intersection of the two paths given above. Here we considered an Fe_{22} cluster with all atoms primary and an Fe_{66} cluster which includes in addition the nearest neighbors as secondary atoms.

Fig. 3 shows the Fe_{30} cluster for the surface sites. Here we are considering two-fold and four-fold sites. The Fe_{30} cluster has six surface and two second layer primary atoms. The secondary atoms consist of ten in the first layer, six in the second layer, and six in the third layer. Note that some of these are at second nearest neighbor distances. The Fe_{39} cluster adds to the Fe_{30} cluster three additional primary atoms (two in the first layer and one in the second layer) and associated secondary atoms leading to an additional four-fold surface site. For each of these clusters the H atom was moved perpendicular to the surface for the two-fold and four-fold sites.

The ground states of the clusters were obtained by an Auf Bau method. The symmetry used in the calculations is C_{2v} for the interior site clusters and C_s for the surface site clusters. The orbitals are filled using the Auf Bau principle until the full complement of electrons is present. The cluster configurations for the interior site clusters are as follows: Fe_{30} has six a_1, three b_2, three b_1, and two a_2 orbitals doubly occupied and one a_1 and one b_2 orbitals singly occupied which leads to a $^3B_2$ state. The triplet state arises here because the singly occupied orbitals belong to an E representation in the full cluster symmetry which is higher than C_{2v}. Fe_{36} has eight a_1, four b_2, four b_1, and two a_2 orbitals doubly occupied. Fe_{48} has eleven a_1, five b_2, five b_1, and three a_2 orbitals doubly occupied. Fe_{66} has twelve a_1, nine b_2, seven b_1, and five a_2 doubly occupied. The cluster configurations for the surface site clusters are as follows: Fe_{30} has nine a' and six a'' orbitals doubly occupied. Fe_{39} has twelve a' and seven a'' orbitals doubly occupied and one a'' orbital singly occupied. The Fe_nH clusters are all doublet states with the exception of the $Fe_{30}H$ interior sites cluster which is a quartet state and Fe_{39} which is a singlet state.

IV. Discussion

Fig. 4 shows the binding energies for the $Fe_{30}H$, $Fe_{36}H$, and $Fe_{48}H$ clusters. As discussed in Section III, for the solid all tetrahedral sites are equivalent and all octahedral sites are equivalent. This behavior is most closely approximated by the $Fe_{36}H$ cluster, where we see pseudo periodic behavior with the tetrahedral sites slightly lower in energy than the octahedral sites. Note that these calculations do not include enough points to demonstrate the shape of the potential (i.e. one would expect an approximately sinusoidal variation between the calculated points). The other clusters, on the other hand, at first appear to exhibit rather different potentials with the $Fe_{30}H$ cluster showing a decrease in energy in moving from the center to the edge of the cluster while the $Fe_{48}H$ cluster shows an increase in energy for motion along the same path. However, the potentials can be made to look very similar for the three clusters by including a correction term (for edge effects) which is linear with distance. Selecting such a correction term to make the two octahedral sites degenerate leads to the corrected curves in Fig. 4b which show a remarkable similarity to each other. From Fig 3b one sees that in all cases the tetrahedral sites are below the octahedral sites. The calculated separations are 0.21eV for $Fe_{30}H$, 0.30 and 0.10eV for $Fe_{36}H$, and 0.28 and 0.11eV for $Fe_{48}H$. Thus, the calculations can be interpreted to indicate a tetrahedral to octahedral separation of 0.10 - 0.30eV.

Fig. 5a shows two cuts through the potential surface for the $Fe_{66}H$ cluster. One path follows one of the periodicity directions in Fig. 1, while the other path is from the central octahedral site toward the trigonal site. Fig. 5b differs from Fig. 5a in that a linear correction has been added to make the potential flat from the center of the cluster to the edge (as was done for Fig. 4). These two cuts through the surface show that the octahedral site is a maximum on the potential energy surface and are consistent with the tetrahedral site being a minimum on the surface with the trigonal site being a saddle point connecting two adjacent tetrahedral sites. A remarkable feature of Fig. 4 is the clearly sinusoidal variation of the energy along the periodicity direction. This result suggests that the $Fe_{66}H$ cluster is exhibiting true periodicity although from comparison of Fig. 4a and Fig. 4b there still appears to be a significant edge effect.

From Fig. 5b the tetrahedral to octahedral separation is 0.23eV and the tetrahedral to trigonal separation is 0.17eV (based on the central octahedral site and the adjacent tetrahedral site). These orderings may be understood based on the following simple geometric argument. The octahedral site does not correspond to a regular octahedron but has two shorter FeH distances ($2.703a_o$) and four longer FeH distances ($3.823a_o$). The tetrahedral site has all FeH distances the same ($3.022a_o$) and the trigonal site has two short FeH distances ($2.819a_o$) and one longer FeH distance ($3.023a_o$). With the one-electron ECP and the same basis set used in the calculations diatomic FeH has a bond length of $2.96a_o$. Clearly one expects an H atom in the solid to prefer an FeH distance longer than for the diatomic molecule. Thus, it should be downhill for the octahedral site with two short bonds to distort toward the tetrahedral or trigonal sites. The tetrahedral site is favored over the trigonal site since it has four reasonable FeH bond lengths while the trigonal site still has one compressed bond distance.

For the octahedral, tetrahedral and trigonal sites some relaxation of the lattice was allowed both with and without the H atom present. The clusters here consisted of six, four, and three primary atoms plus the nearest neighbors as secondary atoms. The resulting cluster sizes are Fe_{30}, Fe_{24}, and Fe_{20}, respectively. Fig. 6 shows the distances which were varied in the geometry optimization. Here only the locations of the primary atoms were varied while the secondary atom locations were fixed. For the bare clusters the Fe_{30} and Fe_{24} cluster geometries were optimized with the constraint that r_1 and r_2 were varied simultaneously; this lead to geometric expansions compared to the BCC geometry of 3.4% and 3.9% for octahedral and tetrahedral, respectively. For the trigonal cluster r_1 and r_2 were varied separately giving a 2.4% increase in r_2 and a 6.5% increase in r_1. For the clusters with the H adatom the increases compared to the bare clusters were: r_1=+10.2% and r_2=-4.8% for octahedral, r_1=+3.8% and r_2=+12.2% for tetrahedral and r_1=+9.7% and r_2=+1.2% for trigonal. The corresponding increases in binding energy are 0.27eV, 0.22eV and 0.29eV for octahedral, tetrahedral, and trigonal. Applying these corrections to the energies from Fig. 5b leads to an estimated tetrahedral to octahedral separation of 0.18eV and an estimated tetrahedral to trigonal separation of 0.10eV. The volume expansion for the tetrahedral site, which is the only site which represents a minimum on the surface, is +21%.

Fig. 1 shows the potential for moving a H atom perpendicular to the (100) surface for two-fold and four-fold sites of the $Fe_{30}H$ surface cluster. Here we see that surface atoms are much more stable ($\sim$1.3eV at the four-fold site) and have a minimum at $\sim 0.5a_o$ above the surface. We expect a barrier for pushing the H atom beneath the surface for a four-fold site because it would be moving in the direction of a second layer Fe atom. For the two-fold sites, on the other hand, a location in the surface is basically an octahedral location and from the studies of interior sites we expect it to be downhill to move to the adjacent tetrahedral site. Indeed it is found that the H atom will move from this location to the interior. Fig. 5 shows similar calculations for the $Fe_{39}H$ surface cluster. Here we see that the $Fe_{39}H$ cluster shows results which are consistent with the $Fe_{30}H$ cluster. The binding energies here are $\sim$1.7eV for site A and $\sim$1.3eV for site B. This difference between the two four-fold sites is another manifestation of cluster edge effects.

As discussed above we expect a large barrier to moving an atom from a four-fold site directly toward a second layer atom. Moving from a four-fold to a two-fold site is uphill by $\sim$1.25eV but it is downhill from here to an interior site; this implies a barrier of $\sim$0.25eV in addition to the endothermicity of $\sim$1.0eV to the process of moving a H atom from a four-fold surface site to an interior site via a two-fold site. However, there may be alternative pathways such as penetrating the surface at a four-fold site followed by sideways movement toward an adjacent tetrahedral site which involves little or no barrier.

From examination of Figs. 5, 7, and 8 we see that the most stable site is the four-fold surface site with an estimated binding energy of 1.3 - 1.7eV while the two-fold surface site shows essentially zero binding energy (based on the $Fe_{39}H$ cluster). Interior sites are less stable than surface sites being bound by about 1.3eV (based on $Fe_{66}H$). This result is consistent with the experimental observation that H atoms are more stable at the surface with only a small fraction of the H atoms moving inside the solid (see section V); however, it is not clear that the binding energies are well enough converged with respect to cluster size to strongly support this conclusion.

V. Comparison to Experiment

The current picture of H_2 chemisorption on an iron surface is that the H_2 molecule first bonds in a weakly bound state which subsequently dissociates leading to two H atoms chemisorbed on the surface[21]. The detailed energetics for H atoms interior to the bulk are not known but overall the interior sites are believed to be less stable than the surface sites [22]. H atoms are known to be quite mobile inside the bulk [20]. The solubility and diffusivity of hydrogen in iron has been reviewed by Kiuchi and McLellan [24]. The quantities which are experimentally accesible (experimental value in parenthesis) are i) the heat adsorption (0.9eV) [22] which is the energy for chemisorption of H_2 on an iron surface (normally as film). Since H_2 is known to dissociate on the surface this quantity is twice the binding energy of an H atom minus the D_e of H_2. ii) the heat of solution (0.3eV) [23] which is as in (ii) except that the two H atoms are in the bulk. Based on an analysis of non-Arrhenius behavior of the solubility it has been inferred that tetrahedral sites are about 0.23eV more stable than octahedral sites, iii) the activation energy for diffusion in the bulk iron lattice (0.1eV) [20], and iv) the volume expansion for a hydrogen atom in the perfect lattice which is $\lesssim$0.17 atomic volumes for BCC iron [25].

Using the experimental D_e of H_2 in conjunction with the heat of adsorption and the heat of solution leads to binding energies of 2.8eV for one H atom at the surface and 2.5eV for one H atom in the bulk. The best calculated values are less than this being 1.3-1.7eV (four-fold surface site) and 1.3eV (interior tetrahedral site), respectively. This is not an unexpected result given the SCF model which typically underestimates binding energies and considering that the same ECP and basis set underestimates the diatomic FeH binding energy by 1.4eV.

The activation energy for diffusion is estimated to be 0.10eV based on the $Fe_{66}H$ cluster. One expects that the effective barrier should be lower than this , since tunneling is known to be important for hydrogen [26]. Thus, it appears that the calculations underestimate this barrier since the experimental barrier is thought to be $\sim$0.1eV. Finally, the calculated volume expansion is 21% in reasonable agreement with the experimental estimate of 17%.

These encouraging results indicate that the SCF cluster model in conjunction with the one-electron ECP and basis set used here provides physically reasonable results and can be relied upon to provide useful information in situations which are experimentally inaccesible, e.g. the interaction of H atoms with defects in the solid.

Acknowledgements

Figures 2 and 3 were prepared at the I.B.M. San Jose Research Laboratory using the I.B.M. implementation of the PLUTO program written by S. Motherwell, J.L. Sussman, Z. Shakked, D. Barnett, and N.H.F. Beebe. The author is indebted to Prof. Klaus Hermann and Dr. Paul S. Bagus for helpful discussions and their kind assistance in the use of Pluto.

The author would also like to acknowledge helpful conversations with Dr. Charles Bauschlicher, Jr., Dr. Richard Jaffe, Dr. Mayes Mullins, and Dr. M.R. Shanabarger.

The author would like to thank Dr. Luis Kahn for making the one-electron Fe ECP available for this work prior to publication.

References

1. M.S. Daw and M.I. Baskes, Phys. Rev. Lett., 50 (1983) 1285 and references quoted therein.

2. L.R. Kahn, unpublished work.

3. S.P. Walch and C.W. Bauschlicher, Jr., J. Chem. Phys., 78 (1983) 4597.

4. C.W. Bauschlicher, Jr., S.P. Walch, and P.E.M. Siegbahn, J. Chem. Phys. 78 (1983) 3347.

5. S.P. Walch and C.W. Bauschlicher, Jr., Chem. Phys. Lett., 94 (1983) 290.

6. I. Shim and K.A. Gingerich, J. Chem. Phys., 77 (1982) 2490.

7. C. Kittle, Introduction to Solid State Physics, Wiley and Sons, New York, p. 407.

8. S.P. Walch, unpublished work.

9. C.W. Bauschlicher, Jr., S.P. Walch, and H. Partridge, J. Chem. Phys., 76 (1982) 1033.

10. C.W. Bauschlicher, Jr., and S.P. Walch, J. Chem. Phys. 76 (1982) 4560.

11. S.P. Walch, C.W. Bauschlicher, Jr., B.O. Roos, and C.J. Nelin, Chem. Phys. Lett., 103 (1983) 175.

12. R.L. Michalopoulos, M.E. Geusic, S.G. Hansen, D.E. Powers, and R.E. Smalley, J. Phys. Chem., 86 (1982) 3914 and references therein.

13. J. Donohue, The Structure of the Elements, Wiley and Sons, New York.

14. T.H. Upton and W.A. Goddard, III, CRC Critical Rev. Solid State Materials Sci., 10 (1981) 261.

15. A.J.H. Wachters, J. Chem. Phys., 66 (1977) 4377.

16. R.F. Stewart, J. Chem. Phys., 66 (1977) 4377.

17. The 4p function is given by: α_i = 0.28016, 0.07190, 0.02442 and C_i = 0.16239, 0.56617, 0.42231.

18. S. Huzinaga, J. Chem. Phys., 42 (1965) 1293.

19. C.W. Bauschlicher, Jr., S.P. Walch, P.S. Bagus, and C.R. Brundle, Phys. Rev. Lett., 50 (1983) 864.

20. A.G. Alefeld and J. Volkl, Eds. Hydrogen in Metals. 1. Basic Properties. Topics in Applied Physics., 28 (Springer, Berlin. 1978).

B.G. Alefeld and J. Volkl, Eds. Hydrogen in Metals. II. Application Oriented Properties. Topics in Applied Physics, 29 (Springer, Berlin. 1978).

21. M.R. Shanabarger in "Advanced Techniques for Characterizing Hydrogen in Metals", N.F. Fiore and B.J. Berkowitz, eds.; The Metalurgical Society of AIME, Warrendale, Pennsylvania, 1982, p. 155.

22. M. Lagos, Surface Science, 122 (1982) L601-L607.

23. O.D. Gonzalez, Trans. TMS-AIME, 245 (1969), 607.

24. K. Kiuchi and R.B. McLellan, Acta Metall. 31 (1983), 961.

25. J.P. Hirth, Met. Trans., 11A (1980), 861.

26. G.C. Schatz and S.P. Walch, J. Chem. Phys. 72 (1980), 776.

Table I Parameters of the GTO Fit of the One-Electron Fe Effective Core Potential [a]

N	ZETA	COEFFICIENTS
F Potential		
2	0.47390366	-1.26119200
2	1.58405370	-9.53136520
2	4.95107780	-25.40468800
2	19.31682400	-64.39665200
2	86.61302200	-190.95396000
2	594.26962000	-733.44870000
1	32.93220700	-1.00000000
S-F Potential		
2	0.77791885	4.11278120
2	2.35091970	20.80044300
2	7.40039490	50.55318300
2	27.76902900	126.11910000
2	175.84886000	515.48734000
0	488.84440000	3.00000000
P-F Potential		
2	0.62727306	2.35615760
2	1.86402300	13.98017900
2	5.77181370	50.95290200
2	18.09789100	144.04543000
2	66.97594900	376.36175000
0	143.17037000	5.00000000
D-F Potential		
2	0.43787116	1.73163370
2	1.90303490	11.35304600
2	7.19745380	45.18231400
2	24.49263100	172.21949000
2	81.70534400	582.84560000
0	152.31608000	7.00000000

[a] The Fe one-electron ECP was developed by Dr. Louis Kahn [2].

Figure Captions

Fig. 1 Calculated potential curves for Fe_2 states arising from the $4s^2 3d^6$ + $4s^1 3d^7$ atomic limit. Curve A is for the high spin state which has no 3d bonding, while curve B is for the low spin state which could have maximal 3d bonding.

Fig. 2 The Fe_{36} cluster for interior sites in BCC Iron. The locations of the primary atoms are indicated by the large circles; the locations of the secondary atoms are indicated by the intermediate size circles. The H atom locations for one periodicity direction are indicated by the small open circles; the H atom locations for the other periodicity direction are indicated by the small solid circles, while a trigonal site is indicated by a triangle.

Fig. 3 The Fe_{30} cluster for surface sites. The conventions are as for Fig. 1.

Fig. 4 Calculated binding energies for octahedral (O) and tetrahedral (T) sites in BCC Iron. Fig. 4a shows the calculated points while Fig. 4b shows the effect of adding a correction term (see text) to compensate for cluster edge effects.

Fig. 5 Calculated binding energies for two cuts through the potential energy surface for H in the Fe_{66} cluster. Curve A is for motion along one of the periodicity directions while curve B is for motion in the direction of a trigonal site. Fig. 5b differs from Fig. 5a in that a correction term has been added to compensate for cluster edge effects (see text).

Fig. 6 The geometric parameters which were varied in studying lattice relaxation for H in octahedral, tetrahedral, and trigonal sites.

Fig. 7 Calculated binding energies for two-fold and four-fold sites on the (100) surface of BCC Iron from the $Fe_{30}H$ cluster.

Fig. 8 Calculated binding energies for two-fold and four-fold sites on the (100) surface of BCC Iron from the $Fe_{39}H$ cluster.

Fig 1

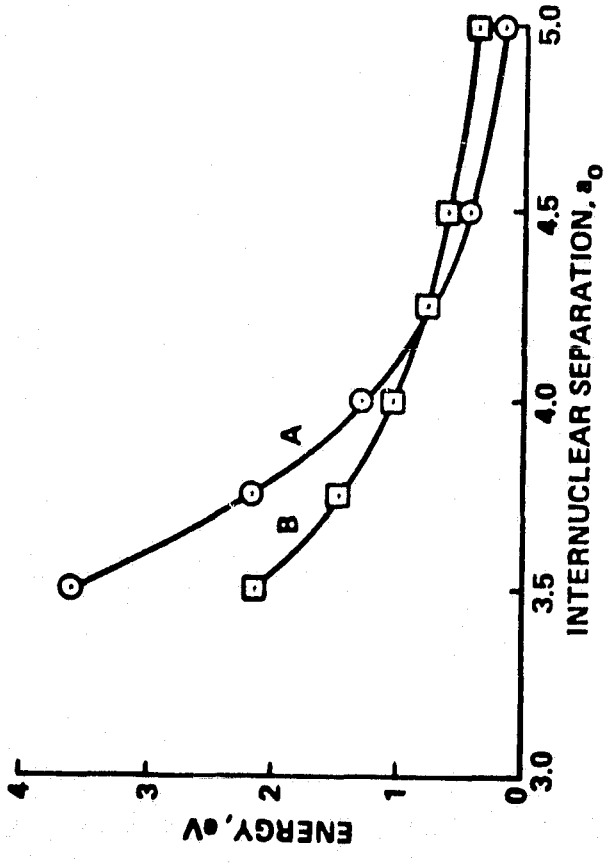

G.
OF FOUR

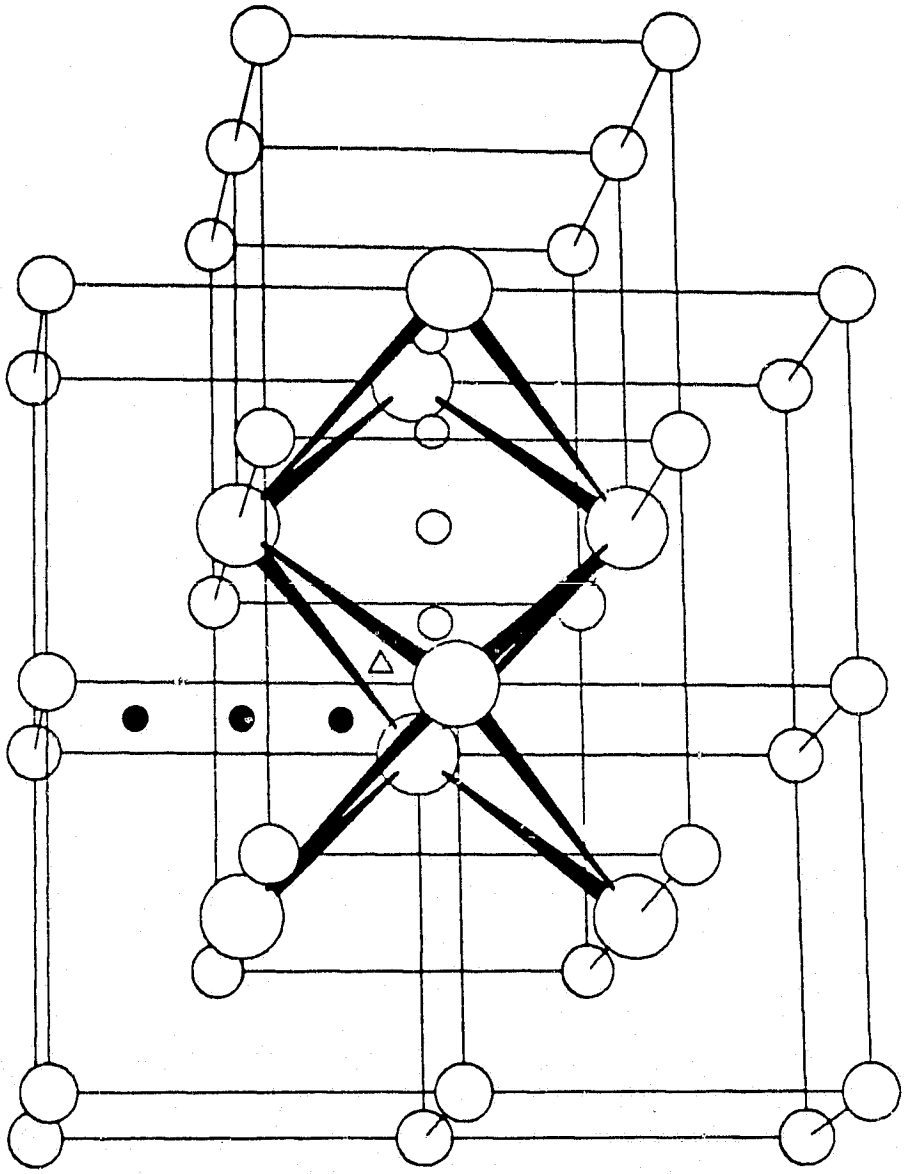

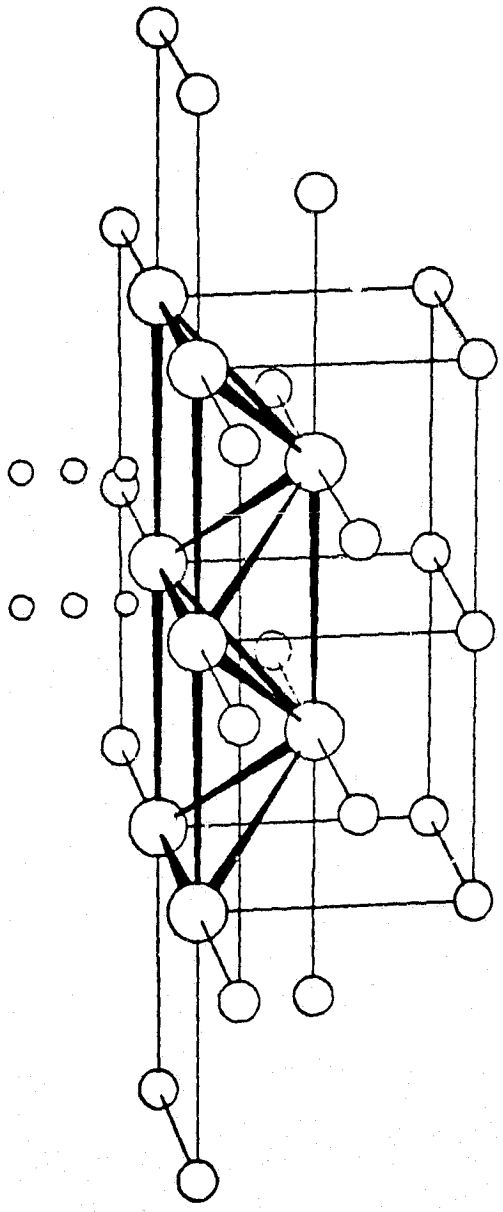

Fig 4a

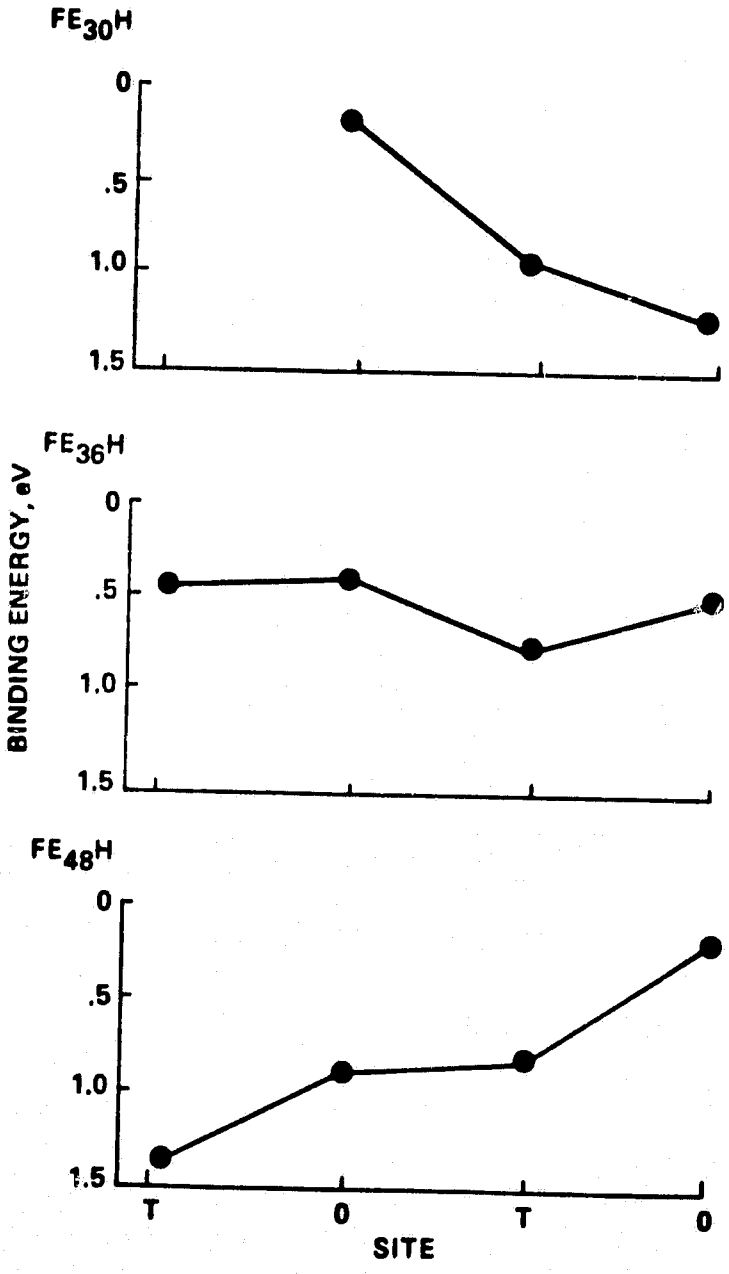

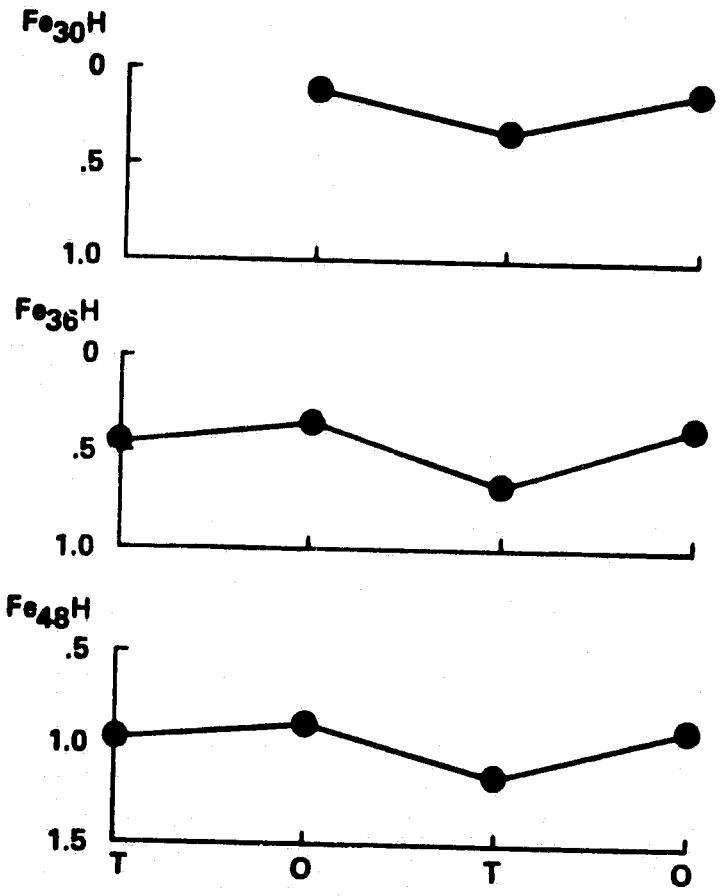

Fig 5a

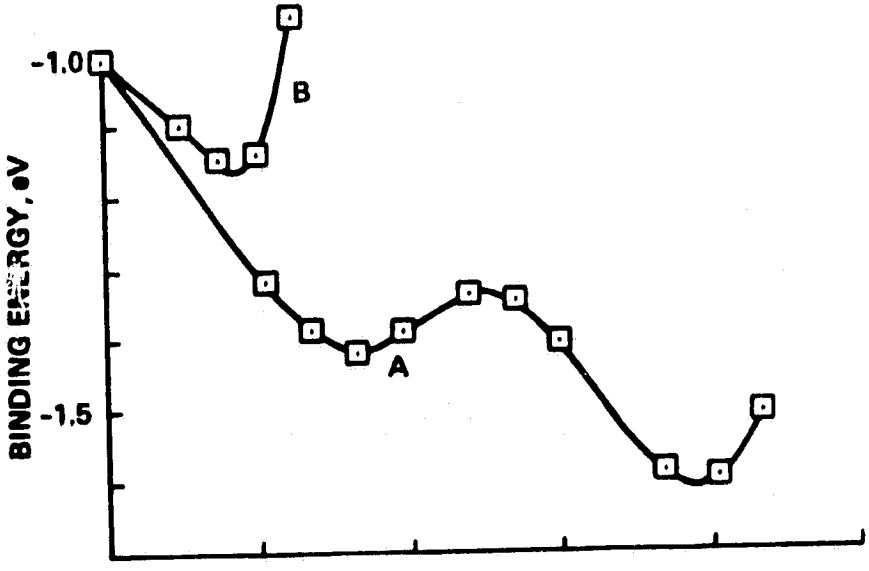

Fig 5b

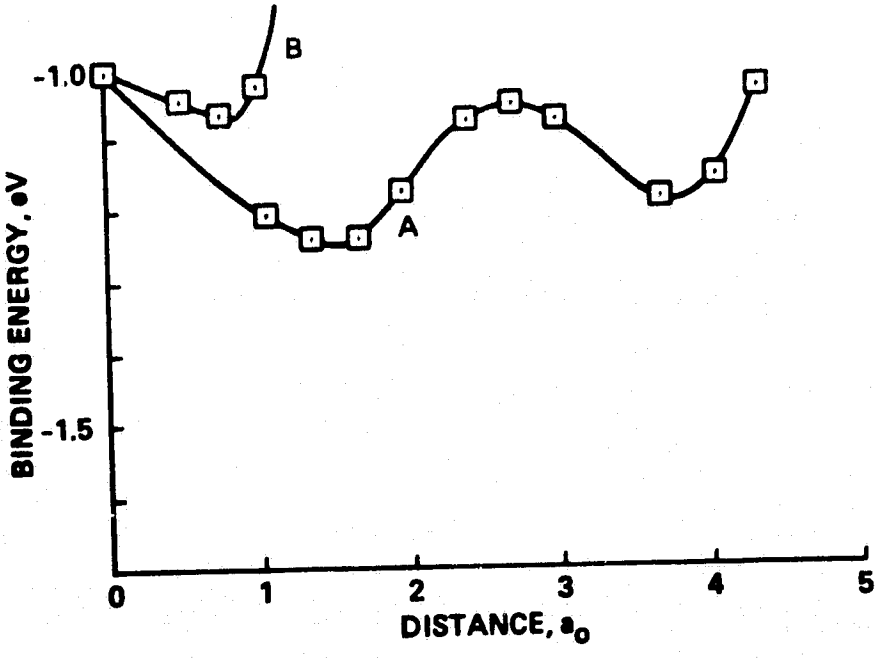

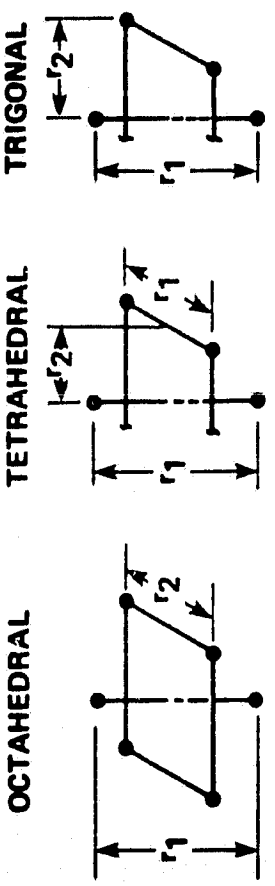

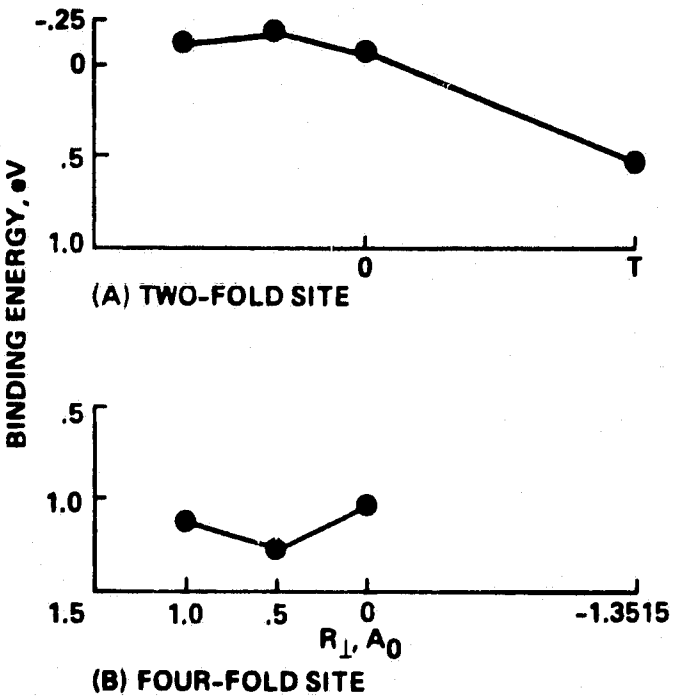

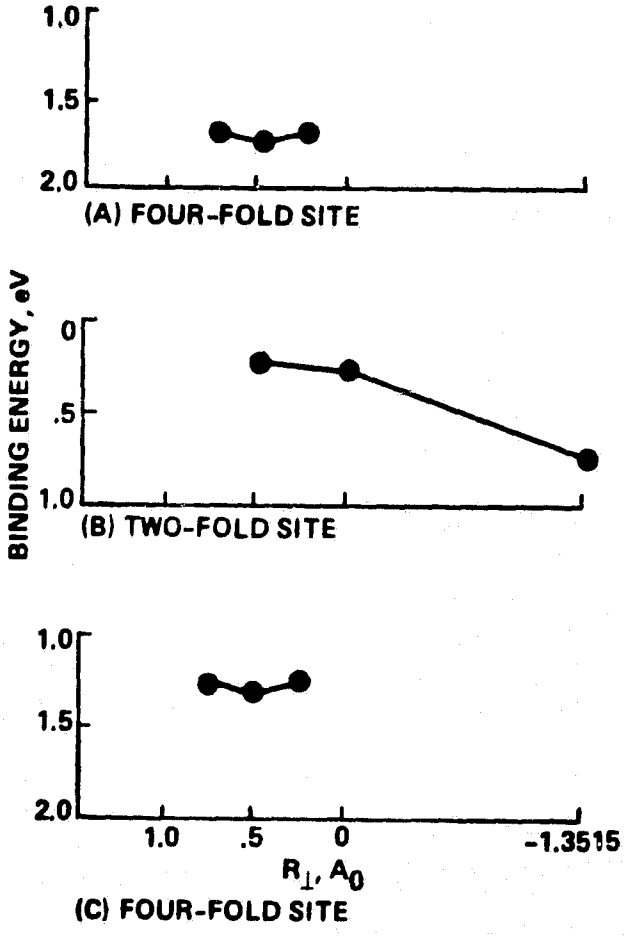
1.0
1.5
2.0
(A) FOUR-FOLD SITE
BINDING ENERGY, eV
0
.5
1.0
(B) TWO-FOLD SITE
1.0
1.5
2.0
1.0
.5
0
-1.3515
$R_\perp, A_0$
(C) FOUR-FOLD SITE

APPENDIX B

The following papers describe the calculations for the TM hydrides and dimers.

CASSCF/CI calculations for first row transition metal hydrides: The TiH ($^4\Phi$), VH ($^5\Delta$), CrH ($^6\Sigma^+$), MnH ($^7\Sigma^+$), FeH ($^{4,6}\Delta$), and NiH ($^2\Delta$) states

Stephen P. Walch[a] and Charles W. Bauschlicher, Jr.[b]

Polyatomics Research Institute,[c] Mountain View, California 94043
(Received 25 October 1982; accepted 28 December 1982)

By consideration of atomic coupling arguments and interaction of $4s^23d^n$ and $4s^13d^{n+1}$ derived terms, the ground states of the transition metal hydrides are predicted to be TiH ($^4\Phi$), VH ($^5\Delta$), CrH ($^6\Sigma^+$), MnH ($^7\Sigma^+$), FeH ($^4\Delta$), CoH ($^3\Phi$), and NiH ($^2\Delta$). All of these systems have been studied by a CASSCF/CI(SD) procedure with the exception of CoH. The calculated parameters derived from the CASSCF/CI(SD) potential curves are in good agreement with the experimental values where known (no information exists for TiH and VH). Inclusion of atomic correlation leads to significantly better agreement with experiment particularly for R_e. These improvements are related to a more balanced description of the atomic states in the correlated wave functions.

I. INTRODUCTION

The chemistry of the transition metals (TM) is especially diverse because of the presence of several low-lying atomic states which may be utilized in bonding. For the first transition row the lowest atomic states are derived from the $4s^23d^n$, $4s^13d^{n+1}$, and $4s^14p^13d^n$ configurations. As we will see the bonding in TM involves a complex interaction among terms arising out of the various atomic levels. A number of studies[1-5] have shown that the separations of the TM atomic states are not well described at the Hartree–Fock (HF) level; however, inclusion of electron correlation does significantly improve the description of the atomic states. Thus, electron correlation has to be included in the molecular calculations.

There have been a number of previous theoretical studies of the TM hydrides. Earlier all-electron studies by Scott and Richards[6-8] and Bagus and Schaefer[9] used HF wave functions which completely neglect electron correlation. More recently Henderson, Das, and Wahl (HDW)[10] and Das[11] have carried out limited MCSCF studies of the TM hydrides. In these studies atomic correlation was largely neglected. This was justified in the work of Das[11] by the observation that for VH the calculated properties of several states were similar in the GVB/POL-CI calculations of Walch[12] which included limited correlation ($4s^2-4p^2$), and in the calculations of HDW which neglected these correlation terms. However, Bauschlicher and Walch[13] pointed out that for ScH neglect of $4s^2-4p^2$ near degeneracy terms leads to an incorrect ordering of the $^1\Sigma^+$ and $^3\Delta$ states. Similarly for NiH Walch and Bauschlicher[14] found that a correct description of the $X^2\Delta$ state of NiH required a balanced description of the $4s^23d^9$ and $4s^13d^9$ states of Ni, and consequently an accurate description of electron correlation was necessary. This conclusion is also substantiated for NiH by the CASSCF/CI calculations of Blomberg *et al.*[15] and had been suggested by the earlier studies of Bagus and Bjorkman[16] and R. Martin[17] in which limited 3*d* shell correlation had been included.

For completeness we also mention the work of Goddard *et al.*[18] on NiH in which electron correlation effects for the Ni atom were included in a semiempirical way using a modified effective core potential. This approach led to properties for NiH in good agreement with experiment at the two configuration MCSCF (GVB) level.

In the present study calculations were carried out for the predicted ground states of TiH($^4\Phi$), VH($^5\Delta$), CrH($^6\Sigma^+$), MnH($^7\Sigma^+$), and NiH($^2\Delta$). For FeH both the $^6\Delta$ and $^4\Delta$ states were studied, since both are likely candidates for the ground state. As discussed in Sec. II, the ground state symmetries are predicted based on a combination of atomic coupling arguments and coupling of $4s^23d^n$ amd $4s^13d^{n+1}$ terms in the molecular system. Electron correlation is included by a CASSCF/CI(SD) treatment. The CASSCF includes near-degeneracy effects ($4s^2-4p^2$) while correlation of the 3*d* electrons is included at the CI level.

II. QUALITATIVE FEATURES OF THE BONDING IN TM HYDRIDES

Figure 1 shows the relative ordering of the $4s^23d^n$ and $4s^13d^{n+1}$ states for the first transition row.[19] The trends in Fig. 1 may be understood in terms of two

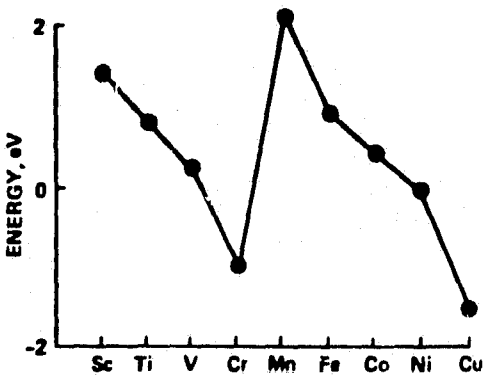

FIG. 1. $4s^13d^{n+1}-4s^23d^n$ excitation energies of scandium to copper $[E(sd^{n+1})-E(s^2d^n)]$. All units are in eV.

[a] Supported under NASA grant NCC2-148.
[b] Present address: NASA Ames Research Center Moffett Field, California 94035.
[c] Mailing address: 1101 San Antonio Road, Suite 420 Mountain View, CA 94043.

 0021-9606/83/074597-09$2.10

TABLE I. Calculated parameters for the TM hydrides.

State		R_e (Å)	ω_e (cm^{-1})	D_e (eV)	$3d$ population
TiH $^4\Phi$	PW[a]	1.83	1407	2.12	2.26
	SR[b]	1.86	1410		
	D[c]	1.91	1331	1.7	
VH $^5\Delta$	PW	1.74	1590	2.30	3.42
	D	1.74	1609	1.77	
CrH $^6\Sigma^+$	PW	1.70	1465	2.10	4.86
	D	1.71	1570	2.0	
	Expt.[d]	1.66	1581		
MnH $^7\Sigma^+$	PW	1.77	1639	1.71	5.06
	D	1.84	1432	1.9	
	Expt.[d]	1.73	1548		
FeH $^6\Delta$	PW	1.72	1560	1.95	6.08
	J[e]	1.62	1560	1.7	
	D	1.77	1380	1.43	
	SR	1.73	1650		
	Expt.[f]	1.77 ± 0.05			
FeH $^4\Delta$	PW	1.60	1710	(3.20)	6.26
	J	1.50	1730	(2.6)	
	Expt.[g]	1.63	1680		
NiH $^2\Delta$	PW	1.47	1982	2.79	8.66
	BSR[h]	1.47	1911	2.76	
	BB[i]	1.49			
	M[j]	1.50	1990	2.34	
	D	1.55	1917	2.5	
	GWRU[k]	1.45	1911	2.76	
	Expt.[d]	1.48	1926.6[l]	≤ 3.16[l]	

[a] Present work (PW).
[b] Scott and Richards (SR) Refs. 6–8.
[c] Das (D) Ref. 11.
[d] Reference 28.
[e] Jaffe (J) Ref. 32.
[f] Stevens, Lineberger, and Feigerle Ref. 30.
[g] Davis Ref. 31.
[h] Blomberg, Siegbahn, and Roos (BSR) Ref. 15 CI results. D_e referenced to $4s^1 3d^9$.
[i] Bagus and Bjorkman (BB) Ref. 16. The R_e value is from CI calculations.
[j] Martin (M) Ref. 17 CI values.
[k] Goddard, Walch, Rappe, and Upton (GWRU) Ref. 18.
[l] The calculated D_e values are with respect to $4s^1 3d^9$ while the experimental D_e, is referenced to $4s^2 3d^8$. The experimental separation is 0.03 eV with $4s^2 3d^8$. Thus, the appropriate D_e value for comparison to the calculation is 3.16 eV (3.19 eV with respect to $4s^2 3d^8$).

competing effects (i) a general stabilization of $3d$ with respect to $4s$ with increasing Z, and (ii) a preference for a maximum number of high spin coupled $3d$ orbitals. For less than half-filled shells both effects tend to stabilize $4s^1 3d^{n+1}$ with respect to $4s^2 3d^n$ for increasing Z, thus the $4s^1 3d^{n+1}$–$4s^2 3d^n$ separation decreases monotonically from Sc–Cr. For Mn $4s^2 3d^5$ is favored over $4s^1 3d^6$ because of the extra high spin coupled $3d$ orbital. Thus, at Mn there is a discontinuity with $4s^2 3d^n$ again becoming lower. For Mn–Cu the $4s^1 3d^{n+1}$–$4s^2 3d^n$ separation once again decreases monotonically due to stabilization of $3d$ with respect to $4s$ for increasing Z.

In addition to the $4s^2 3d^n$ and $4s^1 3d^{n+1}$ atomic configurations the $4s^1 4p^1 3d^n$ configuration is also important. The excitation energy $4s^2 3d^n - 4s^1 4p^1 3d^n$ increases monotonically with increasing Z from ~16 000 cm^{-1} for Sc to ~28 000 cm^{-1} for Cu.[19]

The bonding of a H atom to a transition metal atom may involve either the $4s^2 3d^n$ or $4s^1 3d^{n+1}$ state. For the $4s^2 3d^n$ state the bonding involves formation of sp hybrids arising from interaction of the $4s^2 3d^n$ and $4s^1 4p^1 3d^n$ atomic configurations. This leads to two orbitals sz and $s\bar{z}$ which have the qualitative character $4s + 4p\sigma$ and $4s - 4p\sigma$, respectively. The bonding orbital (two electrons) has the character of a sigma bond between Sc (sz) and H ($1s$) while the $s\bar{z}$ orbital which is singly occupied is hybridized away from the bond pair. For the $4s^1 3d^{n+1}$ state the bonding involves formation of a simple Sc ($4s$)–H ($1s$) bond. We expect the bonding here to be stronger than for the $4s^2 3d^n$ state since no promotion energy is involved. This picture is supported by the population analysis (CASSCF/CISD wave functions) which shows that MnH which is predominately $4s^2 3d^5$ like has valence s and p populations of 1.04 and 0.68 indicating a strong admixture of $4s^1 4p^1 3d^5$ character while CrH which is dominated by $4s^1 3d^5$ has

valence s and p populations of 0.77 and 0.11, i.e., very little admixture of $4p$ character.

Considering these two bonding mechanisms in conjunction with the variation in the $4s^2 3d^n - 4s^1 3d^{n+1}$ separation (Fig. 1) one expects predominately $4s^2 3d^n$ like character for elements where $4s^2 3d^n$ is well below $4s^1 3d^{n+1}$ (e.g., Sc and Mn), predominately $4s^1 3d^{n+1}$ character for elements where $4s^1 3d^{n+1}$ is well below $4s^2 3d^n$ (e.g., Cr and Cu), and mixed character for the other elements with especially strong mixing for elements where $4s^1 3d^{n+1}$ is slightly above $4s^2 3d^n$ (e.g., V and Co). These expectations are borne out by the $3d$ populations in Table I where we see TiH is predominately $4s^2 3d^2$, VH is a mixture of $4s^2 3d^3$ and $4s^1 3d^4$, CrH is predominately $4s^1 3d^5$, MnH is predominately $4s^2 3d^5$, FeH $^6\Delta$ is predominately $4s^2 3d^6$, and NiH is a mixture of $4s^2 3d^8$ and $4s^1 3d^9$.

As pointed out elsewhere,[13] there is an additional complication for ScH where there is a competition between bonding to $s\bar{z}$ and $3d\sigma$ for the $4s^2 3d^1$ configuration. However, we suspect that a "d-bonded" ground state is peculiar to ScH for the following reasons: (i) As one moves from the left to right side of the first transition row both the $3d$ and $4s$ orbitals contract, but the ratio of $\langle r_{4s}\rangle/\langle r_{3d}\rangle$ increases monotonically from 2.364–3.239.[5] Thus bonding to the $4s^2$ pair is favored increasingly as one moves from Sc to elements on the right side of the row. (ii) Formation of the "d-bond" results in loss of exchange energy as the number of $3d$ electrons increases. This effect should be most significant in the center of the row where the maximum number of high spin coupled electrons occurs.

In the previous discussion we considered the interaction between H(1s) and the $4s^2 3d^n$ and $4s^1 3d^{n+1}$ atomic configurations. We now consider how to select the lowest $3d$ orbital occupancies. As discussed in some detail elsewhere,[20] just as one may write a given atomic state as a mixture of determinants it is possible to express a given determinant as a mixture of atomic states. For example, for the Ti atom in the $4s^2 3d^2$ state the configuration $4s^2 3d\sigma^1 3d\delta^1$ is pure ^3F, but the configuration $4s^2 3d\sigma^1 3d\pi^1$ is a mixture of 40% ^3F and 60% ^3P. These relationships have been worked out for the $3d^1$, $3d^2$, $3d^3$, $3d^4$, and $3d^5$ configurations and are given in Table II. Given this information one then expects for Ti that the $4s^2 3d\sigma^1 3d\pi^1$ configuration is 0.62 eV above $4s^2 3d\delta^1 3d\delta^1$ (i.e., 0.6×1.03 where 1.03 is the excitation energy $^3F \rightarrow {}^3P$). Thus in the absence of other effects one expects it to be more favorable to have the configuration $3d\sigma^1 3d\delta^1$ than $3d\sigma^1 3d\pi^1$ and similarly for the other TM hydrides one may pick likely candidates for the ground states from Table I. Note that here we are making use only of atomic information.

Now consider forming a TM hydride. As a first case consider the state of ScH arising out of $4s^2 3d^1$. The SCF configuration here is

$$b^2 s\bar{z}^1 3d^1 \alpha\beta\alpha\alpha , \tag{1}$$

where b is the bond orbital [sz + H(1s)like] and $s\bar{z}$ is an orbital of $4s - 4z$ character. Looking at Table II we see that the three components of ^2D are degenerate and no direct information as to the favorability of $3d\sigma$, $3d\pi$, or $3d\delta$ is obtained from purely atomic information. However in the molecular symmetry $3d\sigma$ and $4s$ mix and in Eq. (1) allowing $s\bar{z}$ to mix in $3d\sigma$ character leads to mixing in a piece of $4s^1 3d^2$ like character:

$$\begin{aligned}
&\delta \text{ particle} \quad b^2 s\bar{z}^1 3d\delta^1 \alpha\beta\alpha\alpha + \lambda\, b^2 3d\sigma^1 3d\delta^1 \alpha\beta\alpha\alpha \;\; 100\%\ {}^3F ;\\
&\pi \text{ particle} \quad b^2 s\bar{z}^1 3d\pi^1 \alpha\beta\alpha\alpha + \lambda\, b^2 3d\sigma^1 3d\pi^1 \alpha\beta\alpha\alpha \;\; 40\%\ {}^3F ;\\
&\sigma \text{ particle} \quad b^2 s\bar{z}^1 3d\sigma^1 \alpha\beta\alpha\alpha .
\end{aligned} \tag{2}$$

Note here that the $3d\delta$ particle leads to $4s^2 3d\sigma^1 3d\delta^1$ which is pure ^3F, the $3d\pi$ particle leads to $4s^2 3d\sigma^1 3d\pi^1$ which is 40% ^3F and 60% ^3P, while the $3d\sigma$ particle leads to no $4s^1 3d^2$ term due to the Pauli principle. Thus hybridizing $4s$ and $3d\sigma$ is equivalent to mixing $4s^2 3d^1$ and $4s^1 3d^2$ character and one expects this process to be more favorable for a $3d\delta$ particle than for a $3d\pi$ particle which is in turn more favorable than for a $3d\sigma$ particle. On this basis one predicts the molecular ordering $^3\Delta < {}^3\Pi < {}^3\Sigma^+$ which is in fact the calculated ordering.[13]

Considering now TiH, from Table II the lowest atomic configurations are

$$b^2 s\bar{z}^1 3d\pi^1 3d\delta^1 \alpha\beta\alpha\alpha\alpha \tag{3}$$

and

$$b^2 s\bar{z}^1 3d\sigma^1 3d\delta^1 \alpha\beta\alpha\alpha\alpha \tag{4}$$

which are pure ^3F for the atomic case. However, Eq. (3) mixes with $b^2 3d\sigma^1 3d\pi^1 3d\delta^1$ which is pure ^4F, while no such mixing is allowed for Eq. (4). Thus one predicts the ground state of TiH is $^4\Phi$ arising from Eq. (3).

TABLE II. Composition of determinants in terms of pure atomic states.

	$3d^1$
(2)	100% ^2D
(1)	100% ^2D
(0)	100% ^2D
	$3d^2$
(21)	100% ^3F
(20)	100% ^3F
(1$\bar{1}$)	80% ^3F, 20% ^3P
(2$\bar{1}$)	60% ^3F, 40% ^3P
(10)	40% ^3F, 60% ^3P
(2$\bar{2}$)	20% ^3F, 80% ^3P
	$3d^3$
(210)	100% ^4F
(21$\bar{1}$)	100% ^4F
(20$\bar{2}$)	80% ^4F, 20% ^4P
(20$\bar{1}$)	60% ^4F, 40% ^4P
(21$\bar{2}$)	40% ^4F, 60% ^4P
(10$\bar{1}$)	20% ^4F, 80% ^4P
	$3d^4$
(210$\bar{1}$)	100% ^5D
(210$\bar{2}$)	100% ^5D
(21$\bar{1}\bar{2}$)	100% ^5D
(20$\bar{1}\bar{2}$)	100% ^5D
(10$\bar{1}\bar{2}$)	100% ^5D
	$3d^5$
(210$\bar{1}\bar{2}$)	100% ^6S

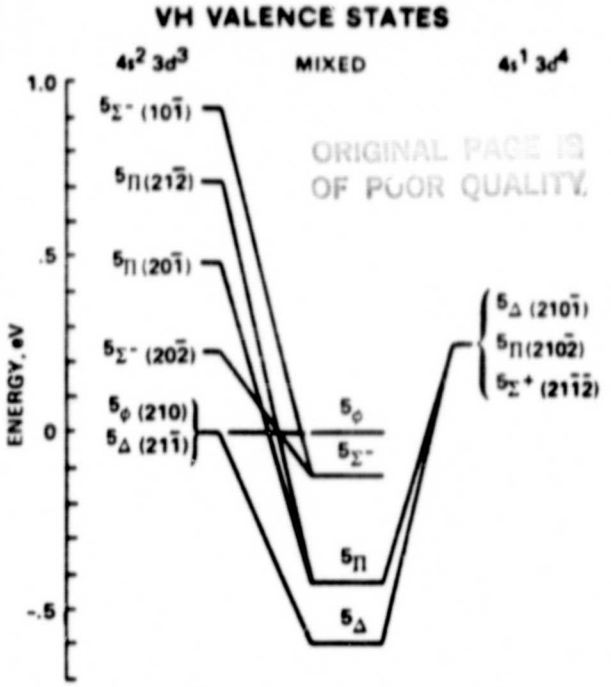

FIG. 2. Origin of VH valence states. The first column shows the ordering of the $4s^2 3d^3$ derived terms and the last column shows the ordering of the $4s^1 3d^4$ derived terms while the center column shows the calculated ordering of molecular states.

Similarly for VH the most favorable choice is

$$b^2 s\bar{z}^1 3d\delta^1 3d\pi_x^1 3d\pi_y^1 , \tag{5}$$

which mixes with

$$b^2 3d\sigma^1 3d\delta^1 3d\pi_x^1 3d\pi_y^1 \alpha\beta\alpha\alpha\alpha , \tag{6}$$

leading to a $^5\Delta$ ground state.

For CrH mixing of $4s$ and $3d\sigma$ couples

$$b^2 s\bar{z}^1 3d\delta_{xy}^1 3d\delta^1{}_{x^2-y^2} 3d\pi_x^1 3d\pi_y^1 \alpha\beta\alpha\alpha\alpha\alpha$$

and (7)

$$b^2 3d\sigma^1 3d\delta_{xy}^1 3d\delta^1{}_{x^2-y^2} 3d\pi_x^1 3d\pi_y^1 \alpha\beta\alpha\alpha\alpha\alpha$$

leading to a $^6\Sigma^+$ ground state.

For a less than half-filled $3d$ shell the above analysis predicts the ground state spin and spatial symmetry independent of whether the molecular state is predominately $4s^2 3d^n$ or $4s^1 3d^{n+1}$. On the other hand, for a more than half-filled $3d$ shell the spin multiplicity depends on whether the atomic character is $4s^2 3d^n$ or $4s^1 3d^{n+1}$ like. Here the low spin states are expected to involve strong coupling of $4s^1 3d^{n+1}$ and $4s^2 3d^n$ derived terms as for the elements with less than half-filled $3d$ shells, but the high spin states should involve less coupling of $4s^2 3d^n$ and $4s^1 3d^{n+1}$ because the high spin coupling arising from $4s^1 3d^{n+1}$ is expected to be repulsive. By an argument analogous to the above (substituting holes for particles) one predicts that the ground states of the remaining hydrides are MnH($^{6,7}\Sigma^+$), FeH($^{4,6}\Delta$), CoH($^{3,5}\Phi$), and NiH($^{2,4}\Delta$) where the higher spin multiplicity corresponds to $4s^2 3d^n$ and the lower multiplicity corresponds to $4s^1 3d^{n+1}$.

To further confirm the qualitative arguments made above we also compare the predicted ordering of the low-lying states to the calculated POL-CI ordering[12] for VH. Figure 2 shows the molecular terms arising out of the V $4s^2 3d^3$ and $4s^1 3d^4$ atomic states (based on Table II and the experimental atomic separations.[19]) The left- and right-hand columns of Fig. 2 show the atomic $4s^2 3d^3$ and $4s^1 3d^4$ states while the center column (labeled "mixed") shows the calculated molecular ordering. Here the $^5\Phi$ mixed energy is fixed at the energy of the $4s^2 3d^3$ ($^5\Phi$) term since no mixing of atomic states is expected for $^5\Phi$ (because only one $^5\Phi$ term arises).

The most noticeable feature of Fig. 2 is a large stabilization of the $^5\Delta$ and $^5\Pi$ states as compared to the atomic $4s^2 3d^3$ separation. For the $^5\Delta$ state this effect is due to admixture of $^5\Delta(21\bar{1})$ terms as above. [Note that we use an abbreviated notation for the $3d$ orbital occupancy here and in Fig. 2, e.g., $^5\Delta(21\bar{1})$ is equivalent to Eq. (5) and $^5\Delta(210\bar{1})$ is equivalent to Eq. (6).] This admixture of $4s^2 3d^3$ and $4s^1 3d^4$ character is associated with a decrease of $0.15 a_0$ in R_e as compared to $^5\Phi$, and is also consistent with the CASSCF/CI population of 3.42 $3d$ electrons (Table I). For $^5\Pi$ the situation is more complex in that there are two major configurational mixing effects. The dominant configuration here is $^5\Pi(20\bar{1})$; however, there is significant admixture of $^5\Pi(21\bar{2})$ and $^5\Pi(210\bar{2})$. The latter configuration coupling mixes $4s^2 3d^3$ and $4s^1 3d^4$ character and is probably responsible for the decrease in R_e by $0.09 a_0$ as compared to $^5\Phi$. Finally, the $^5\Sigma^-$ state shows significant coupling of $^5\Sigma^-(10\bar{1})$ and $^5\Sigma^-(20\bar{2})$ leading to stabilization with respect to $^5\Phi$ but no admixture of $4s^2 3d^3$ and $4s^1 3d^4$ character which is consistent with $^5\Phi$ and $^5\Sigma^-$ having nearly identical R_e values.

III. CALCULATIONAL DETAILS

The TM basis sets start with Wachters (14s 9p 5d) primitive set[21] augmented with Wachters two $4p$ functions, the diffuse d function of Hay,[22] and a set of f polarization functions. The f exponents used were Ti (1.2), V(1.4), Cr(1.6), Mn(1.8), Fe(2.0), Co(2.2), and Ni(2.4). These exponents were selected by linear extrapolation of the optimum CI(SD) values for Fe and Ni.[1,4,5] These values are near the optimum values for a single and double CI when the $3s$ and $3p$ are correlated.[5] Since we did not correlate the transition metal $3s$ and $3p$ electrons a better choice of exponents may have been those optimized for only $3d$ and $4s$ correlation.[3] However, the $4f$ functions are found to be unimportant for the TM hydrides[13] and the $3d$ correlation energy and atomic splitting are somewhat insensitive to the choice of f exponent. Thus, this defect in the f basis is of no serious consequence. This basis set was contracted to [5s 4p 3d1f] using the general contraction feature of BIGGMOLI.[23]

The H basis set starts with the (6s) primitive set of van Duijneveldt[24] with two additional diffuse s functions added in an even tempered manner, while the p functions were selected as a (211) contraction of a four term GTO fit[25] to an STO $2p$ with an exponent of 1.0; (8s 4p)/[5s 3p]. The innermost contracted p function is similar in spatial extent to the usual single p function, while the outer two p functions are diffuse functions

TABLE III. CASSCF wave function for MnH.

Configuration										
6σ	7σ	8σ	9σ	$1\delta_{x^2-y^2}$	$1\delta_{xy}$	$3\pi_x$	$4\pi_x$	$3\pi_y$	$4\pi_y$	Coefficient
2	1	0	1	1	1	1	0	1	0	0.988
0	1	2	1	1	1	1	0	1	0	0.092
2	1	0	1	1	1	1	2	1	0	0.065
2	1	0	1	1	1	1	0	1	2	0.065

appropriate to H^-. This basis set obtains all but ~0.02 eV of the electron affinity (E.A.) of H^-.

In the CASSCF calculations the Ar cores of the TM atoms are kept doubly occupied in all configurations; the active space consists of the orbitals derived from the transition metal 4s, 4p, and 3d orbitals and the H(1s) orbital, i.e., 6σ–9σ, 3π–4π, and 1δ. In the above the 9σ, 3π, and 1δ orbitals are transition metal 3d like, 6σ is the bond pair, 7σ is the $s\bar{s}$ orbital, and 8σ introduces left–right correlation of the bond pair, while 4π introduces angular correlation of the bond pair. Note that at $R = \infty$ 6σ is a transition metal 4s orbital, 7σ is the H(1s) orbital, and 8σ and 4π are transition metal 4p orbitals (near degeneracy effect), while as R decreases the orbitals evolve much as in a 2-1 chemical reaction.[26] Note also that for cases where the $3d\sigma$ orbital is not occupied (TiH and VH) the 9σ orbital is mostly $H(2p\sigma)$ like and there is no occupied $3d\sigma$ like orbital. The 4π orbital is mostly $H(2p\pi)$ like, a result which is consistent with the nature of the 9σ orbital for TiH and VH. Note that the TM hydrides contain a significant component of TM^+H^- character (H population 0.22 for MnH CASSCF CISD wave function).

Because the CASSCF procedure introduces some ambiguities into the calculations (e.g., the 9σ orbital is hydrogen like for TiH but is transition metal $3d\sigma$ like for CrH), it is difficult to obtain a consistent description of the bonding in the TM hydrides at the CASSCF level. Therefore, the CASSCF calculations were followed by CI(SD) calculations. The starting set of reference configurations for these calculations were the GVB configurations:

$$\begin{pmatrix} 6\sigma^2 7\sigma^1 \\ 6\sigma^1 8\sigma^1 7\sigma^1 \\ 8\sigma^2 7\sigma^1 \end{pmatrix} 3d^n \quad \mathrm{TM}(4s^2 3d^n) + \mathrm{H}\,, \tag{8a}$$

$$\begin{pmatrix} 6\sigma^2 \\ 6\sigma^1 8\sigma^1 \\ 8\sigma^2 \end{pmatrix} 3d^{n-1} \quad \mathrm{TM}(4s^1 3d^{n-1}) + \mathrm{H}\,. \tag{8b}$$

Table III shows the configurations in the CASSCF for the $^7\Sigma^+$ state of MnH, a case which is predominately $4s^2 3d^n$ like. Here one sees that the dominant correlation terms are the GVB configurations (8a). For the $^6\Sigma^+$ state of CrH which is derived from $4s^1 3d^5$ the dominant terms in the CASSCF are the GVB configurations (8b). For this reason configurations (8a) were used as reference configurations for TiH and MnH which are predominately $4s^2 3d^n$ like and configurations (8b) were used as reference configurations for CrH which is predominately $4s^1 3d^{n-1}$ like. However, for VH and NiH and for the $^4\Delta$ state of FeH there is a strong admixture of $4s^2 3d^n$ and $4s^1 3d^{n-1}$ character, and more extensive reference lists were used as indicated in Sec. IV.

The CASSCF/CI calculations were carried out with BIGGMOLI[23]-SWEDEN[27] using the NASA Ames CRAY 1S. The calculated R_e, D_e, and ω_e values were obtained via a Dunham analysis of the points near R_e. In those fits in general only three terms are used. Based on a comparison of three and four term fits for NiH we estimate that use of this small number of computed points leads to errors of $\langle 0.01 a_0$ for R_e, $\langle 50$ cm^{-1} for ω_e, and $\langle 0.01$ eV for D_e.

IV. DISCUSSION

A. TiH

Table IV presents the CASSCF and CI energies for the $^4\Phi$ state of TiH, while Table I gives the derived potential curve parameters. The reference configurations for the CI are configurations (8a). Note from Table I that the 3d population is 2.26 which is consistent with using a $4s^2 3d^2$ reference. No experimental information exists for TiH, however the calculated results are compared to the calculated results of Das (D)[11] and Scott and Richards (SR).[6–8] Here one sees that the present results show a shorter bond length and larger binding energy—a result consistent with the higher level of electron correlation included in the present calculation.

B. VH

Table V gives the CASSCF and CI energies for the $^5\Delta$ state of VH obtained using Eq. (8a) as reference configurations. Because of the large amount of $4s^1 3d^4$ character in the CI wave function (see Table I and VI A) more extensive CI calculations were carried out

TABLE IV. Calculated energies for the $^4\Phi$ state of TiH.

R, a_0	CASSCF	CI
20.0	−848.926 21	−848.935 98
4.00	−848.983 19	
3.75	−848.992 04	−849.013 69
3.50	−848.993 85	−849.016 76
3.25	−848.990 61	−849.015 21

TABLE V. Calculated energies for the $^1\Delta$ state of VH.

R, a_0	CASSCF	CI
20.0	−943.404 39	−943.429 86
3.50	−943.469 91	−943.510 13
3.25	−943.469 72	−943.512 16
3.00	−943.463 13	−943.508 35

TABLE VIA. VH extended CI results.

Case	Energy	3d population	% reference
4$A\sigma$, 3 reference	−943.512 16	3.36	92
4$A\sigma$, 5 reference	−943.513 01	3.37	92
5$A\sigma$, 5 reference	−943.513 53	3.39	93
5$A\sigma$, 8 reference	−943.514 34	3.42	94

TABLE VIB. VH 5$A\sigma$, 8 reference CI energies.

R, a_0	E
3.50	−943.512 15
3.25	−943.514 34
3.00	−943.510 62

(Table VI). In Table VI the designation 4$A\sigma$ denotes that there are four active sigma orbitals 6σ–9σ. The 5$A\sigma$ designation denotes a more extensive MCSCF in which a 10σ orbital was added to the active space. The 10σ orbital is mostly 3$d\sigma$ like and is important for describing orbital readjustment effects concomitant with the mixing of Eqs. (5) and (6) in the CI. The reference configurations for the extended CI calculations are given in Table VII. The 3 reference list consists of configurations (8a) while the 5 and 8 reference lists include the remaining configurations in Table VII. The 5 and 8 reference lists were selected based on CI calculations using the 3 reference list with the 4$A\sigma$ and 5$A\sigma$ CASSCF orbitals, respectively. Note that the 5 reference list includes additional correlation of the bond pair, mainly angular correlation involving H(2p), which is not included in the 3 reference list. The 8 reference list differs from the 5 reference list in that single excitations from 7σ into the remaining sigma active orbitals are included.

TABLE VIII. Calculated energies for the $^6\Sigma^+$ state of CrH.

R, a_0	GVB	CI
20.0	−1043.833 14	−1043.906 02
3.50	−1043.883 85	−1043.979 88
3.25	−1043.884 34	−1043.983 20
3.00	−1045.879 99	−1043.981 50

From Table VIA we see that the extended CI calculations lead to results rather similar to the calculations using only Eq. (8a) as a reference set. Calculations using a larger V basis set (14s 11p 6d 2f)/[8s 7p 4d 2f] show a very similar population and this population is only slightly changed by natural orbital iterations. From this we conclude that the strong mixing of d^3 and d^4 observed in the current CASSCF/CI (SD) calculations is converged with respect to basis set and level of correlation.

Finally, Table VIB gives energies obtained at the 5$A\sigma$, 8 reference CI level. The potential curve parameters given in Table I are derived from these energies. We note from Table I that the potential curve parameters obtained here are in good agreement with the calculations of Das[11] and the earlier results of Walch.[10]

C. CrH

For CrH the ground $^6\Sigma^+$ state is predominately $4s^1 3d^5$ like, thus the CASSCF was based on Eq. (8b) (3σ 1π 1δ active space). The CASSCF was followed by a SDCI using Eq. (8b) as references. [Note that the CASSCF in this case has a smaller active space than for the other cases. The smaller active space here omits angular correlation effects; however, these effects are included at the CI(SD) level and these calculations are consistent with those for the other hydrides.] The calculated R_e and ω_e are in reasonable agreement with experiment[28]; the bond length is too long by ~0.04 Å and ω_e is too small by 100 cm^{-1}. The results of the present calculations (Table I and Table VIII) are in good agreement with the results of Das[11]—a not unexpected result given that the MCSCF model used by Das is the same as ours for this particular system, and one expects very little mixing of $4s^2 3d^4$.

D. MnH

Table IX gives the calculated CASSCF and CI energies for MnH. The reference configurations for the CI

TABLE VII. Reference configurations for VH extended CI calculations.

Reference	6σ	7σ	8σ	9σ	10σ	1$\delta_{x^2-y^2}$	1δ_{xy}	3π_x	4π_x	3π_y	4π_y
3	2	1	0	0	0	0	1	1	0	1	0
3	0	1	2	0	0	0	1	1	0	1	0
3	0	1	0	2	0	0	1	1	0	1	0
5	0	1	0	0	0	0	1	1	2	1	0
5	0	1	0	0	0	0	1	1	0	1	2
8	2	0	1	0	0	0	1	1	0	1	0
8	2	0	0	1	0	0	1	1	0	1	0
8	2	0	0	0	1	0	1	1	0	1	0

TABLE IX. Calculated energies for the $^7\Sigma^+$ state of MnH.

R, a_0	CASSCF	CI
20.0	−1150.373 88	−1150.439 99
3.50	−1150.423 84	−1150.501 63
3.25	−1150.423 47	−1150.502 47
3.00	−1150.416 50	−1150.497 02

TABLE X. Calculated energies for the $^6\Delta$ state of FeH.

R, a_0	CASSCF	CI
20.0	−1262.951 01	−1263.052 17
3.50	−1262.999 75	−1263.114 20
3.25	−1263.001 36	−1263.117 16
3.00	−1262.996 84	−1263.114 36

are Eq. (8a) which is consistent with the $3d$ population of 5.06. From Table I one sees that the calculated R_e is ~0.04 Å longer than experiment while the calculated ω_e is 90 cm^{-1} larger than experiment.[28] Comparing our results to Das',[11] we see that his R_e is larger than ours by ~0.07 Å (and in poorer agreement with experiment), and his ω_e is smaller than experiment by ~110 cm^{-1}. Given the longer R_e and smaller ω_e in the calculations of Das it is puzzling to note that his D_e is *larger* than ours. Note that in all other cases Das' binding energies are smaller. We suspect that overestimation of D_e in this case is due to neglect of $4s^2 - 4p^2$ near degeneracy which is more important for the $4s^2 3d^5$ atomic asymptote than for the molecular region. Another puzzling point here is Das' comment that the HF configuration is not dominant for MnH, since we find that in the CASSCF the HF configuration is dominant for all R. (See Table III.)

E. FeH

Table X gives the calculated CASSCF and CI energies for the $^6\Delta$ state of FeH. These calculations were carried out in the same way as the MnH calculations. For FeH more extended calculations were also carried out to examine the question of the separation of the $^6\Delta$ and $^4\Delta$ states of FeH. The $^6\Delta$ state of FeH is dominated by

$$6\sigma^2 7\sigma^1 9\sigma^1 1\delta^1_{x^2-y^2} 1\delta^2_{xy} 3\pi_x^1 3\pi_y^1 , \quad (9)$$

while we find the $^4\Delta$ state is a strong mixture of the quartet coupling of Eq. (9) and

$$6\sigma^2 9\sigma^2 1\delta^1_{x^2-y^2} 1\delta^2_{xy} 3\pi_x^1 3\pi_y^1 , \quad (10)$$

which is best viewed as the $^4\Delta$ configuration arising from $4s^1 3d^7$. In the CASSCF calculations the $^4\Delta$ state has the 7σ and 9σ orbitals mixed, i.e., $7\sigma \cong s\bar{z} + 3d\sigma$ and $9\sigma \cong s\bar{z} - 3d\sigma$. With these orbitals the $^4\Delta$ state has five dominant configurations which are the reference configurations given in Table XI. The dominant configurations for the $^6\Delta$ state on the other hand, also given in Table XI are more clearly defined consisting of Eq. (9) plus left–right and angular correlation of the bond pair.

Table XII gives the calculated energies for the $^6\Delta$ and $^4\Delta$ states of FeH using the reference configurations given in Table XI. Here we find the $^6\Delta$ state is 0.09 eV below $^4\Delta$ at the CI(SD) plus Davidson's correction level of calculation, while the best experimental estimate[29] places $^6\Delta$ ~0.25 eV above $^4\Delta$.

GVB+1+2 calculations with the present basis set for Eqs. (9) and (10) at $R = 20.0a_0$ give a separation of 1.34 eV as compared to the experimental $^5F - {}^5D$ atomic separation of 0.88 eV. Since the $^4\Delta$ state is a strong mixture of $4s^2 3d^6$ and $4s^1 3d^7$ derived terms, one might expect that further improvement in the $^5F - {}^5D$ separation would depress $^4\Delta$ with respect to $^6\Delta$. However, the same CASSCF/CI (SD) calculation with a larger $[6s\,5p\,4d\,1f]$ basis set,[29] which gives a $^5F - {}^5D$ atomic separation of 1.11 eV, leads to the same separation of 0.08 eV with $^6\Delta$ below $^4\Delta$, and the $3d$ population remains the same as with the smaller basis set. This result is consistent with our studies[14] of NiH, where we found a correct mixing of $4s^2 3d^8$ and $4s^1 3d^9$ (as reflected in the bond shortening) at a level of calculation where the separation was still in error by ~0.5 eV.

From Table XII one sees that there is a differential Davidson's correction for the $^4\Delta - {}^6\Delta$ separation of FeH of 0.19 eV (based on $^6\Delta$ at $3.25a_0$ and $^4\Delta$ at $3.00a_0$). This large differential Davidson's correction is consistent with the differential percentage reference in the CI (SD) wave functions (92% for $^4\Delta$ and 95% for $^6\Delta$). Because of the size of the differential Davidson's correction we suspect that the ground state of FeH is $^4\Delta$ (in agreement with experiment) and that the remaining error in our calculated separation is due to a need for

TABLE XI. Reference configurations for FeH extended CI calculations.

	6σ	7σ	8σ	9σ	$1\delta_{x^2-y^2}$	$1\delta_{xy}$	$3\pi_x$	$4\pi_x$	$3\pi_y$	$4\pi_y$
$^6\Delta$	2	1	0	1	1	2	1	0	1	0
	0	1	2	1	1	2	1	0	1	0
	0	1	0	1	1	2	1	2	1	0
	0	1	0	1	1	2	1	0	1	2
$^4\Delta$	2	2	0	0	1	2	1	0	1	0
	2	0	0	2	1	2	1	0	1	0
	2	1	0	1	1	2	1	0	1	0
	0	2	2	0	1	2	1	0	1	0
	1	1	1	1	1	2	1	0	1	0

TABLE XII. Calculated energies for the $^6\Delta$ and $^4\Delta$ states of FeH.

	$^6\Delta$		$^4\Delta$	
R, a_0	CASSCF	CI	CASSCF	CI
20.0	−1262.951 01	−1263.052 17[a]		−1263.003 02[c]
3.50	−1262.999 75	−1263.114 83		
		(−1263.120 69)[b]		
3.25	−1263.001 36	−1263.117 87	−1262.980 74	−1263.105 80
		(−1263.123 74)		(−1263.117 71)
3.00	−1262.996 84	−1263.115 05	−1262.978 61	−1263.107 69
		(−1263.121 09)		(−1263.120 38)
2.75			−1262.968 50	−1263.102 64
				(−1263.116 20)

[a] From Table X using the GVB reference configurations [Eq. (8a)].
[b] Values in parenthesis include Davidson's correction.
[c] From a GVB + 1 + 2 calculation for the $^4\Delta$ state of FeH.

higher excitations in our CI wave function.

From Table I we see that the calculated R_e and ω_e for the $^4\Delta$ state and the calculated R_e for the $^6\Delta$ state are in good agreement with experiment.[30,31] Comparing to other calculated results, Das[11] studied only the $^6\Delta$ state and finds a longer R_e, smaller ω_e, and smaller D_e than in the present calculations. Jaffe[32] carried out an ECP/CI study of the $^6\Delta$ and $^4\Delta$ states of FeH. His results show shorter bond lengths for both states (a result which is believed to be due to defects in the ECP); however the other calculated parameters are in reasonable agreement with the present results.

F. NiH

For NiH the CASSCF calculations converged to a solution somewhat similar to the $^4\Delta$ FeH calculations. The $3d$ population here is ~8.2 for $R = 2.75 a_0$. Attempts to obtain a solution which was dominated by $4s^1 3d^9$ converged to the same result even when started from $4s^1 3d^9$ like GVB vectors. It was found that correlating the $3d\sigma$ orbital which stabilizes $4s^1 3d^9$ with respect to $4s^2 3d^8$ lead to stabilization of the $4s^1 3d^9$ like solution. However, for consistency, calculations were carried out using the $4s^2 3d^8$ like orbitals. The GVB–CI calculations were carried out and the natural orbitals were used in a CI using the reference configurations in Table XIII. This calculation leads to a $3d$ population of ~8.7 indicating strong mixing between $4s^1 3d^9$ and $4s^2 3d^8$ at the CI level. Note that the results here confirm the conclusion reached in the earlier MCSCF/POL-CI studies[14] of NiH that MCSCF leads to incorrect mixing of $4s^2 3d^8$ and $4s^1 3d^9$, and that this defect is corrected at the CI level. Correlating the $3d$ orbitals leads to a $4s^1 3d^9$ like solution as is the case for HF wave functions, while the present CASSCF calculations tend to bias the calculation toward $4s^2 3d^8$.

From Table I we see that the calculated parameters for NiH (derived from the energies given in Table XIV) are in good agreement with experiment.[26] Note that the D_e value is obtained by comparison to a GVB + 1 + 2 calculation for NiH at large R ($4s^1 3d^9$ like solution). This is the most appropriate state to compare it to since the NiH wave function near R_e is mostly $4s^1 3d^9$ like. Note also that the calculated R_e is slightly smaller than experiment, a result that reflects a bias in the present calculations toward $4s^2 3d^8$ like orbitals. By contrast the MCSCF/POL-CI calculations[14] which converged to $4s^1 3d^9$ like orbitals lead to an R_e somewhat longer than experiment, a result which reflects a corresponding bias toward $4s^1 3d^9$ like orbitals.

The present calculations are in good agreement with the CASSCF/CI calculations of Blomberg *et al.*,[15] in spite of the omission of $4f$ functions in the calculations of Ref. 15. This result is consistent with the small importance of $4f$ functions in ScH.[13] By comparison the calculations of Das[11] show an R_e significantly larger than experiment, which we view as indicative of the need for additional atomic correlation. Interestingly the calculations of GWRU[18] which are only two configuration MCSCF but incorporate atomic correlation in a semiempirical way are in good agreement with the present calculations.

TABLE XIII. Reference configurations for NiH CI calculations.

6σ	7σ	8σ	9σ	$1\delta_{x^2-y^2}$	$1\delta_{xy}$	$3\pi_x$	$3\pi_y$
2	0	0	2	2	1	2	2
1	0	1	2	2	1	2	2
0	0	2	2	2	1	2	2
2	0	2	0	2	1	2	2

TABLE XIV. Calculated energies for the $^2\Delta$ state of NiH.

R, a_0	CASSCF	CAS CI[a]	NO/CI[a]
3.25	−1507.376 39	−1507.600 35	−1507.606 47
3.00	−1507.377 79	−1507.610 21	−1507.617 35
2.75	−1507.373 35	−1507.614 40	−1507.620 65
2.50	−1507.359 32	−1507.610 09	−1507.614 40

[a] The asymptotic energy is −1507.517 99 from a GVB + 1 + 2 calculation based on a $4s^1 3d^9$ + H(1s) like GVB solution.

V. CONCLUSIONS

The bonding in the TM hydrides is found to involve strong admixture of terms from the $4s^2 3d^n$ and $4s^1 3d^{n+1}$ states of the TM atoms. The bonding in the $4s^2 3d^n$ state is found to arise by formation of sp hybrids sz

and $s\bar{s}$ where s is $4s-4s$ like and $s\bar{s}$ is $4s-4s$ like. The bond pair involves singlet pairing the s and H(1s) orbitals while the $s\bar{s}$ orbital is singly occupied and hybridized away from the bond pair. The bonding in the $4s^1 3d^{n+1}$ state involves formation of a $4s-$H(1s) bond pair.

By consideration of atomic coupling arguments and interaction of $4s^2 3d^n$ and $4s^1 3d^{n+1}$ derived terms, the ground states of the TM hydrides are predicted to be TiH ($^4\Phi$), VH($^5\Delta$), CrH($^6\Sigma^+$), MnH($^7\Sigma^+$), FeH($^4\Delta$), CoH($^3\Phi$), and NiH($^2\Delta$). All of these systems have been studied by a CASSCF CI (SD) procedure with the exception of CoH. In addition studies have been carried out for the $^6\Delta$ state of FeH.

We find strong mixing of $4s^2 3d^n$ and $4s^1 3d^{n+1}$ for VH and NiH where the $4s^2 3d^n$ and $4s^1 3d^{n+1}$ states are close in energy. TiH, MnH, and FeH ($^6\Delta$) are found to be predominately $4s^2 3d^n$ like, while CrH is found to be predominately $4s^1 3d^{n+1}$ like. These trends are consistent with the ordering of the atomic states.

The calculated R_e and D_e values derived from the CASSCF/CI (SD) potential curves are in good agreement with the available experimental information (no information exists for TiH and VH). Inclusion of atomic correlation leads to significantly better agreement with experiment particularly for R_e. These improvements are related to a more balanced description of the atomic states in the correlated wave functions.

ACKNOWLEDGMENTS

We thank Bjorn Roos and Per Siegbahn for use of their programs. We thank Rich Jaffe for helpful discussions on FeH.

[1] R. L. Martin, Chem. Phys. Lett. **75**, 290 (1980).
[2] T. H. Dunning, Jr., B. H. Botch, and J. F. Harrison, J. Chem. Phys. 72, 3419 (1980).
[3] B. H. Botch, T. H. Dunning, Jr., and J. F. Harrison, J. Chem. Phys. 75, 3466 (1981).
[4] C. W. Bauschlicher, Jr., and S. P. Walch, J. Chem. Phys. **74**, 5922 (1981).
[5] C. W. Bauschlicher, Jr., S. P. Walch, and H. Partridge, J. Chem. Phys. 76, 1033 (1982).
[6] P. R. Scott and W. G. Richards, J. Phys. B 7, 500 (1974); 7, 347 (1974).
[7] P. R. Scott and W. G. Richards, J. Phys. B 7, 1079 (1974).
[8] P. R. Scott and W. G. Richards, J. Chem. Phys. **63**, 1690 (1975).
[9] P. S. Bagus and H. F. Schaefer III, J. Chem. Phys. **58**, 1844 (1973).
[10] G. A. Henderson, G. Das, and A. C. Wahl, J. Chem. Phys. **63**, 2805 (1980).
[11] G. Das, J. Chem. Phys. **74**, 5766 (1981).
[12] S. P. Walch, unpublished results quoted by G. Das in Ref. 11.
[13] C. W. Bauschlicher, Jr. and S. P. Walch, J. Chem. Phys. 76, 4560 (1982).
[14] S. P. Walch and C. W. Bauschlicher, Jr., Chem. Phys. Lett. **86**, 66 (1982).
[15] M. R. A. Blomberg, P. E. M. Siegbahn, and B. J. Roos, Mol. Phys. (in press).
[16] P. S. Bagus and C. Bjorkman, Phys. Rev. A **23**, 461 (1981).
[17] R. Martin (unpublished results).
[18] W. A. Goddard III, S. P. Walch, A. K. Rappe, and T. H. Upton, J. Vac. Sci. Technol. **14**, 416 (1977).
[19] Average of M_J's from C. E. Moore, *Atomic Energy Levels*, Natl. Bur. Stand. (U.S.) Circ. **467** (1949).
[20] S. P. Walch, Ph.D. thesis, California Institute of Technology, 1977.
[21] A. J. H. Wachters, J. Chem. Phys. 66, 4377 (1977).
[22] P. J. Hay, J. Chem. Phys. **66**, 4377 (1977).
[23] R. C. Raffenetti, BIGGMOLI: Program No. 328, Quantum Chemistry Program Exchange, Indiana University, Bloomington, Indiana (1977).
[24] F. B. van Duijneveldt, "Gaussian Basis Sets for the Atoms H–Ne for Use in Molecular Calculations," Research Report RJ 945, IBM, San Jose, California, (1st December, 1971).
[25] R. F. Stewart, J. Chem. Phys. 52, 431 (1970).
[26] S. P. Walch, T. H. Dunning, Jr., R. C. Raffenetti, and F. W. Bobrowicz, J. Chem. Phys. 72, 406 (1980).
[27] SWEDEN is a vectorized SCF-MCSCF-Direct-CI written by P. E. M. Sigbahn, B. Roos, and C. W. Bauschlicher, Jr.
[28] H. P. Huber and G. Herzberg, *Molecular Spectra and Molecular Structure. IV. Constants of Diatomic Molecules* (Van Nostrand Reinhold, New York, 1979).
[29] This basis is a (15*s* 12*p* 6*d* 3*f*) {6*s* 5*p* 4*d* 1*f*} basis set. The primitive *s* and *p* basis sets differ from Wachters' in that the 4*s* and 4*p* functions are triple zeta whereas Wachters' basis is double zeta. The 4*s* functions were optimized for $^5D(s^2d^6)$, while the 4*p* functions were optimized for $^7F(4s^14p^13d^6)$ and the resulting 4*p* functions were mutliplied by 1.5 to make them more suitable for describing $4s^2 \rightarrow 4p^2$ correlation. (The final exponents are $\alpha_{4s}=0.1294$, 0.08287, 0.03789 and $\alpha_{4p}=0.2454$, 0.1249, 0.05307.) The 3*d* basis was contracted to four functions. The 4*f* function is a 3 term GTO fit to an STO with exponent 3.75.
[30] A. E. Stevens, W. C. Lienberger, and C. S. Feigerle (unpublished results).
[31] S. Davis (private communication).
[32] R. Jaffe (unpublished results).

THEORETICAL EVIDENCE SUPPORTING THE $^4\Delta$ GROUND-STATE ASSIGNMENT FOR FeH

Stephen P. WALCH *
Polyatomics Research Institute, 1101 San Antonio Road, Suite 420, Mountain View, California 94043, USA

Received 9 November 1983; in final form 19 December 1983

The results of GVB/MRSD CI calculations for the $^5\Delta$ state of FeH^- are combined with the results of previous CAS SCF/MRSD CI calculations for the $^4\Delta$ and $^6\Delta$ states of FeH to provide theoretical confirmation of the qualitative arguments used by Stevens, Feigerle, and Lineberger to assign the lowest state of FeH as $^4\Delta$. The calculated electron affinity of FeH and the calculated R_e and ω_e for the $^5\Delta$ state of FeH^- are in good agreement with experimental estimates.

Recently Stevens, Feigerle and Lineberger [1] (SFL) have reported photodetachment experiments for FeH^- and MnH^-. For FeH^- the lowest photodetachment transition exhibits a vibrational progression while a second transition which is 0.24 eV higher exhibits no vibrational progression. SFL interpret these experiments using a theoretical model in which FeH^- has the configuration

$$b^2 s\bar{s}^1 3d\sigma^2 3d\delta^3 3d\pi^2 \quad ^5\Delta, \tag{1}$$

where b is a bond pair orbital and $s\bar{s}$ is an sp hybrid directed away from the bond pair [2]. Removing an electron from the above configuration leads to two low-lying FeH neutral states: (i) ionization of the $s\bar{s}$ electron leads to a $^4\Delta$ state with the configuration

$$b^2 3d\sigma^2 3d\delta^3 3d\pi^2 \quad ^4\Delta \tag{2}$$

and (ii) ionization of a $3d\sigma$ electron leads to a $^6\Delta$ state with the configuration

$$b^2 s\bar{s}^1 3d\sigma^1 3d\delta^3 3d\pi^2 \quad ^6\Delta. \tag{3}$$

SFL argue that (i) involves ionizing an antibonding orbital ($s\bar{s}$) and this involves a significant reduction in equilibrium bond length (R_e) while (ii) involves ionizing a non-bonding orbital ($3d\sigma$) and should involve little change in R_e. Thus SFL assign the lower transition with a long vibrational progression to $^4\Delta$ and the upper vertical transition to $^6\Delta$.

* Supported by NASA Grant NCC2-148.

The bond length and vibrational frequency (ω_e) for the $^4\Delta$ state are known directly from experiment [3]. SFL were able to estimate R_e and ω_e for the $^6\Delta$ state of FeH and the $^5\Delta$ state of FeH^- by comparing computed and experimental spectra.

Previously Walch and Bauschlicher (WB) [2] carried out CAS SCF/CI SD calculations for the $^6\Delta$ and $^4\Delta$ states of FeH. In the present paper GVB CI SD calculations are reported for the $^5\Delta$ state of FeH^-. The calculated spectroscopic parameters are compared to experiment in table 1. Here one sees that photodetachment to the $^6\Delta$ state of FeH involves little change in R_e (<0.01 Å) while photodetachment to the $^4\Delta$ state involves a large decrease in R_e (0.12 Å). The calculated R_e and ω_e for the $^6\Delta$ state of the neutral and for the $^5\Delta$ state of FeH^- are in reasonable agreement with the values obtained by SFL. Also the calculated electron affinity (EA) is in good agreement with the value measured by SFL. Thus the present calculations in conjunction with the previous calculations by WB substantiate the assignments of SFL. However the qualitative features of the wavefunctions are different from the simple picture above in that the $^4\Delta$ state of FeH and the $^5\Delta$ state of FeH^- show strong mixing of $3d^6$ and $3d^7$ (see table 1), whereas the analysis of SFL is based on pure $3d^7$ character for these states.

The basis set used for FeH^- is Wachters' (14s9p5d) set [4] augmented with: (i) two diffuse 4s functions selected in an even-tempered fashion, (ii) Wachters'

0 009-2614/84/$ 03.00

Table 1
Calculated CAS SCF/CI results for FeH

State		R_e (Å)	ω_e (cm^{-1})	T_e (eV)	3d population
FeH $^6\Delta$	calc. [2]	1.72	1560	−0.08	6.08
	exp. [1]	1.77 ± 0.05	1550	0.25	
FeH $^4\Delta$	calc. [2]	1.60	1710	0.00	6.26
	exp. [3]	1.63	1680	0.00	
FeH$^-$ $^5\Delta$	calc. a)	1.72	1282	−0.78	6.50
	exp. [1]	1.79 ± 0.03	1300 ± 140	−0.93	

a) Present work. The calculated spectroscopic constants are obtained via a Dunham analysis of the CI plus Davidson's correction energies at 3.00, 3.25, and 3.50a_0. The CI energies at 3.25a_0 are −1263.12366 (−1263.14914) where the value in parentheses includes Davidson's correction.

two 4p functions and one even-tempered 4p diffuse function, (iii) the diffuse 3d function of Hay [5], and (iv) a single set of 4f functions (α_{4f} = 2.0). The resulting basis was contracted using the general contraction feature of BIGGMOLI [6]: (16s12p6d1f)/[7s5p3d1f]. The H basis set was the (8s4p)/[5s3p] basis used in ref. [2]. The calculations were carried out using BIGGMOLI–SWEDEN [‡].

Before considering FeH$^-$, we first consider the calculated EA for the Fe atom as a function of basis set and level of electron correlation (table 2). Two different types of CI calculations were carried out. The MRSD CI has as reference configurations the SCF configutation for the $4s^1 3d^7$ state of Fe and the SCF plus three components of the $4s^2 \rightarrow 4p^2$ near degeneracy for the $4s^2 3d^7$ configuration of Fe$^-$. All single and double excitations from the above configurations are included in the CI. The core–valence CI (CV CI) [7] has the same set of reference configurations but allows only a single electron outside the $3d^7$ configuration. The qualitative idea is that the major differential correlation between the $4s^2 3d^7$ and $4s^1 3d^7$ states includes the valence correlation effects due to the 4s electrons and the core–valence correlation effects between the 4s and 3d electrons. The intrapair 3d correlation, on the other hand, remains relatively constant between the two states since they have the same number of 3d electrons. This expectation is substantiated by the results in table 2 where one sees that the CV CI result is in reasonable agreement with the MRSD + Davidson's correction [8] result. The [7s5p3d1f] basis set is the same basis set used for FeH$^-$, while the [7s5p4d2f] basis uses a more flexible [4d] contraction and replaces the single set of 4f functions by a (3)/[2] 4f basis based on a three-term fit [9] to a Slater 4f with exponent 2.25. This exponent was optimized for the $4s^1 3d^7$ state of the Fe atom at the CV CI level. From table 2 one sees that at the CV CI level the smaller basis set is within 0.04 eV of the larger basis set result for the EA.

Table 2
Calculation of electron affinity for Fe

Basis set	Method	Electron affinity a)
[7s5p3d1f]	CV CI	0.72
	MRSD	0.65 (0.78) b)
[7s5p4d2f]	CV CI	0.76
	exp. c)	1.00

a) $4s^2 3d^7/4s^1 3d^7$.
b) Value in parentheses includes Davidson's correction.
c) Extrapolated based on the error for CV CI for Cu and Ni.

No experimental value exists for the EA of Fe atom. The EA reported by Hotop and Lineberger [10], 0.25 eV, is based on SCF calculations plus an estimate of correlation effects. A more reliable estimate may be obtained by noting that CV CI with large basis sets (equivalent to the larger basis set used here) underestimates the EA of Cu [11] and Ni [12] by 0.23 and 0.24 eV, respectively. Assuming the same error for the EA of Fe leads to 1.00 eV with respect

‡ SWEDEN is a vectorized SCF MC SCF direct CI written by P.E.M. Siegbahn, B. Roos and C.W. Bauschlicher Jr.

Table 3
Reference configurations for FeH CI calculations

	6σ	7σ	8σ	9σ	$1\delta_{x^2-y^2}$	$1\delta_{xy}$	$3\pi_x$	$4\pi_x$	$3\pi_y$	$4\pi_y$
FeH $^6\Delta$	2	1	0	1	1	2	1	0	1	0
	0	1	2	1	1	2	1	0	1	0
	0	1	0	1	1	2	1	2	1	0
	0	1	0	1	1	2	1	0	1	2
FeH $^4\Delta$	2	2	0	0	1	2	1	0	1	0
	2	0	0	2	1	2	1	0	1	0
	2	1	0	1	1	2	1	0	1	0
	0	2	2	0	1	2	1	0	1	0
	1	1	1	1	1	2	1	0	1	0
FeH^- $^5\Delta$	2	1	0	2	2	1	1	0	1	0
	0	1	2	2	2	1	1	0	1	0
	2	1	1	1	2	1	1	0	1	0
	2	2	0	1	2	1	1	0	1	0

to $4s^1 3d^7$ or 0.12 eV with respect to $4s^2 3d^6$. For the H atom the basis set used here leads to an error of ≈0.02 eV in the EA.

The calculations for FeH^- used a GVB wavefunction to define the orbitals. this calculation was followed by multireference singles and doubles CI (MRSD CI). Given the size of the CI calculations the use of GVB orbitals for FeH^- as compared to CAS SCF orbitals for FeH [2] is expected to be of little importance. In the GVB MRSD CI calculations the Ar cores of the transition metal atoms are kept doubly occupied in all configurations; the active space consists of the orbitals derived from the transition metal 4s, 4pσ, and 3d orbitals and the H(1s) orbital, i.e. $6\sigma-9\sigma$, 3π, and 1δ. In the above the 9σ, 3π, and 1δ orbitals are transition metal 3d like, 6σ is the bond pair, 7σ is the $s\bar{s}$ orbital, and 8σ introduces left–right correlation of the bond pair. Table 3 gives the reference configurations which were used in the MRSD CI for the $^5\Delta$ state of FeH^-. The GVB wavefunction [13] includes the first two configurations in table 3. The first configuration for FeH^- is the SCF configuration which corresponds to eq. (1), while the second configuration introduces left–right correlation of the bond pair. The remaining two configurations correspond to $3d^6$ components of the wavefunction which are found to be sufficiently important that they are included as reference configurations in the MRSD CI.

The molecular constants given in table 1 were obtained via a Dunham analysis of the CI SD plus Davidson's correction energies. As noted in ref. [2] since only three computed points are used in the Dunham analysis, there may be small uncertainties introduced in the derived spectroscopic parameters. These errors are estimated to be <0.01 Å for R_e and 50 cm^{-1} for ω_e.

The computed FeH EA is 0.43 eV. These systems have large Davidson's corrections: 0.69, 0.35, and 0.16 eV for FeH^- $^5\Delta$, FeH $^4\Delta$, and FeH $^6\Delta$, respectively. These large Davidson's corrections correlate with the % reference in the CI wavefunctions: 88, 92, and 95% for $^5\Delta$, $^4\Delta$, and $^6\Delta$, respectively. Including the differential Davidson's correction leads to 0.78 eV as our best estimate of the EA of FeH. This value is 0.15 eV smaller than experiment. This result is somewhat better than might be expected based on the calculated Fe atom EA, but is consistent with the population analysis which indicates a large amount of H^- character. Thus the error in the FeH EA may be intermediate between the errors for the EAs of the Fe and H atoms.

We conclude that the present calculations in conjunction with the previous results of WB substantiate SFL's assignment of $^4\Delta$ as the lowest state of FeH with $^6\Delta$ 0.25 eV higher. (Calculations [2] still show the $^6\Delta$ state 0.08 eV below $^4\Delta$, i.e. an error of 0.33 eV in the $^4\Delta-^6\Delta$ separation.) The key feature here is that photodetachment from the $^5\Delta$ state of FeH^- to give the $^6\Delta$ state of FeH is calculated to lead to little change in R_e (<0.01 Å) while photodetachment

to the $^4\Delta$ state of FeH leads to a large decrease in R_e (0.12 Å). Thus the calculations are in agreement with observation of a vibrational progression for photodetachment to $^4\Delta$ but no vibrational progression for photodetachment to $^6\Delta$ as predicted by SFL based on a simple theoretical model. However the qualitative description of the system is more complex than the simple model adopted by SFL in that the $^4\Delta$ state of FeH and the $^5\Delta$ state of FeH^- show strong mixing of $3d^6$ and $3d^7$ character whereas the analysis of SFL is based on pure $3d^7$ character for these states.

The calculated R_e and ω_e values for the $^4\Delta$ state of FeH are in good agreement with the values measured by Davis [3] while the calculated R_e and ω_e values for the $^6\Delta$ state of FeH and the $^5\Delta$ state of FeH^- are in reasonable agreement with the values obtained by SFL from comparison of calculated and experimental spectra. Finally the calculated EA of FeH^- is in reasonable agreement with the value reported by SFL.

References

[1] A.E. Stevens, C.S. Feigerle and W.C. Lineberger, J. Chem. Phys. 78 (1983) 5420.
[2] S.P. Walch and C.W. Bauschlicher Jr., J. Chem. Phys. 78 (1983) 4597.
[3] S. Davis, unpublished results quoted in ref. [1].
[4] A.J.H. Wachters, J. Chem. Phys. 66 (1977) 4377.
[5] P.J. Hay, J. Chem. Phys. 66 (1977) 4377.
[6] R.C. Raffenetti, BIGGMOL1, Program No. 328, Quantum Chemistry Program Exchange, Indiana University, Bloomington, Indiana (1977).
[7] H. Partridge, C.W. Bauschlicher Jr., S.P. Walch and B. Liu, J. Chem. Phys. 79 (1983) 1866.
[8] S.R. Langhoff and E.R. Davidson, Intern. J. Quantum Chem. 8 (1974) 61.
[9] R.F. Stewart, J. Chem. Phys. 52 (1970) 431.
[10] H. Hotop and W.C. Lineberger, J. Phys. Chem. Ref. Data 4 (1975) 539.
[11] C.W. Bauschlicher Jr., S.P. Walch and H. Partridge, Chem. Phys. Letters 103 (1983) 291.
[12] S.P. Walch, unpublished.
[13] W.A. Goddard III, T.H. Dunning Jr., W.J. Hunt and P.J. Hay, Accounts Chem. Res. 6 (1973) 368.

CAS SCF CI CALCULATIONS FOR THE $^3\Sigma_g^-$, $^1\Sigma_g^+$, $^3\Sigma_u^+$, AND $^5\Delta_u$ STATES OF Sc_2

Stephen P. WALCH and Charles W. BAUSCHLICHER Jr.
Polyatomics Research Institute, 1101 San Antonio Road, Suite 420, Mountain View, California 94043, USA

Received 14 July 1982; in final form 19 October 1982

CAS SCF CI(SD) calculations have been carried out for the $^3\Sigma_g^-$, $^1\Sigma_g^+$, $^3\Sigma_u^+$, and $^5\Delta_u$ states of Sc_2 using large gaussian basis sets. The $^3\Sigma_g^-$, $^1\Sigma_g^+$, and $^3\Sigma_u^+$ states arise from the $^2D(4s^23d^1) + {}^2D(4s^23d^1)$ limit of Sc_2 and are found to be only weakly bound ($D_e \approx 0.06$ eV and $R_e \approx 8.0a_0$). The $^5\Delta_u$ state arises from the $^2D(4s^23d^1) + {}^4F(4s^13d^14p^1)$ atomic limit. This state is found to be strongly bound relative to its limits ($D_e \approx 0.8$ eV and $R_e \approx 7.0a_0$).

1. Introduction

Recently the Sc_2 molecule has been the subject of considerable theoretical study [1,2]. The interest in this system arises because of the relevance of metal metal bonds to problems in materials science and because theoretical studies find only weakly bound states (at least out of the lowest $^2D(4s^23d^1) + {}^2D(4s^23d^1)$ atomic limit) for Sc_2 in contrast to mass spectrometric experiments [3] which had been interpreted to indicate strong bonding.

Das [1] has carried out an MC SCF study of the singlet and triplet states arising out of the $^2D(4s^23d^1) + {}^2D(4s^23d^1)$ and the $^2D(4s^23d^1) + {}^4F(4s^13d^2)$ asymptotes of Sc_2 using a Slater basis set in conjunction with a pseudopotential. For the $^1\Sigma_g^+$ state of Sc_2 Das finds a D_e of ≈ 4 kcal/mole and an R_e of $\approx 9.5a_0$ which he attributes to van der Waals terms arising primarily out of the $4s^2 \rightarrow 4p^2$ near-degeneracy effect for the $^2D(4s^23d^1)$ state of Sc. However, as Das points out, by making choices for R_e and the degeneracy factors consistent with the calculations, the mass spectrometric experiments are consistent with a binding energy in the range of 3–5 kcal/mole. Das also considered the possibility of bound states arising from the $^2D + {}^4F$ limit but found no significant binding at least for singlet and triplet states (quintet states also arise from this limit but were not considered).

Wood, Doran, Hillier and Guest (WDHG) [2] also carried out MC SCF CI calculations using a small gaussian basis set. They concluded that the lowest state was $^5\Sigma_u^-$ arising from the $^2D + {}^4F$ asymptote. Their calculations showed a binding energy of 1.12 eV with respect to $^2D + {}^4F$ and 0.55 eV with respect $^2D + {}^2D$. However, due to basis set deficiencies they find a $^4F - {}^2D$ atomic separation of 0.57 eV compared to an experimental separation of 1.43 eV. Correcting for the error in the asymptotic separation the $^5\Sigma_u^-$ state is unbound by 0.31 eV with respect to $^2D + {}^2D$ and it does not appear that $^5\Sigma_u^-$ is the ground state of Sc_2 as suggested by WDHG.

The present calculations were undertaken to determine (i) the nature of the bonding and the magnitude of the binding energy for states arising out of the $^2D(4s^23d^1) + {}^2D(4s^23d^1)$ asymptote, and (ii) the nature of the bonding arising out of the $^2D(4s^23d^1) + {}^4F(4s^13d^2$ or $4s^14p^13d^1)$ atomic limit. The calculations reported here are more extensive than those of Das or WDHG and involve extensive MC SCF or CAS SCF followed by CI(SD) using large gaussian basis sets. In agreement with Das we find that the states arising out of the $^2D + {}^2D$ limit are weakly bound, however we use the interacting correlated fragments (ICF) method [4] to more accurately determine the binding energy. We have also investigated a $^5\Delta_u$ state arising out of the $^2D(4s^23d^1) + {}^4F(4s^14p^13d^1)$ atomic limit. Here we find a binding energy relative to the limits above of ≈ 0.8 eV at an R_e of $\approx 7.0a_0$. We also estimate a binding energy relative to the corresponding limit of $\geqslant 0.5$ eV for

0 009-2614/83/0000–0000/$ 03.00

the state arising from $^2D + {}^4F(4s^1 3d^2)$. For Sc_2 this latter limit is 1.43 eV above $^2D + {}^2D$ and this state does not cross the states arising out of $^2D + {}^2D$. However, we find similar states for V_2 and it appears that in the case of V_2 the lowest bond state is of this character [5] and thus this state of Sc_2 is relevant to bonding in the lowest states of other transition metal dimers.

2. Calculational details

The Sc basis set starts with the Wachters (14s9p5d) primitive set [6] augmented with Wachters' two additional 4p functions, the diffuse d function of Hay [7], and a set of f polarization functions ($\alpha = 1.4$). Two different contracted basis sets were constructed from this primitive set. Basis set I was contracted in a segmented fashion for use with MOLECULE [8]. The contraction scheme used here was contraction 3 of table VI of ref. [6]. This contraction was used for the s and p functions, while the d functions were contracted (3111). In this basis set the f functions were omitted and the 4p functions were scaled by $(1.5)^{1/2}$. Basis set I was used for the CAS SCF calculations. The final basis is (14s11p6d)/[8s6p4d]. Basis set II was generally contracted for use with BIGGMOLI [9] resulting in a (14s11p6d1f)/[6s6p3d1f] contracted set. Here the 4p functions were left unscaled. This larger basis set was used in the ICF calculations.

The CAS SCF CI calculations were carried out with MOLECULE [8]–SWEDEN [10] using the NASA Ames CRAY 1S. The ICF calculations were carried out with BIGGMOLI [9]–noname [11] using the NASA Ames CDC 7600.

In the calculations the 18-electron Ar cores were kept doubly occupied in all configurations. In the CAS SCF calculations these orbitals were optimized at the CAS SCF level, while in the calculations using noname the core orbitals were obtained from a HF calculation on the $^3\Sigma_u^+$ state of Sc_2.

3. Discussion

The low-lying states of the Sc atom are the $^2D(4s^2 3d^1)$ state which is the ground state, the $^4F(4s^1 3d^2)$ state which is at 1.43 eV, and the $^4F(4s^1 4p^1 3d^1)$ state which is at 1.96 eV [12] (the

Table 1
Reference configurations for the CI(SD) calculation

State	Configuration															
	g			u			$3d\pi_x$		$3d\pi_y$		$3d\delta_{xy}$		$3d\delta_{x^2-y^2}$	
	4s	3dσ	4pσ	4s	3dσ	4pσ	g	u	g	u	g	u	g	u
$^5\Delta_u$	2	1	1	1	0	0	0	0	0	0	1	0	0	0
	1	0	1	2	1	0	0	0	0	0	1	0	0	0
	1	1	0	2	0	1	0	0	0	0	1	0	0	0
	2	0	0	1	1	1	0	0	0	0	1	0	0	0
	1	1	1	2	0	0	0	0	0	0	0	1	0	0
	2	0	1	1	1	0	0	0	0	0	0	1	0	0
	2	1	0	1	0	1	0	0	0	0	0	1	0	0
	1	0	0	2	1	1	0	0	0	0	0	1	0	0
	2	1	0	1	1	0	0	0	0	0	0	1	0	0
	1	1	0	2	1	0	0	0	0	0	1	0	0	0
$^3\Sigma_u^+$	2	1	0	2	1	0	0	0	0	0	0	0	0	0
$^1\Sigma_g^+$	2	2	0	2	0	0	0	0	0	0	0	0	0	0
	2	0	0	2	2	0	0	0	0	0	0	0	0	0
$^3\Sigma_g^-$	2	0	0	2	0	0	1	0	1	0	0	0	0	0
	2	0	0	2	0	0	0	1	0	1	0	0	0	0

energy levels are averaged over the m_j values). As indicated earlier the present calculations concentrate on states arising out of the $^2D + {}^2D$ and $^2D + {}^4F$ limits. In these calculations we include the 4s, 4p, and 3d electrons in the valence space, thus the $4s^2 \rightarrow 4p^2$ near degeneracy [13] which is important for the ^2D state is included at the MC SCF level. Correlation of the 3d orbitals on the other hand is treated at the CI level.

Table 1 shows the dominant configurations for the $^3\Sigma_g^-$, $^1\Sigma_g^+$, $^3\Sigma_u^+$, and $^5\Delta_u$ states which were considered here. The reference configurations in table 1 are the dominant configurations at all R as derived from small CI calculations. These configurations may also be understood by considering the degeneracies which occur at large R (due to the degeneracy of the corresponding g and u orbitals at large R. The $^3\Sigma_u^+$ state requires only one reference configuration, the $^1\Sigma_g^+$ and $^3\Sigma_g^-$ states require two reference configurations, and the $^5\Delta_u$ state requires eight configurations to dissociate to $^2D(4s^2 3d^1) + {}^4F(4s^2 3d^1 4p^1)$. The remaining two $^5\Delta_u$ configurations describe the $^5\Delta_u$ state arising from $^2D(4s^2 3d^1) + {}^4F(4s^1 3d^2)$.

In order to keep the CAS SCF calculations of reasonable size, restrictions were placed on the orbital occupancies as indicated in table 2. These restrictions arise by noting the number of sigma electrons associated with each state and allowing up to double excitations from the sigma block to the pi block. These excitations correspond to $4s^2 \rightarrow 4p\pi^2$ atomic excitations. Note that for the $^5\Delta_u$ state an additional restriction that the sigma plus pi blocks contain five electrons could have been imposed. The CAS SCF calculations in each case were followed by CI(SD) calculations from the reference configurations in table 1.

Table 2
Constraints on orbital occupancies for the CAS SCF calculations

State	Constraint	Number of configurations
$^5\Delta_u$	sigma block 3–5 electrons	5430
$^3\Sigma_u^+$	sigma block 4–6 electrons sigma + pi block 6 electrons	651
$^3\Sigma_g^-$	sigma block 2–4 electrons sigma + pi block 6 electrons	2520

The calculated energies for the CAS SCF CI(SD) calculations are given in table 3, while fig. 1 shows the calculated potential curves [CAS SCF CI(SD) calculations] for the $^3\Sigma_g^-$, $^1\Sigma_g^+$, $^3\Sigma_u^+$, and $^5\Delta_u$ state. Qualitatively the $^1\Sigma_g^+$ and $^3\Sigma_u^+$ states arise from $^2D(4s^2 3d\sigma^1) + {}^2D(4s^2 3d\sigma^1)$ with singlet and triplet pairing of the $3d\sigma$ orbitals, while the $^3\Sigma_g^-$ state arises from $^2D(4s^2 3d\pi^1) + {}^2D(4s^2 3d\pi^1)$ and the $^5\Delta_u$ state arises out of the $^2D(4s^2 3d\sigma^1) + {}^4F(4s^1 4p\sigma^1 3d\delta^1)$ limit.

Concentrating first on the states which arise out of the $^2D + {}^2D$ limit, the basic feature of the calculated curves is very weak binding at large R ($\approx 8.0\, a_0$) and repulsive behavior at smaller R. The weak binding at large R appears to arise from the $4s^2 \rightarrow 4p^2$ near degeneracy, i.e. $4s_\xi \rightarrow 4p_\zeta \times 4s_\tau \rightarrow 4p_\tau$. The binding energy at the CI level for $R = 8.0\, a_0$ is ≈ 0.045 eV for the $^1\Sigma_g^+$ state, ≈ 0.045 eV for the $^3\Sigma_g^-$ state, and ≈ 0.029 eV for the $^3\Sigma_u^+$ state. Note that the CAS SCF curves are repulsive at all R. Note also that in the van der Waals region (i.e. $\geq 8.0\, a_0$) the states arising from the various occupancies of the 3d electrons are very close in energy. However, at small R the 3d orbital occupancies do split the curves significantly. At small R one sees that $^1\Sigma_g^+$ is significantly below $^3\Sigma_u^+$ indicating some $3d\sigma - 3d\sigma$ bonding character. However it appears that the repulsion between the $4s^2$ pairs becomes large before sufficient $3d\sigma - 3d\sigma$ overlap is obtained to stabilize this state. Given that we are in the small overlap region it appeared likely that a one-electron bond which varies with distance like S would be more favorable than a two-electron bond which varies with distance like S^2. The $^3\Sigma_g^-$ state may be thought of as having two one-electron π bonds and indeed at small R this state drops below $^1\Sigma_g^+$ although $^1\Sigma_g^+$ and $^3\Sigma_g^-$ are nearly degenerate at R values near the van der Waals minimum.

Looking now at the $^5\Delta_u$ state, the bonding here arises basically out of the $4s^2 + 4s^1$ interaction. Based on our studies of the transition metal hydrides [14] we expect this to be an attractive interaction. The reason for this attractive interaction is the presence of the low-lying $4s^1 4p^1 3d^n$ states of the transition metal atom (e.g. in Sc $4s^1 4p^1 3d^1$ is at 1.96 eV). Interaction of $4s^2 3d^n$ and $4s^1 3d^n 4p^1$ leads to the formation of sp hybrids one of which has the character s + z denoted by sz and the other of which has the character s − z

Table 3
Calculated CAS CI(SD) energies for various states of Sc_2 [a]

State		R = 6.0	R = 6.5	R = 7.0	R = 7.5	R = 8.0	R = 100.0
$2\,^5\Delta_u$	CAS [b]	−0.36792	−0.37342	−0.37616	−0.36977	−0.36927	−0.36125
	CI						
$^5\Delta_u$	CAS	−0.43128	−0.43829	−0.43943	−0.43727	−0.43346	−0.41337
	CI	−0.44667	−0.45304	−0.45344	−0.45071	−0.44652	−0.42288
$^3\Sigma_u^+$	CAS	−0.44923		−0.46732		−0.47295	−0.47595
	CI	−0.46754		−0.48270		−0.48575	−0.48466
$^1\Sigma_g^+$	CAS [c]						
	CI	−0.47578		−0.48488		−0.48632	−0.48463
$^3\Sigma_g^-$	CAS	−0.46023		−0.47010		−0.47346	
	CI	−0.47934		−0.48514		−0.48594	

a) In hartree relative to −1519.0.
b) Higher root from the $^5\Delta_u$ CAS calculation.
c) $^3\Sigma_u^+$ vectors were used for the CI.

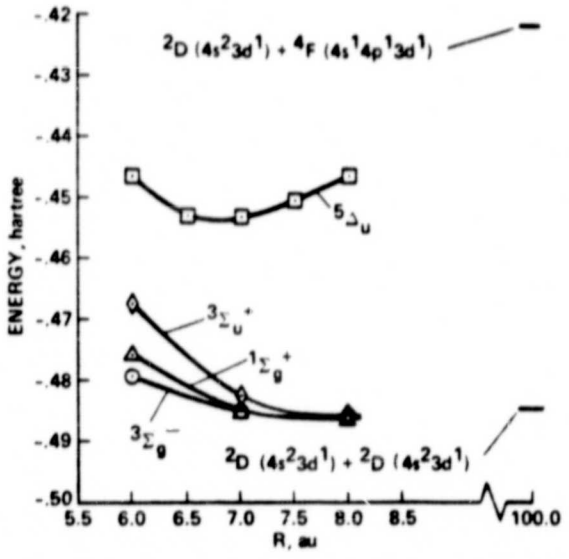

Fig. 1. Potential energy curves for the low-lying states of Sc_2 from CAS SCF CI (SD) calculations. The locations of the $^2D + {}^2D$ and $^2D + {}^4F(4s^14p^13d^1)$ asymptotes are indicated.

denoted by $s\bar{z}$. This leads in the case of the transition metal hydride to an sz–H(1s) bond and a singly occupied $s\bar{z}$ orbital, and in the case of the transition metal dimers to states which may be represented by the following structures:

In the case of the $^5\Delta_u$ state the remaining electrons are in $3d\sigma$, $4p\sigma$, $3d\delta_{xy}$ orbitals which are orthogonal to the bond orbitals and therefore the high spin (i.e. quintet state) is favored.

From fig. 1 one sees that the $^5\Delta_u$ state is bound by ≈ 0.8 eV with respect to $^2D(4s^23d^1) + {}^4F(4s^14p^13d^1)$. The atomic asymptote here is calculated to be at 1.68 eV (1.96 eV experimental). Note that experimentally the $^4F(4s^13d^2)$ state is below the $^4F(4s^14p^13d^1)$ state, while in the calculations the $^4F(4s^14p^13d^1)$ state is lower at both the CAS SCF and CI levels. This results from the larger 3d correlation [15] in the $^4F(4s^13d^2)$ state. Since 3d correlation is not included in the CAS SCF calculations the $^4F(4s^14p^13d^1)$ state is lower at the CAS SCF level and the resulting orbital bias makes this state also at the CI level. This problem makes it difficult to study the corresponding $4s^13d^2$ derived state. However, this state is observed as a higher root in the CAS SCF ($2\,^5\Delta_g$ state in table 3) and using these CI energies the binding energy is predicted to be ≤0.3 eV smaller for the $^5\Delta_g$ state derived from $^2D + {}^4F(4s^13d^2)$ than for the $^5\Delta_g$ state derived from $^2D + {}^4F(4s^14p^13d^1)$. Thus we predict a D_e of ≥ 0.5 eV for the $^5\Delta_g$ state derived from $^2D + {}^4F(4s^13d^2)$. Assuming this and noting that the $4s^13d^{n+1} - 4s^23d^n$ separations for Ti and V are 0.81 and 0.25 eV, res-

pectively [12], we predict that the mixed state will be unbound by $\leqslant 0.3$ eV with respect to the $4s^2 3d^n + 4s^2 3d^n$ limit for Ti_2 and bound by $\geqslant 0.25$ eV for the same limit in V_2. Indeed the lowest state in V_2 is found to arise from this atomic limit [5]. At the other end of the row the mixed states are expected to be important for Fe_2 and Co_2.

Comparing to WDHG, their calculations show a deeper well and shorter R_e for the $^5\Sigma_u^-$ state (R_e = 4.86 a_0 and D_e = 1.12 eV) than do our calculations for the $^5\Delta_u$ state ($R_e \approx 7.0\,a_0$ and $D_e \approx 0.8$ eV). We have also studied states of $^5\Sigma_u^-$ symmetry at the MC SCF POL CI level [16] and find two states, one of which is derived from $^2D(4s^2 3d\pi^1) + {}^4F(4s^1 4p\sigma^1 3d\pi^1)$, and the other of which is derived from $^2D(4s^2 3d\delta^1) + {}^4F(4s^1 4p\sigma^1 3d\delta^1)$. Both states are bound by ≈ 0.8 eV with the first state having an R_e of $\approx 6.5\,a_0$ and the second state having an R_e of $\approx 7.0\,a_0$. It is not clear why the results of WDHG are so different from ours. We do note however that their total energies for Sc_2 are more than 3.0 hartree more positive than ours, and suspect that some of the difference may arise from basis set deficiencies in the calculations of WDHG (e.g. basis set superposition error).

Now we consider the calculation of the binding energy of the states arising out of the $^2D(4s^2 3d^1) + {}^2D(4s^2 3d^1)$ limit. In these calculations we used basis set II. The calculations consisted of MC SCF followed by POL CI [17] and ICF [4] calculations. The ICF method has been shown to lead to reliable binding energies for weakly bound systems, e.g. Be_2 [4]. Since the minimum in the van der Waals binding curve for Sc_2 occurs at $R > 8.0\,a_0$ and the 3d interactions are small at this distance, we arbitrarily studied the $^3\Sigma_u^+$ and $^1\Sigma_g^+$ states which arise from $4s^2 3d\sigma^1 + 4s^2 3d\sigma^1$ (see table 4).

In these calculations the orbitals were obtained from MC SCF calculations with the 4s, 4p and 3dσ in the valence space. The MC SCF configurations consisted of all single and double excitations within the valence space from the reference configurations in table 1 (one for $^3\Sigma_u^+$ and two for $^1\Sigma_g^+$). These MC SCF calculations were then followed by CI. The POL CI calculations include single and double excitations from the reference configurations but with no more than one electron outside the valence space. To approximate the ICF method the orbitals were localized using the transformation

Table 4
Calculated MC SCF POL CI energies for the $^3\Sigma_u^+$ and $^1\Sigma_u^+$ states of Sc_2 [a]

R	MC SCF		POL CI	
	$^3\Sigma_u^+$	$^1\Sigma_g^+$	$^3\Sigma_u^+$	$^1\Sigma_g^+$
20.0	−0.50699	−0.50699	−0.50833	−0.50830
10.0		−0.50679		−0.50935
9.0		−0.50614		−0.50974
8.0	−0.50390	−0.50443	−0.50934	−0.50983
7.5		−0.50287		−0.50954
7.0	−0.49815	−0.50027		−0.50839
6.0		−0.48773		−0.49896

[a] In hartree relative to −1519.0.

$\phi_\xi = 2^{-1/2}\phi_g + 2^{-1/2}\phi_u$, $\phi_\tau = 2^{-1/2}\phi_g - 2^{-1/2}\phi_u$,

and in addition to the POL CI list configurations of the form

$\phi_\xi \to v \times \phi_\tau \to v$,

which allows two electrons into the virtuals were also included. (Note that this calculation was carried out for the $^3\Sigma_u^+$ state since for this state the energy is invariant to the transformation given above.) From table 5 we see that the ICF method gives a binding energy of 0.046 eV (1.1 kcal/mole) while the POL CI method leads to 0.041 eV (for the [6s6p3d1f] basis set). Combining this result with the POL CI estimate of the separation between $^3\Sigma_u^+$ and $^1\Sigma_g^+$ leads to an estimated binding energy of 0.061 eV (1.4 kcal/mole) for the $^3\Sigma_g^-$ or $^1\Sigma_g^+$ state of Sc_2.

Das using an MC SCF model obtains a D_e of ≈ 4 kcal/mole, whereas we obtain no binding at the

Table 5
Calculated MC SCF CI energies for the $^3\Sigma_u^+$ state of Sc_2

R	MC SCF POL CI		MC SCF ICF	
	[6s6p3d]	[6s6p3d1f]	[6s6p3d]	[6s6p3d1f]
20.0	−0.50833 h	−0.50947	−0.50835	−0.50952
	0.000 eV	0.000	0.000	0.000
8.0	−0.50934	−0.51099	−0.51000	−0.51120
	−0.027	−0.041	−0.045	−0.046

[a] In hartree relative to −1519.0.

CAS SCF level. Das' MC SCF differs from ours in that he includes only the dispersion terms $4s_i \rightarrow 4p_i \times 4s_j \rightarrow 4p_j$ while we include all valence configurations among the 4s, 4p, and 3d orbitals. Including these additional terms tends to decrease the importance of the dispersion terms and we see a repulsive curve at the CAS SCF level but obtain a D_e of 1.4 kcal/mole at the ICF level. We suspect that Das' MC SCF potential curve is too attractive, although his conclusion that the experimental results may be reinterpreted in terms of a weak bonding model remains valid.

4. Conclusions

We have studied the $^3\Sigma_g^-$, $^1\Sigma_g^+$, $^3\Sigma_u^+$, and $^5\Delta_u$ states of Sc_2 using CAS SCF CI(SD) wavefunctions in a large gaussian basis set. We find that the states arising out of the $^2D(4s^2 3d^1) + {}^2D(4s^2 3d^1)$ limit show only weak bonding (≈ 0.06 eV at $R \approx 8.0\, a_0$). At this distance 3d electrons are only weakly coupled and the bonding appears to be largely of the van der Waals type arising out of the $4s^2 \rightarrow 4p^2$ near degeneracy.

The $^5\Delta_u$ state which arises out of the $^2D(4s^2 3d^1) + {}^4F(4s^1 4p^1 3d^1)$ limit is found to be strongly bound with respect to $^2D + {}^4F(4s^1 4p^1 3d^1)$ (≈ 0.8 eV at $R \approx 7.0\, a_0$). The bonding in this state is a result of interaction between the 4s orbital of the $4s^1 3d^1 4p^1$ configuration and sp hybrids arising out of the $4s^2 3d^1$ and $4s^1 3d^1 4p^1$ states. States arising out of $^2D(4s^2 3d^1) + {}^4F(4s^1 3d^2)$ are predicted to be bound by $\lesssim 0.3$ eV less with respect to $^2D + {}^4F(4s^1 3d^2)$. While this atomic asymptote is too high (1.43 eV) in Sc_2 for this state to drop below the $^2D(4s^2 3d^1) + {}^2D(4s^2 3d^1)$ asymptote, for V_2 the corresponding asymptote is at 0.25 eV leading to states from this mixed asymptote being the lowest state. WDHG report a significantly shorter R_e (4.86 a_0) and somewhat deeper D_e (1.12 eV) for a $^5\Sigma_u^-$ state. However, our calculations indicate similar results for $^5\Sigma_u^-$ and $^5\Delta_u$. We suspect that the differences between our results and those of WDHG are at least partly due to basis set deficiencies in the calculations of WDHG.

We have also studied the binding energy of the $^3\Sigma_u^+$ state using the ICF method. This leads to the estimate of $D_e = 0.046$ eV for $^3\Sigma_u^+$ and 0.061 eV for $^1\Sigma_g^+$ or $^3\Sigma_g^-$. This result is in agreement with the weak binding model proposed by Das.

Acknowledgement

We thank Björn Roos for helpful discussions and thank Björn Roos and Per Siegbahn for use of their programs.

References

[1] G. Das, Chem. Phys. Letters 86 (1982) 482.
[2] C. Wood, M. Moran, I.H. Hillier and M.F. Guest, Faraday Symp. 14 (1980) 159.
[3] J. Drowart and R.E. Honig, J. Phys. Chem. 61 (1957) 6801.
[4] B. Liu and A.D. McLean, J. Chem. Phys. 72 (1980) 3418.
[5] B. Roos and C.W. Bauschlicher Jr., unpublished results.
[6] A.J.H. Wachters, J. Chem. Phys. 58 (1973) 4452.
[7] P.J. Hay, J. Chem. Phys. 66 (1977) 4377.
[8] J. Almlof, MOLECULE, a gaussian integrals program.
[9] R.C. Raffenetti, BIGGMOLI, Program No. 328, Quantum Chemistry Program Exchange, Indiana University, Bloomington (1977).
[10] P.E.M. Siegbahn, B. Roos and C.W. Bauschlicher Jr., SWEDEN, a vectorized SCF MC SCF direct CI.
[11] C.W. Bauschlicher Jr. and B.H. Lengsfield III, Noname, a general SCF MC SCF open ended CI program.
[12] C.E. Moore, Atomic Energy Levels, Circular 467 (National Bureau of Standards, Washington, 1949).
[13] C.W. Bauschlicher Jr., S.P. Walch and H. Partridge, J. Chem. Phys. 76 (1982) 1003.
[14] S.P. Walch and C.W. Bauschlicher Jr., Chem. Phys. Letters 86 (1982) 66;
C.W. Bauschlicher Jr. and S.P. Walch, J. Chem. Phys. 76 (1982) 4560.
[15] B.H. Botch, T.H. Dunning Jr. and J.F. Harrison, J. Chem. Phys. 75 (1981) 3466.
[16] S.P. Walch, unpublished results.
[17] P.J. Hay and T.H. Dunning Jr., J. Chem. Phys. 64 (1976) 5077;
T.H. Dunning Jr., S.P. Walch and A.F. Wagner, Theoretical Studies of Selected Reactions in the Hydrogen Oxygen System, in: Potential energy surfaces and dynamics calculations, ed. D.G. Truhlar (Plenum Press, New York, 1981), and references therein.

Theoretical evidence for multiple one-electron 3*d* bonding in a first row transition metal dimer: The $^5\Sigma_u^-$ state of Sc_2

Stephen P. Walch[a)]

Polyatomics Research Institute,[b)] Mountain View, California 94043

Charles W. Bauschlicher, Jr.

NASA Ames Research Center, Moffett Field, California 94035
(Received 3 June 1983; accepted 26 July 1983)

Recently, the Sc_2 molecule has been the subject of considerable theoretical study.[1-3] The interest in this system arises because previous theoretical studies have found only weakly bound states for Sc_2 in contrast to mass spectrometric experiments which had been interpreted to indicate strong bonding ($D_e = 26 \pm 5$ kcal/mol).[4] Previous studies of Sc_2 by Das[2] and by Walch and Bauschlicher[3] indicated that states arising from the $^2D + ^2D$ atomic limit were closely spaced and only weakly bound with large R_e values ($\sim 8.0a_0$). Reinterpreting the mass spectrometric experiments using a larger molecular degeneracy and larger R_e (the original analysis used $R_e = 5.14a_0$, $\omega_e = 230$ cm^{-1}, and $g = 5$), Das concluded that the mass spectrometric results were consistent with weak binding. However, more recently matrix isolation studies have indicated a bound $^5\Sigma$ state of Sc_2.[5] This state appears to be bound with respect to the $^2D + ^2D$ atomic limit, but clearly cannot arise from this asymptote. Walch and Bauschlicher[3] found a $^5\Delta_g$ state which was bound by ~ 0.8 eV with respect to the $^2D + ^4F(4s^1 4p^1 3d^1)$ atomic limit, but unbound with respect to $^2D + ^2D$. States arising out of the $^2D + ^4F(4s^1 3d^2)$ atomic limit were not studied in detail; however, given the experimental evidence for a bound $^5\Sigma$ state of Sc_2 with a 3*d* population of ~ 3.0, together with a known computational bias toward the $^4F(4s^1 4p^1 3d^1)$ state relative to the $^4F(4s^1 3d^2)$ state,[6] a reinvestigation of the $^5\Sigma_u^-$ state arising from $^2D + ^4F(4s^1 3d^2)$ was carried out.

In this communication we report extensive CASSCF/CI(SD) calculations which show that this $^5\Sigma_u^-$ state is bound with respect to the $^2D + ^2D$ atomic limit. We find that the bonding in this state involves three one-electron 3*d* bonds and believe this to be strong theoretical evidence of multiple 3*d* bonding in a first row transition metal dimer.

The $^5\Sigma_u^-$ state had previously been suggested as the ground state of Sc_2 by Wood, Moran, Hillier, and Guest[1] however this assignment was not convincing because correcting for their asymptotic error the $^5\Sigma_u^-$ state was not bound with respect to the lowest limit.

The basis set was the $(14s11p6d)/[8s6p4d]$ basis set described in Ref. 3. An extended basis $(14s12p6d3f)/[8s7p4d2f]$ was also used. This basis has three 4*p* functions[7] optimized for the $^4F(4s^1 4p^1 3d^1)$ state of Sc and two 4*f* functions obtained as a (21) contraction of a three term GTO fit to a Slater 4*f* with exponent 1.6. The extended basis gave an energy improvement of $0.003\,39h = 0.092$ eV for the CASSCF of the $^5\Sigma_u^-$ state at $R = 5.0a_0$.

As in the previous calculations,[3] the CASSCF space consisted of the orbitals derived from the atomic 4*s*, 4*p*, and 3*d* orbitals. The dominant configuration ($c_1 = 0.85$ for CASSCF at $R = 5.0a_0$) for the $^5\Sigma_u^-$ state is

$$4s\sigma_g^2 3d\sigma_g^1 4s\sigma_u^1 3d\pi_{x_u}^1 3d\pi_{y_u}^1 . \quad (1)$$

Constraints were placed on the orbital occupancies; here the σ block had four electrons, the π block had two electrons, and the δ block had zero electrons in all configurations. The reference configurations for the CI(SD) were selected as those configurations (ten) with CI coefficients > 0.05 in the CASSCF wave function near R_e. This leads to 87% reference in the CI(SD) wave function for the $^5\Sigma_u^-$ state at $R = 5.0a_0$ as compared to 86% reference for the large R asymptote, the $^3\Sigma_u^+$ state at $R = 50.0a_0$. The valence populations derived from the CASSCF/CI(SD) calculation are $4s = 2.60$, $4p = 0.83$, and $3d = 2.57$.

Figure 1 shows the calculated CASSCF/CI(SD) potential curve for the $^5\Sigma_u^-$ state together with the states which were previously computed.[3] The $^5\Sigma_u^-$ state is most closely related to the $^3\Sigma_g^-$ state which has the configuration

$$4s\sigma_g^2 4s\sigma_u^2 3d\pi_{x_u}^1 3d\pi_{y_u}^1 . \quad (2)$$

As discussed elsewhere,[3] for the states derived from the $^2D + ^2D$ asymptote, the 3*d* overlap is small and in the small S region one expects one-electron bonds which vary with distance like S to be more favorable than two-electron bonds which vary with distance like S^2. Thus the $^3\Sigma_g^-$ state which involves two one-electron π bonds is more favorable than the $^1\Sigma_g^+$ state which has a single

 0021-9606/83/193590-02$02.10

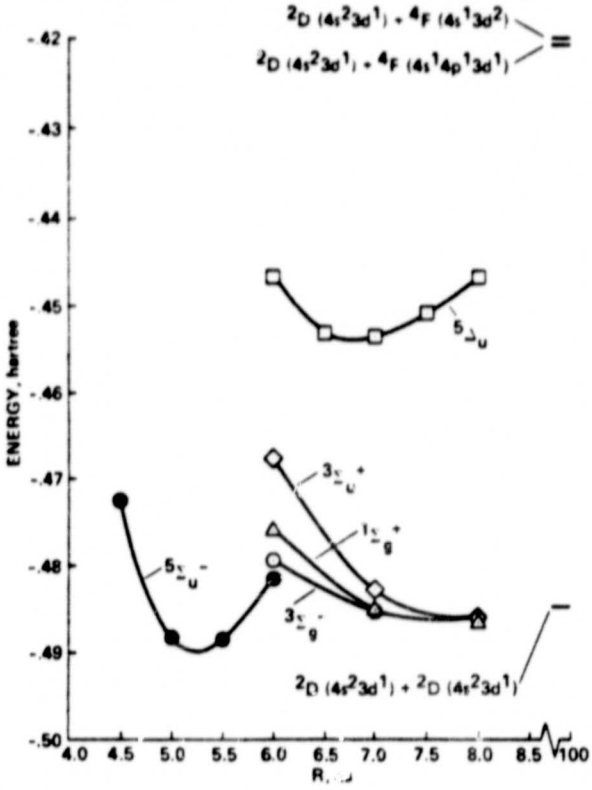

FIG. 1. Potential energy curves for the low-lying states of Sc_2 from CASSCF CI(SD) calculations. The locations of the $^2D + {}^2D$, $^2D + {}^4F(4s^1 4p^1 3d^2)$, and $^2D + {}^4F(4s^1 3d^2)$ asymptotes are indicated.

two-electron σ bond. Promoting an electron of the $^3\Sigma_g^-$ state from the $4s\sigma_u$ antibonding orbital to the $3d\sigma_g$ orbital leads to the $^5\Sigma_u^-$ state which has an additional one-electron $3d\sigma$ bond and reduced 4s repulsion due to removal of an electron from the $4s\sigma_u$ orbital. Given these factors, it is not surprising that the $^5\Sigma_u^-$ state has a smaller R_e and is more stable than the $^3\Sigma_g^-$ state.

A Dunham analysis of a parabolic fit to the $^5\Sigma_u^-$ potential leads to $R_e = 5.27a_0$ and $\omega_e = 184$ cm^{-1}. The binding energy is estimated to be 0.44 eV (10.1 kcal/mol) including (i) a small differential Davidson's correction (−0.03 eV), (ii) a correction for the error in the asymptotic separation (+0.26 eV), and (iii) a correction for the energy improvement with the extended basis (+0.09 eV). The calculated R_e and ω_e values are very close to the assumed values. In the limit of *no* 3*d* interactions $^4F + {}^2D$ leads to a molecular degeneracy of 280 which would lead to an ~16 kcal/mol decrease[2] in the experimental estimate of D_e and excellent agreement with experiment. However, the actual degeneracy will be much lower than this, possibly approaching 5, and thus the calculated D_e is smaller than current experimental estimates by at least 10 kcal/mol. The calculated ω_e is slightly smaller than the current estimate[9] of 238.9 cm^{-1} which is consistent with the underestimation of D_e.

[a]Supported by NASA grant # NCC2-148.
[b]Mailing address: 1101 San Antonio Road, Suite 420.
[1]G. Wood, M. Moran, I. H. Hillier, and M. F. Guest, Faraday Symp. **14**, 159 (1980).
[2]G. Das, Chem. Phys. Lett. **86**, 482 (1982).
[3]S. P. Walch and C. W. Bauschlicher, Jr., Chem. Phys. Lett. **94**, 290 (1983).
[4]G. Verhaegen, S. Smoes, and J. Drowart, J. Chem. Phys. **40**, 239 (1964).
[5]L. B. Knight, Jr., R. J. Van Zee, and W. Weltner, Jr., Chem. Phys. Lett. **94**, 296 (1983).
[6]For example, valence CI calculations with the molecular basis set lead to $^4F(4s^1 4p^1 3d^1)$ 0.50 eV too low with respect to $^4F(4s^1 3d^2)$.
[7]The 4*p* functions are 0.13616, 0.059357, 0.025136.
[8]R. F. Stewart, J. Chem. Phys. **52**, 431 (1970).
[9]D. P. DiLella, W. Limm, R. H. Lipson, M. Moskovitts, and K. V. Taylor, J. Chem. Phys. **77**, 5263 (1982).

Extended CASSCF Calculations for Transition Metal Dimers: the $Ti_2\ ^1\Sigma_g^+$, $V_2\ ^3\Sigma_g^-$, and $Cr_2\ ^1\Sigma_g^+$ States

Stephen P. Walch*
Polyatomics Research Institute+
Mountain View, Calif. 94043

The results of extended active space CASSCF calculations are reported for Ti_2, V_2, and Cr_2. Molecular orbitals derived from atomic 4p and 3d' are found to be very important leading to improved binding energies for Ti_2 and V_2 and to a bound curve for Cr_2. The Cr_2 calculated spectroscopic parameters are (experimental values in parenthesis) R_e = 1.78 Å (1.68 Å), ω_e = 383 cm^{-1} (480 cm^{-1}) and D_e = 0.71 eV (1.56 eV).

*S.P. Walch was supported by NASA grant NCC2-148
+Mailing Address: 1101 San Antonio Rd., Suite 420
Mountain View, Calif. 94043

Recently the transition metal dimers have been of considerable experimental [1-5] and theoretical [6-10] interest both because of the diverse nature of the bonding in the transition metal dimers and because of the difficulty in calculating accurate potential curves for those dimers which exhibit multiple two-electron 3d bonding (especially Cr_2). To date the most extensive study of V_2 and Cr_2 has been carried out by Walch et al. [6]. These calculations were CASSCF calculations with the 4s and 3d transition metal orbitals in the active space. This choice of the active space is appropriate for the states considered, V_2 $^3\Sigma_g^-$ and Cr_2 $^1\Sigma_g^+$, since they arise from the $4s^13d^n + 4s^13d^n$ atomic asymptotes. The calculated CASSCF curve for V_2 gave good R_e and ω_e values and also these authors correctly predicted the ground state of V_2 to be $^3\Sigma_g^-$ prior to experimental determination [4]. However, the calculated binding energy for V_2 was only 0.33 eV (relative to $4s^23d^4 + 4s^23d^4$) compared to the current experimental value of 1.8 eV [4] and Cr_2 did not give a bound curve although a shoulder was observed near the region of the experimental R_e.

The usual approach to correcting those defects is the use of configuration interaction (CI). However, the brute force application of CI techniques to V_2 and Cr_2 is not practical due to the large size of the CI expansions encountered. For example, Walch et al. [6] estimate $\sim$57 million configurations are needed to describe the potential curve for the Cr_2 molecule, whereas the current computational capability is only about one million configurations. Walch et al. were able to carry out a CI calculation for the $^1\Sigma_g^+$ state of Ti_2 which exhibits a triple two-electron 3d bond (σ, π_x, π_y) and used this result to estimate the binding energies of V_2 and Cr_2 assuming a triple bonded picture for V_2, i.e., that the 3dδ orbitals are nonbonding. The preliminary estimate [6] was an increase in binding energy of $\sim$2.0 eV which has now been refined to 1.57 eV leading to predicted D_e's of $\sim$1.7 eV for V_2 (relative to $4s^23d^3 + 4s^23d^3$) and 0.2eV for Cr_2 (relative to $4s^13d^5 + 4s^13d^5$). This model is probably realistic for V_2 where the 3dδ orbitals are singly occupied leading to only weak one-electron bonds but we now believe it is not reasonable for Cr_2 where the 3dδ orbitals are double occupied (vide infra).

In order to get around these difficulties we have used a CASSCF approach to estimate the dominant correlation effects missing in the CASSCF calculations with only 4s and 3d in the active space. For the transition metal atoms we find that the most important additional terms are derived from 3d' and 4p and these are also found to be the most important additional molecular correlation terms. Here 3d' is a tight diffuse correlating orbital for the 3d. Table 1 shows the efrect of including these

additional correlation terms for the Ti atom. Concentrating on the description of the $4s^2 3d^2 \rightarrow 4s^1 3d^3$ excitation energy we see that SCF underestimates the excitation energy. Including the 4p orbital lowers $4s^2$ relative to to $4s^1$ and leads to an overestimation of the excitation energy, while inclusion of 3d' lowers $3d^3$ relative to $3d^2$ leading to a calculated separation that is close to the CI value when both 4p and 3d' are included. The remaining 0.2 eV discrepancy with experiment is due to core-valence correlation involving the 3p shell [11]. Thus inclusion of 4p and 3d' enables an accurate description of the relative energies of atomic states involving different numbers of 4s and 3d electrons. This improved atomic description has been shown to be important for describing molecular potential curves [12]. An analagous argument for the importance of 3d' has been made by Dunning, Botch, and Harrison [13].

To the extent that charge transfer terms are important for the transition metal dimers, we also expect 4p and 3d' to be important since 4p improves the description of terms arising from

$$3d^n + 4s^2 3d^n \qquad (1)$$

while 3d' improves the description of terms arising from

$$4s^1 3d^{n-1} + 4s^1 3d^{n+1} \qquad (2)$$

Indeed, Goodgame and Goddard [14] have suggested that the difficulty in describing the transition metal dimers arises from difficulties in describing the ionic terms [especially (2)]. If this explanation is correct our calculations include directly the correlation corrections which they include by empirical modification of the integrals.

The dominant configurations [6] for the molecules considered here are:

$$Ti_2 \quad {}^1\Sigma_g^+ \; 4s\sigma_g^2 3d\sigma_g^2 3d\pi_{xu}^2 3d\pi_{yu}^2 \qquad (3)$$

$$V_2 \quad {}^1\Sigma_g^+ \; 4s\sigma_g^2 3d\sigma_g^2 3d\pi_{xu}^2 3d\pi_{yu}^2 3d\delta_{xyg}^1 3d\delta_{x^2-y^2g}^1 \qquad (4)$$

$$Cr_2 \quad {}^1\Sigma_g^+ \; 4s\sigma_y^2 3d\sigma_g^2 3d\pi_{xu}^2 3d\pi_{yu}^2 3d\delta_{xyg}^2 3d\delta_{x^2-y^2g}^2 \qquad (5)$$

The calculations use the [8s6p4d2f] basis set described previously [6] and the MOLECULE-SWEDEN programs [15]. As in the previous calculations the occupations are constrained by symmetry. For example for Ti_2 the dominant configuration has four electrons in sigma, two in π_x, and two in π_y.

For the CASSCF within the 4s and 3d orbitals we impose the constraints that four electrons be distributed among $4s\sigma_g$, $4s\sigma_u$, $3d\sigma_g$, and $3d\sigma_u$, two electrons be distributed among $3d\pi_{xu}$ and $3d\pi_{xg}$, and two electrons be distributed among $3d\pi_{yu}$ and $3d\pi_{yg}$. This set of constraints leads to a CASSCF which mimics the GVB wavefunction [16]. Here we use GVB in the more general sense of allowing all possible spin couplings of the 4s and 3d atomic like orbitals with simultaneous orbital optimization. The active space was then augmented by addition of 3d' and 4p. Here the additional active orbitals were added separately by symmetry blocks. For Ti_2 $3d\sigma'$, $3d\sigma'$ plus $4p\sigma$, $3d\pi'_x$, $3d\pi'_x$ plus $4p\pi_x$ were added in separate calculations. The same occupation constraints were imposed except that in the calculation with $3d\pi'_x$ plus $4p\pi_x$ the sigma block was constrained to two to four electrons and the π_x block to two to four electrons thus allowing the $4s^2 \rightarrow 4p\pi_x^2$ near degeneracy terms. These orbital constraints in addition to keeping the calculations of tractable size also lead to a wavefunction which dissociates to Hartree-Fock atoms (for the $4s^13d^n + 4s^13d^n$ limit considered here). For Cr_2 and V_2 $3d\sigma'$, $3d\pi'_x$ and $3d\delta'_{xy}$ were added in separate calculations. For the Ti_2 calculations the $4p\sigma$ contribution was obtained as the $3d\sigma'$ plus $4p\sigma$ contribution minus the $3d\sigma'$ contribution and similarly for the $4p\pi_x$ contribution. The $3d\pi'$, $4p\pi$, and $3d\delta'$ contributions were calculated as twice the $3d\pi'_x$, $4p\pi_x$ and $3d\delta'_{xy}$ contributions, respectively. The CASSCF energies and energy contributions for each of the added active space orbitals are given in Table 2, Table 3, and Table 4 for Ti_2, V_2, and Cr_2, respectively.

Figure 1 shows the calculated potential curves for the $^1\Sigma_g^+$ state of the Ti_2 molecule. The CI calculation was a multireference singles and doubles CI from nine references leading to $\sim$180,000 CSFs. For comparison to the CASSCF curves the CI energies are shifted to make the asymptotic CI energy equal to the asymptotic SCF energy for the $4s^13d^3 + 4s^13d^3$ limit (i.e. we are comparing binding energies). From Fig. 1 it is clear that both 3d' and 4p make important contributions to the binding energy with 3d' somewhat more important than 4p. It is also evident from Fig. 1 that the extended CASSCF procedure used here obtains a very large percentage of the extra binding energy obtained in the CI. However, estimating ΔE 3d' bysumming the separately calculated $3d\sigma'$ and $3d\pi'$ components as was done here overestimates the effect of 3d' as compared to a calculation in which all the 3d' components are included in one calculation. For Ti_2 including $3d\sigma'$, $3d\pi'_x$, and $3d\pi'_y$ in one calculation with occupation constraints as above increases ΔE 3d' by 0.01436h for the molecule at $R = 3.75a_0$ and by 0.03852h for the separated atoms; thus the differential effect of 3d' is reduced from $\sim$32mh to $\sim$8mh. The dominant atomic correlation terms are of the form

$$3d_i \rightarrow 3d'_i \times 3d_j \rightarrow 3d'_j \qquad (6)$$

This result indicates that these terms may not be viewed as "atomic correlation" because they are less important for the molecule than for the atom. On the other hand, the 4p correlation does not contribute for the $4s^13d^n$ state of the atom and we do not expect the 4p correlation effect to be significantly reduced by a more extensive MCSCF calculation. Given these results we must view as fortuitous the good D_e for Ti_2 obtained by including 3d' and 4p correlation estimates based on calculations which dissociate to SCF atoms. However, our intention here is to use this method to extrapolate from the Ti_2 case where we are able to do an adequate CI treatment to the V_2 and Cr_2 cases where the calculations exceed present computational capabilities. We believe that the correlation effects which are included in these calculations will be the most important differential effects between molecules in this series. For simplicity in performing the extrapolation we use the extended CASCF results directly since the D_e obtained for Ti_2 in this way is within 0.08eV of the CI value.

Table 5 shows the calculated spectroscopic parameters for Ti_2 (obtained via a Dunham analysis of the points in Table 2). Here we see that the calculated ω_e is in good agreement with experiment. The calculated D_e is smaller than the mass spectrometrically determined D_e but the experimental value may be too large as is the case for V_2 where a more recent determination via predissociation reduces D_e by $\sim$0.7eV.

Table 6 shows the calculated spectroscopic constants for V_2. Here the effect of 4p was estimated from the Ti_2 calculations. This was done by shifting the ΔE 4p curves for Ti_2 toward shorter R by $0.36a_o$ which is twice the difference between $\langle r_{4s} \rangle$ for Ti $4s^13d^3$ and V $4s^13d^4$[11]. From Table 6 we see that R_e, D_e, and ω_e are all in good agreement with experiment for V_2. In particular the calculated D_e is in good agreement with the recent experimental value determined from predissociation [4] but is considerably smaller than the mass spectrometric value [17].

Fig. 2 shows calculated potential curves for Cr_2. Here as for V_2 the effect of 4p was estimated from the Ti_2 results but shifted toward shorter R by $0.64a_o$ which is twice the difference between $\langle r_{4s} \rangle$ for Ti $4s^13d^3$ and Cr $4s^13d^5$ [11]. The most significant feature of Fig. 2 is the appearance of a well in the region where a shoulder had been observed in the CASSCF curve [6]. Thus, Cr_2 exhibits rather different behavior from Ti_2 or V_2 in that 3d' correlation in Ti_2 and V_2 deepened the well but did not significantly change R_e or ω_e, while for Cr_2 3d' correlation converts a shoulder on the curve into a well. This behavior implies considerable R dependence in the 3d correlation as is evident from Fig. 3 where the $3d\sigma$, $3d\pi$, and $3d\delta$ components of the 3d' correlation are plotted. The $3d\delta$ component shows an especially strong R dependence and it is this term which is mainly respon-

sible for the difference between Cr_2 and V_2 or Ti_2. In fact from Table 3 one sees that for V_2 the ΔE $3d\delta$ is small ($\sim$0.010) and not strongly R dependent. Thus a triple bond model based on Ti_2, as used in ref 6, is an appropriate zero order approximation for V_2 but not for Cr_2.

From Fig. 2 one sees that there is some anharmonicity in the calculated Cr_2 curve. However, this anharmonicity decreases as the calculation is improved and neither the CASSCF + 3d' or the CASSCF + 3d' + 4p curves show any resemblance to the very peculiar potential curve obtained in the recent local spin density (LSD) calculations [20]. Also the LSD wavefunction is described as antiferromagnetic even near R_e whereas our wavefunction shows this spin coupling at large R but becomes a multiple 3d bond near R_e.

Table 7 shows the calculated spectroscopic constraints for Cr_2. Here the best calculation has R_e too long by 0.10 Å and ω_e too small by 97 cm^{-1}. This result is consistent with underestimating the binding energy. However it seems probable based on what is known about the binding energy of V_2 that Cr_2 is bound by considerably less than 1.56eV. The most likely source of error in the Cr_2 potential curve is the estimation of the Δ4p using the Ti_2 results. Shifting the R_e by $0.64a_o$ based on the relative 4s sizes for the Ti and Cr atoms is a somewhat arbitrary assumption although the potential is not particularly sensitive to the choice of this parameter since very similar spectroscopic parameters are obtained for a shift of 0.50. It is also possible that the Δ4p is slightly larger for Cr_2 than for Ti_2 due to the smaller 4s orbital size. However Bagus and Bauschlicher report that $4s^2 \rightarrow 4p^2$ is nearly constant for the atoms varying from 0.76 for Sc to 0.85 for Cu [11]. Unfortunately, the calculation of Δ4p by the technique used for Ti_2 would involve a very large CASSCF calculation (which we may carry out in the future) since the Cr_2 CASSCF for $3d\sigma'$ involves $\sim$20,000 configurations.

One further possible source of error in the Cr_2 calculation is core-valence correlation [21] involving the 3p shell. This effect would be more likely to be important for Cr than for V or Ti since $\langle r_{3d}\rangle/\langle r_{3p}\rangle$ is only 1.39 for Cr while the corresponding ratio is 1.47 for V and 1.56 for Ti [11]. However, calculations on the $4s^1 3d^5$ state of the Cr atom [22] show that singles and doubles CI out of the 4s and 3d electrons leads to a slight contraction ($\delta\langle r\rangle = -0.09a_o$) of the 4s and a slight expansion ($\delta\langle r\rangle = 0.04a_o$) for the 3d, while simultaneous inclusion of single excitations out of the 3p has little additional effect. This result makes a significant core-valence effect due to the 3p shell seem unlikely.

We conclude that inclusion of 3d' and 4p in the valence space leads to a very significant improvement in the potential curves for Ti_2, V_2, and Cr_2. The calculated R_e, D_e, and ω_e are in excellent agreement with experiment for V_2. For Ti_2 the calculated ω_e is in excellent agreement with experiment but the calculated D_e is $\sim$0.3eV (with respect to $4s^23d^2 + 4s^23d^2$) which is smaller than the mass spectrometric value of $\sim$1.3eV. However, based on previous experience with the mass spectrometric D_e for V_2 which has been shown to be too large by $\geq$ 0.68eV, we believe the calculated D_e is more reliable. We predict an R_e for Ti_2 of 1.97 Å. To date no experimental determination of this quantity exists. For Cr_2 we report the first variational calculations with proper dissociation which have the inner multiple 3d bonded well. The R_e is too long by $\sim$0.10 Å and the ω_e is too small by $\sim$97 cm^{-1} but this still represents a significant improvement over previous calculations. The calculated D_e is 0.71eV which is smaller than the mass spectrometric estimate of 1.56eV. Given the large R_e and small ω_e in the Cr_2 potential curve it is quite likely that the true D_e is larger than the calculated D_e although we doubt that it is as large as 1.56eV.

Acknowledgments

I would like to acknowledge very help discussions with Dr. Bowen Liu.

Dr. Charles Bauschlicher, Jr. has made numerous improvements to the CASSCF program which contributed significantly to this work, also Dr. Bauschlicher and Dr. Constance Nelin redimensioned the CASSCF program to permit these calculations.

I would also like to thank Dr. Charles Bauschlicher, Jr., Prof. William A. Goddard III, Dr. Marvin Goodgame, Dr. Stephen Langhoff, and Dr. Constance Nelin for helpful discussions.

References

1. D.L. Michalopoulos, M.E. Geusic, S.G. Hansen, D.E. Powers and R.E. Smalley, J. Phys. Chem. 86 (1982) 3914.
2. V.E. Bondybey and J.H. English, Chem. Phys. Lett. 94 (1983) 443.
3. S.J. Riley, E.K. Parks, L.G. Pobo, and S. Wexler, J. Chem. Phys. 79 (1983) 2577.
4. P.R.R. Langridge-Smith, M.D. Morse, G.P. Hansen, R.E. Smalley and A.J. Merer, J. Chem. Phys. 80 (1984) 593.
5. L.B. Knight, Jr., R.J. Van Zee, and W. Weltner, Jr., Chem. Phys. Lett. 94 (1983) 296.
6. S.P. Walch, C.W. Bauschlicher, Jr., B.O. Roos, and C.J. Nelin, Chem. Phys. Lett. 103 (1983) 175.
7. A.D. McLean and B. Liu, Chem. Phys. Lett. 101 (1983) 144.
8. M.M. Goodgame and W.A. Goddard III, Phys. Rev. Letters 48 (1982) 135; J. Phys. Chem. 85 (1981) 215.
9. S.P. Walch and C.W. Bauschlicher, Jr., J. Chem. Phys. 79 (1983) 3590.
10. C.W. Bauschlicher Jr., S.P. Walch and P.E.M. Siegbahn, J. Chem. Phys. 78 (1983) 3347.
11. C.W. Bauschlicher, Jr., S.P. Walch, and H. Partridge, J. Chem. Phys. 76 (1982) 1033.
12. S.P. Walch and C.W. Bauschlicher, Jr., Chem. Phys. Lett. 86 (1982) 66.
13a. T.H. Dunning, Jr., B.H. Botch, and J.F. Harrison, J. Chem. Phys. 72 (1980) 3419.
13b. B.H. Botch, T.H. Dunning, Jr., and J.F. Harrison, J. Chem. Phys. 75 (1981) 3466.
14. M.M. Goodgame and W.A. Goddard III, paper presented at the Sixth West Coast Theory Conference, Los Alamos, New Mexico, April 1984.
15. SWEDEN is a vectorized SCF MCSCF direct CI written by P.E.M. Siegbahn, B.O. Roos, and C.W. Bauschlicher, Jr.
16. W.A. Goddard, III, T.H. Dunning, Jr., W.J. Hunt, and P.J. Hay, Accounts Chem. Res. 6 (1973) 368.
17. A. Kant and S.H. Lin, J. Chem. Phys. 51 (1965) 1644.
18. A. Kant and B. Strauss, J. Chem. Phys. 45 (1966) 3161.
19. D.P. DiLella, W. Limm, R.H. Lipson, M. Moskovits, and K.V. Taylor, J.Chem. Phys. 77 (1982) 5263.
20. B. Delley, A.J. Freeman, and D.E. Ellis, Phys. Rev. Lett., 50 (1983) 488.
21. H. Partridge, C.W. Bauschlicher, Jr., S.P. Walch, and B. Liu, J. Chem. Phys. 79 (1983) 1866.
22. C.W. Bauschlicher, Jr., unpublished results.

Table 1. CASSCF/CI Calculations for the Ti Atom

	$4s^2 3d^2$ state	$4s^1 3d^3$ state	Δ E (eV)
SCF	-.37208	-.35146	0.56
CASSCF (4s,4p,3d)	-.40292	-.35146	1.40
CASSCF (4s,4p,3d,3d')	-.40756	-.37072	1.00
CASSCF (4s,4p,3d,3d', 4f)		-.38366	
CI [a]	-.42234 (-.42649)	-.38981 (-.39093)	.89 (0.97)
exp			0.81

[a]Values in parenthesis include Davidson's correction

Table 2. Energy Contributions and CASSCF Energies for Ti_2 $^1\Sigma_g^+$

	R = 3.50	3.75	4.00	4.25
CASSCF [a]	-.71240	-.71684	-.71051	-.69821
ΔE $3d\sigma'$	0.01323	0.01238	0.01094	0.01105
ΔE $4p\sigma$	0.00749	0.00773	0.00829	0.00810
2x ΔE $3d\pi'_x$	0.01700	0.01970	0.02364	0.02840
2x ΔE $4p\pi_x$	0.01504	0.01476	0.01320	0.01100

[a]The CASSCF energies are referenced to -1969.0 hartree

Table 3. Energy Contributions and CASSCF Energies for V_2 $^3\Sigma_g^-$

	R = 3.15	3.25	3.50	3.75
CASSCF [a]	-.69183	-.69666	-.69407	-.68236
Δ E $3d\sigma'$	0.00987	0.00997	0.00932	0.00769
2x ΔE $3d\pi'_x$	0.01726	0.01854	0.02194	0.02478
2x ΔE $3d\delta'_{xy}$	0.00870	0.00924	0.01058	0.01156

[a]The CASSCF energies reported here are slightly lower than the values reported in ref. 6 which suffered from incomplete orbital optimization. The CASSCF energies are referenced to -1885.0 hartree.

Table 4. Energy Contributions and CASSCF Energies for Cr_2 $^1\Sigma_g^+$

	R = 3.00	3.25	3.35	3.50	3.75
CASSCF [a]	-.53455	-.54502	-.54764	-.55206	-.56157
Δ E $3d\sigma'$	0.01136	0.01120	0.01087	0.01011	0.00834
2x ΔE $3d\pi_x'$	0.01930	0.02158	0.02178	0.02118	0.01804
2x ΔE $3d\delta'_{xy}$	0.02950	0.02978	0.02856	0.02560	0.01936

[a]The energies reported here are slightly lower than the values reported in ref. 6 which suffered from incomplete orbital optimization. The CASSCF energies are referenced to -2086.0 hartree.

Table 5. Calculated Spectroscopic Constants for Ti_2

	CAS	CAS+3d'	CAS+3d'+4p	CI	Exp.
R_e, Å	1.97	2.00	1.99	1.97	-----
D_e, eV	0.37	1.25	1.86	1.94	2.91[a]
ω_e, cm^{-1}	436	423	442	438	407.9[b]

[a]Mass spectrometric value (ref. 17) energy referenced to $4s^1 3d^3 + 4s^1 3d^3$

[b]ref. 19

Table 6. Calculated Spectroscopic Constants for V_2

	CAS	CAS+3d'	CAS+3d'+4p (est.)	Exp.
R_e , Å	1.76	1.79	1.79	1.76[a]
D_e , eV	0.60	1.68	2.29	2.29[a], 2.97[b]
ω_e , cm	564	533	545	537.5[c]

[a]ref. 4 The D_e value is from predissociation

[b]mass spectrometric value (ref. 17) referenced to $4s^13d^4+4s^13d^4$

[c]ref.19

Table 7. Calculated Spectroscopic Constants for Cr_2

	CAS	CAS+3d'	CAS+3d'+4p (est.)	Exp.
R_e, Å	----	1.81	1.78	1.68 [a]
D_e, eV	-1.4	0.13	0.71	1.56 [b]
ω_e, cm^{-1}	----	308	383	480 [c]

[a] ref. 1-3.

[b] mass spectrometric value (ref. 18)

[c] ref.19

Figure Captions

Fig. 1. Calculated potential curves for the $^1\Sigma_g^+$ state of Ti_2.

Fig. 2. Calculated potential curves for the $^1\Sigma_g^+$ state of Cr_2.

Fig. 3. Calculated energy contributions for 3d" orbitals for Cr_2.

Fig. 1

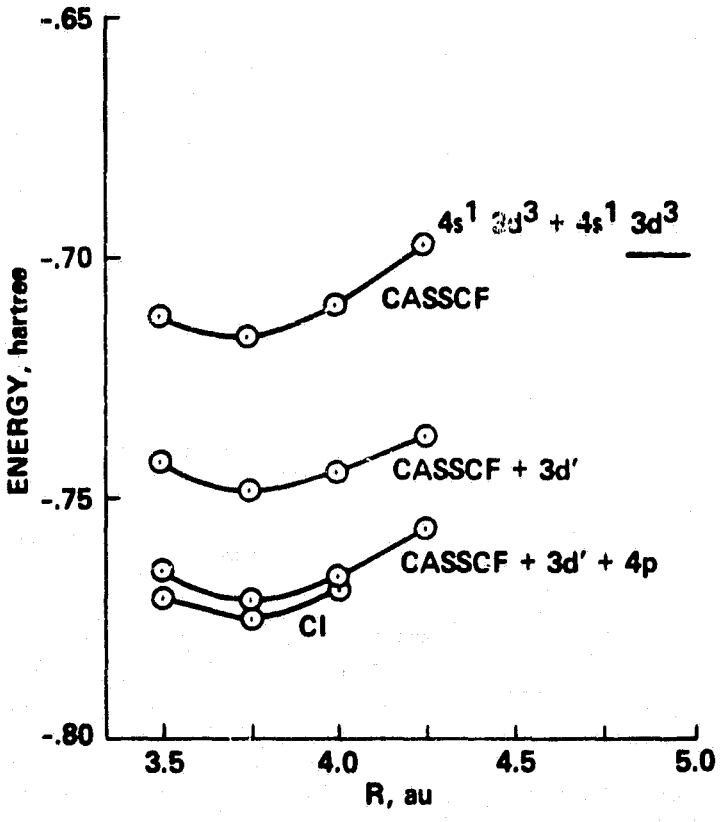

Fig. 2

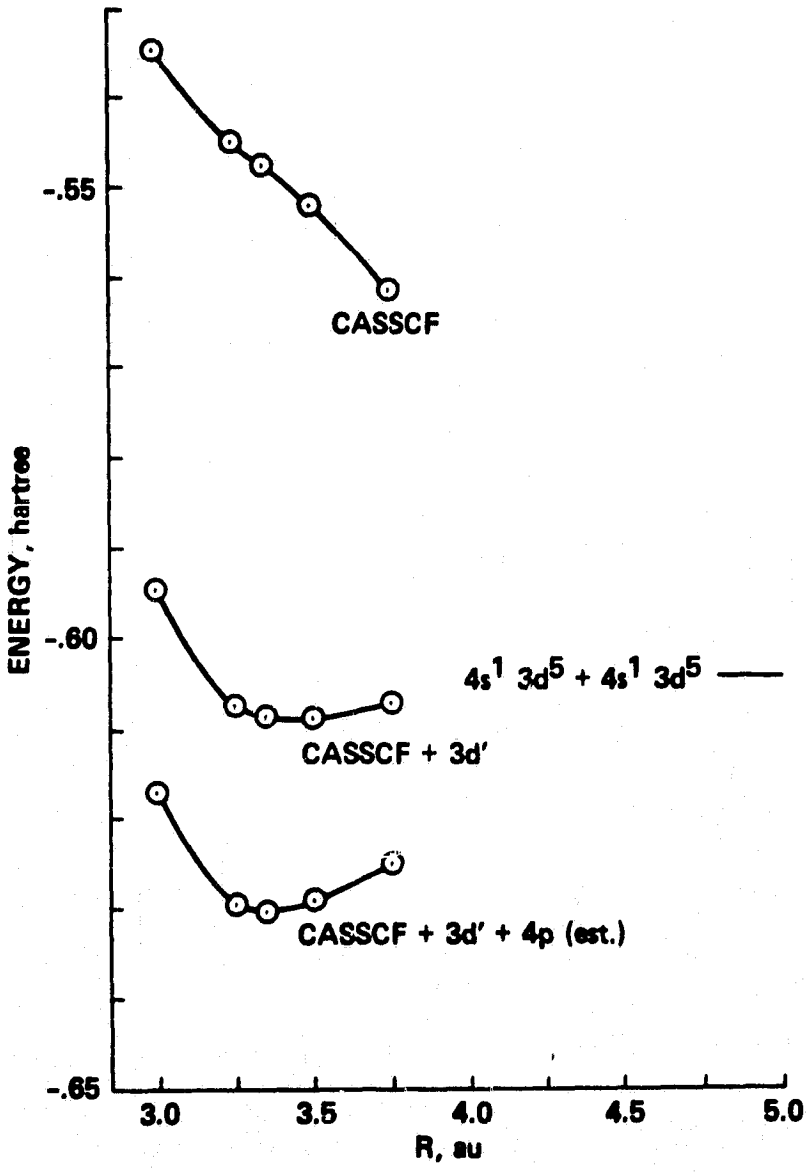
-.55
-.60
-.65
ENERGY, hartree
CASSCF
CASSCF + 3d'
CASSCF + 3d' + 4p (est.)
$4s^1\ 3d^5 + 4s^1\ 3d^5$
3.0
3.5
4.0
4.5
5.0
R, au

Fig. 3

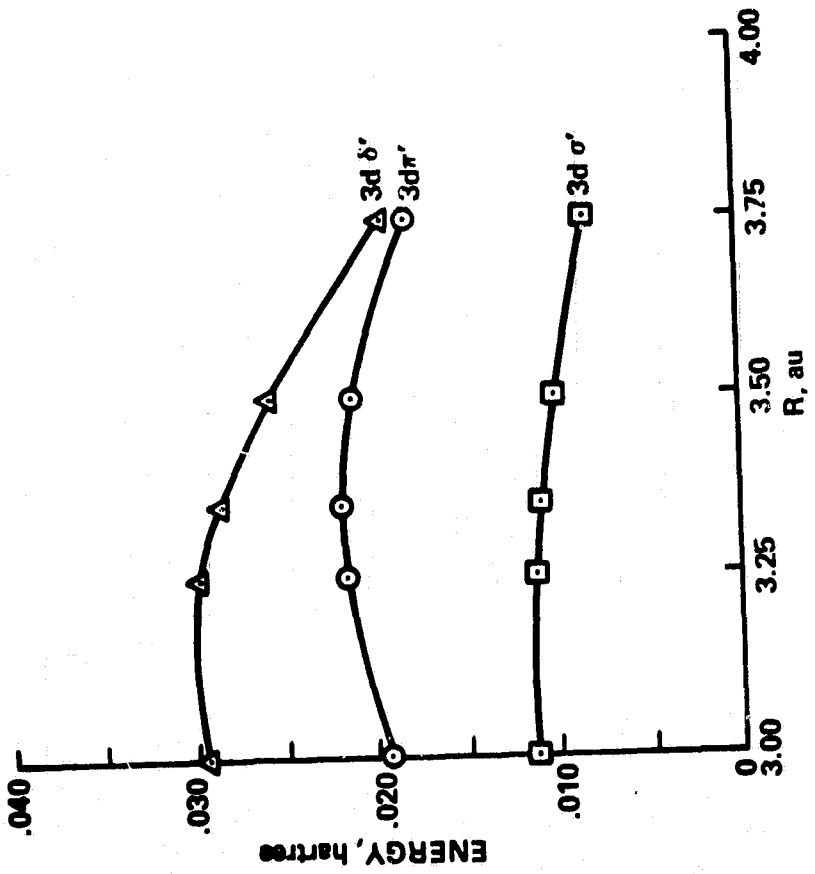

THEORETICAL EVIDENCE FOR MULTIPLE 3d BONDING IN THE V_2 AND Cr_2 MOLECULES

Stephen P. WALCH ‡
Polyatomics Research Institute, 1101 San Antonio Road, Suite 420, Mountain View, California 94043, USA

Charles W. BAUSCHLICHER Jr.
NASA Ames Research Center, Moffett Field, California 94035, USA

Bjorn O. ROOS
Department of Theoretical Chemistry, P.O. Box 740, S-220 07 Lund, Sweden

and

Constance J. NELIN
Analatom Inc., 253 Humboldt Court, Sunnyvale, California 94089, USA

Received 29 September 1983; in final form 13 October 1983

Calculated CAS SCF potential curves are reported for the $^3\Sigma_g^-$ state of V_2 and the $^1\Sigma_g^+$ state of Cr_2. At the CAS SCF level the $^3\Sigma_g^-$ state of V_2 is calculated to be bound (R_e = 1.77 Å, ω_e = 593.6 cm^{-1}, D_e = 0.33 eV) and to involve a triple 3d bond; while the Cr_2 potential curve is not bound but shows a shoulder near the experimental R_e and the wavefunction shows multiple 3d bonding in this region.

It is now clear from experimental work that the Cr_2 molecule has a very short bond length [1], 1.68 ± 0.01 Å. This short bond has generally been thought to involve a quintuple 3d bond arising out of the 3dσ, 3dπ, and 3dδ orbitals of the Cr_2 $4s^13d^5 + 4s^13d^5$ asymptote. Given the $\langle r \rangle$ for the Cr atomic orbitals [2] $\langle r_{4s} \rangle$ = 1.94 Å, $\langle r_{3d} \rangle$ = 0.72 Å one sees that at the equilibrium bond distance (R_e) of Cr_2 the 3d orbitals are at a reasonable distance for bonding but that this R value is well inside the optimal bonding radius for the 4s electrons and they are expected to be non-bonding or antibonding.

At larger R values one would expect the spin coupling to change from predominately 3d–3d bonding to 4s–4s bonding, since at large R the 4s orbitals have a much larger overlap than the 3d orbitals. The situation at large R is expected to be somewhat complex because the ground state of the Cr atom is high-spin ^6S arising out of $4s^13d^5$. As pointed out by Goodgame and Goddard [3], forming a 4s–4s bond with the remaining electrons high-spin-coupled results in the loss of a large amount of exchange interaction. As a result the lowest molecular state in the large R region is found to be an antiferromagnetic singlet state which couples the two Cr atoms into a singlet but still preserves the maximum number of atomic exchange interactions.

For Mo_2 Goodgame and Goddard [3] found an inner and outer well with the inner well corresponding to multiple 3d bonding while the outer well corresponded to the antiferromagnetic coupling. The perplexing problem is why the Goodgame and Goddard Cr_2 calculation did not show a similar 3d bonding solution in the inner region.

In this paper we present complete active space self consistent field (CAS SCF) calculations [4] with large

‡ Supported by NASA grant NCC2-148.

0 009-2614/83/$ 03.00

gaussian basis sets for the $^3\Sigma_g^-$ state of V_2 and the $^1\Sigma_g^+$ state of Cr_2. These calculations show very clear evidence for a triple 3d bond in V_2; the bonding involves 3dσ and 3dπ two-electron bonds with the remaining two electrons involved 3dδ one-electron bonds. The bond length here is 1.77 Å compared to an experimental value [5] of 1.757 Å and the vibrational frequency is 593.6 cm^{-1} compared to an experimental value [6] of 537.5 cm^{-1}. The calculated binding energy at the CAS SCF level is only 0.33 eV compared to 2.48 eV for experiment [7]. For Cr_2, while the wavefunction shows clear evidence of quintuple 3d bonding at small R (<1.85 Å), the calculated potential curve shows only a marked shoulder at ≈1.7 Å and is still repulsive by ≈1.4 eV compared to current interpretations [8] of the experimental estimate of D_e (1.0 ± 0.3 eV). At the present time it is not computationally feasible to do configuration interaction (CI) calculations for the $^3\Sigma_g^-$ state of V_2 or for the $^1\Sigma_g^+$ state of Cr_2 at the level of our previous calculations on Sc_2 [9,10]. An idea of the size of the CI for Cr_2 may be obtained by noting that a multireference singles and doubles CI (MRSD CI) for Cr_2 using the basis set with 4f functions and the 3088 configuration CAS SCF defined below as reference configurations leads to 57 million configurations in D_{2h} symmetry. However, less extensive MRSD CI calculations [11] have been carried out for a $^1\Sigma_g^+$ state of Ti_2 which shows triple 3d bonding, 3dσ and 3dπ as in V_2 and Cr_2, respectively. Here we find an increase in D_e of ≈2.0 eV for CI as compared to CAS SCF. Applying this correction to the V_2 and Cr_2 CAS SCF results leads to 2.3 and 0.6 eV as our best estimates of the D_e of V_2 and Cr_2, respectively. We believe that these calculations provide the first convincing theoretical evidence for multiple two-electron 3d bonding in a first-row transition metal dimer. Multiple one-electron 3d bonding had been observed previously for Sc_2 by Walch and Bauschlicher [9].

The spd basis sets used here were the (14s11p6d)/[8s6p4d] segmented sets which have been described previously [10]. These basis sets were augmented with two 4f functions. The 4f functions were optimized based on SDCI calculations for the $4s^13d^4$ and $4s^13d^5$ configurations of the V and Cr atoms using a (14s11p6d3f)/[8s6p4d1f] basis set. The optimum exponents (STO) were 2.7 and 3.2 for V and Cr, respectively. The [2f] contraction is a (21) contraction based on Stewart's [12] three-term fit of a gaussian f function to a Slater 4f.

The CAS SCF space for these calculations consisted of the orbitals derived from the atomic 4s and 3d orbitals. Constraints were placed on the orbital occupancies. For V_2 the σ block had four electrons, π_x and π_y had two electrons each, and δ_{xy} and $\delta_{x^2-y^2}$ had one electron each. For Cr_2 the δ_{xy} and $\delta_{x^2-y^2}$ blocks had two electrons each and the other occupancies were the same as for V_2. These constraints basically correspond to a generalized valence bond [13] (GVB) treatment of these systems. Here we use GVB in the more general sense of allowing all possible spin couplings of the 4s and 3d atomic like orbitals with simultaneous orbital optimization. For Cr_2 these orbital constraints reduce the CAS SCF calculation from 28784 configurations to 3088 configurations in D_{2h} symmetry. The dominant configurations in the small R region are the SCF configurations:

$$4s\sigma_g^2 3d\sigma_g^2 3d\pi_{xu}^2 3d\pi_{yu}^2 3d\delta_{xy,g}^1 3d\delta_{x^2-y^2,g}^1 \quad (1)$$

for V_2 and

$$4s\sigma_g^2 3d\sigma_g^2 3d\pi_{xu}^2 3d\pi_{yu}^2 3d\delta_{xy,g}^2 3d\delta_{x^2-y^2,g}^2 \quad (2)$$

for Cr_2. At $R = 3.00\ a_0$ the percent SCF (C_0^2) in the CAS SCF wavefunction is 76% for V_2 and 56% for Cr_2. This clearly indicates the need for an MC SCF treatment of these systems.

Table 1 gives the natural orbital occupancies of the CAS SCF wavefunctions for V_2 and Cr_2 at $R = 3.0$ and $3.5\ a_0$. In discussing the results in table 1 it is useful to consider an analogy to the H_2 molecule. Here including only left–right correlation leads to a two-configuration MS SCF,

$$C_1\ 1s\sigma_g^2 + C_2\ 1s\sigma_u^2. \quad (3)$$

Near R_e the $1s\sigma_g^2$ (SCF) configuration dominates but at large R, $C_1 \approx C_2$. As discussed elsewhere, in terms of the generalized valence bond (GVB) wavefunction [13], the relative weights of the two configurations are related to the overlap of the two H(1s) like GVB orbitals ϕ_l and ϕ_r with C_1 dominant indicative of a large overlap $\langle\phi_l|\phi_r\rangle$ while $C_1 \approx C_2$ implies a very small overlap. In interpreting table 1 we can thus compare the overlaps of each pair by comparing the natural orbital occupancies of the bonding and antibonding combinations of each atomic like orbital. Looking first at Cr_2, where each possible 3d pair is doubly occupied, we see that the above analysis indicates the 3d overlaps are in the order

Table 1
CAS SCF natural orbital occupancies for V_2 and Cr_2 at $R = 3.00\,a_0$ and $3.50\,a_0$

State	R	Natural orbital occupation [a]							
		$4s\sigma_g$	$3d\sigma_g$	$4s\sigma_u$	$3d\sigma_u$	$3d\pi_{xu}$	$3d\pi_{xg}$	$3d\delta_{xyg}$	$3d\delta_{xyu}$
$V_2\ ^3\Sigma_g^-$	3.00	1.93	1.83	0.09	0.15	1.90	0.10	0.93	0.07
	3.50	1.93	1.81	0.07	0.18	1.85	0.15	0.87	0.13
$Cr_2\ ^1\Sigma_g^+$	3.00	1.90	1.83	0.11	0.16	1.85	0.15	1.68	0.32
	3.50	1.85	1.60	0.15	0.39	1.66	0.34	1.29	0.71

[a] The 4sσ and 3dσ natural orbitals are a mixture of 4s and 3dσ at $R = 3.00\,a_0$ but show only slight amounts of mixed character at $R = 3.5\,a_0$.

$$\langle 3d\pi | 3d\pi \rangle \approx \langle 3d\sigma | 3d\sigma \rangle > \langle 3d\delta | 3d\delta \rangle. \quad (4)$$

Given this analysis one expects the lowest state in V_2 to arise by distributing two electrons among the 3dδ orbitals, since the 3dσ and 3dπ orbitals are in the large overlap region near R_e and the 3dδ orbitals have much smaller overlaps in this region. Thus it is favorable for the 3dσ and 3dπ electrons to form two-electron bonds. Furthermore the small overlap of the 3dδ orbitals makes one-electron bonding more favorable than two-electron bonding [10]. Thus the $^3\Sigma_g^-$ state arising from $3d\delta_{xy}^1 3d\delta_{x^2-y^2}^1$ is expected to be below the $^1\Sigma^+$ and $^1\Gamma$ states arising out of $3d\delta_{xy}^2$ and $3d\delta_{x^2-y^2}^2$. These arguments are consistent with the observation of a $^3\Sigma$ ground state with a short bond length for V_2 [5] and are also consistent with the much weaker bonding in Cr_2 as compared to V_2 due to the necessity of two-electron 3dδ bonding (unfavorable in the small overlap region) in Cr_2.

Table 2
V_2 CAS SCF energies $^3\Sigma_g^-$ state

R	CAS SCF energy [a,b]	
	[8s6p4d]	[8s6p4d2f]
3.00	−0.64007	−0.67220
3.15		−0.69119
3.25	−0.67716	−0.69621
3.50	−0.68402	−0.69390
3.75	−0.67798	
4.00	−0.67051	

[a] In au relative to −1885.0.
[b] The asymptotic energies (based on atomic SCF calculations) are $4s^23d^3 + 4s^23d^3$ − 1885.68586, $4s^13d^4 + 4s^23d^3$ − 1885.68076, and $4s^13d^4 + 4s^13d^4$ − 1885.67566.

Tables 2 and 3 give the CAS SCF energies for V_2 and Cr_2 while the results are plotted in figs. 1 and 2. A very striking feature of these calculations is the large effect of 4f functions in the basis set. This effect has also been noted by McLean and Liu [14] for SCF calculations on Cr_2 using a large Slater basis set. Table 4 shows the change in SCF energy at $R = 3.0\,a_0$ as a function of the completeness of the 4f basis set. The contractions shown in table 4 are based on the gaussian fits of Stewart [12] for an STO of 3.2. The largest basis set is the basis set used in the molecular calculations. The total effect of 4f functions for this basis is 1.17 eV as compared to 1.11 eV in the calculations of McLean and Liu. The slightly larger effect of 4f functions in our calculations probably reflects a slightly poorer spd basis in our calculations. A perhaps surprising feature of table 4 is the relatively good results with much less complete 4f basis sets. In particular a single set of 4f primitives obtains 1.01 eV of

Table 3
Cr_2 CAS SCF energies $^1\Sigma_g^+$ state

R	CAS SCF energy [a,b]	
	[8s6p4d]	[8s6p4d2f]
3.00	−0.50554	−0.53396
3.25	−0.53004	−0.54482
3.50	−0.54536	−0.55196
3.75	−0.55917	−0.56151
4.00	−0.57231	

[a] In au relative to −2086.0.
[b] The Cr_2 asymptotic energy (based on atomic SCF calculations) is −2086.60456 for $4s^13d^5 + 4s^13d^5$.

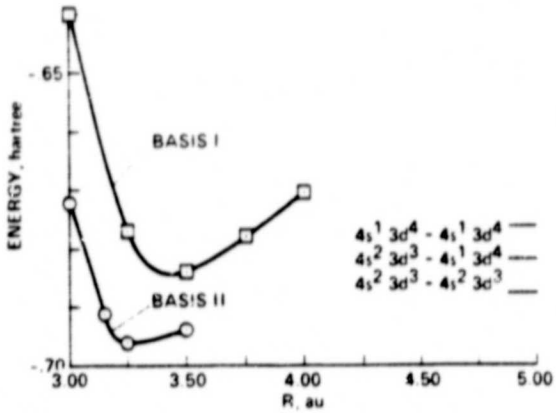

Fig. 1. Calculated CAS SCF potential curves for the $^3\Sigma_g^-$ state of V_2. Basis I is the [8s6p4d] basis while basis II is the [8s6p4d2f] basis.

the 1.17 eV effect obtained with the best 4f basis set. From table 4 one sees that the effect of 4f functions is slightly smaller at the CAS SCF level than at the SCF level.

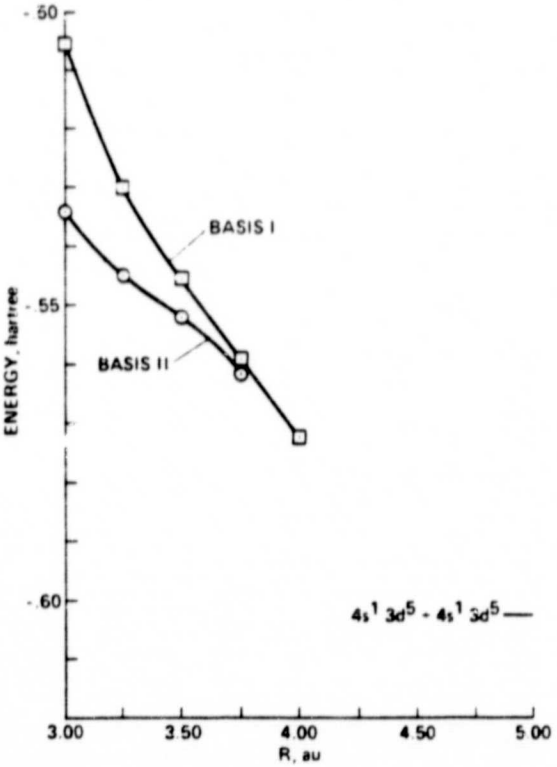

Fig. 2. Calculated CAS SCF potential curves for the $^1\Sigma_g^+$ state of Cr_2. Basis I and basis II are the same size as in fig. 1.

Table 4
Comparison of 4f basis sets for Cr_2 $^1\Sigma_g^+$

4f basis	SCF energy
none	-2085.82353
(1)/[1]	-2085.86064
(2)/[1]	-2085.86190
(3)/[1]	-2085.86250
(3)/[2]	-2085.86640

An interesting feature of fig. 1 is that the effect of 4f functions is very R dependent and shifts the R_e value of V_2 to smaller R. From fig. 2 one also sees that the addition of 4f basis functions results in a distinct shoulder on the Cr_2 potential curve in the region of the experimental R_e. While this feature is not evident in the calculation without 4f functions, the nearly linear behavior from 4.00 to 3.25 a_0 is indicative of some additional bonding interaction occurring in this region.

Comparing to Goodgame and Goddard we note that our configuration space contains all the configurations included in the GVB wavefunction. Our basis set is more extensive than that of Goodgame and Goddard which is only double zeta in the 3d space and has no 4f functions. As pointed out by McLean and Liu [14] a major weakness in the Goodgame and Goddard calculations is the very limited basis set and this clearly accounts for missing the shoulder on the Cr_2 curve at small R.

Kok and Hall [15] claim to obtain a correct bond length for Cr_2 using essentially a perfect pairing GVB wavefunction [13]. However this result is clearly an artifact of the failure of their wavefunction to dissociate properly.

We conclude that the ground states of both V_2 and Cr_2 are characterized by multiple 3d bonding. Given this, it is not surprising that 4f functions are found to be very important in the basis set. This new theoretical result demonstrates the diverse nature of transition metal bonding in that Sc_2 has been shown to have multiple one-electron 3d bonding [9], V_2 and Cr_2 are now shown to have multiple two-electron 3d bonding, and Cu_2 [16] has been shown to be predominately 4s–4s bonding with the 3d electrons essentially atomic like.

References

[1] D.L. Michalopoulos, M.E. Geusic, S.G. Hansen, D.E. Powers and R.E. Smalley, J. Phys. Chem. 86 (1982) 3914;
Y.M. Efremov, A.N. Samoilova and L.V. Gurvich, Opt. Spectry. 36 (1974) 381;
V.E. Bondybey and J.H. English, Chem. Phys. Letters 94 (1983) 443.
[2] C.W. Bauschlicher Jr., S.P. Walch and H. Partridge, J. Chem. Phys. 76 (1982) 1033.
[3] M.M. Goodgame and W.A. Goddard III, Phys. Rev. Letters 48 (1982) 135; J. Phys. Chem. 85 (1981) 215
[4] P.E.M. Siegbahn, A. Heiberg, B.O. Roos and B. Levy, Physica Scipta 21 (1980) 323.
[5] P.R.R. Langridge-Smith, M.D. Morse, G.P. Hansen, R.E. Smalley and A.J. Merer, J. Chem. Phys., to be submitted for publication.
[6] D.P. Dilella, W. Limm, R.H. Lipson, M. Moskovitts and H.V. Taylor, J. Chem. Phys. 77 (1982) 5263.
[7] A. Kant and S.-S. Lin, J. Chem. Phys. 51 (1969) 1644.
[8] A. Kant and B. Strauss, J. Chem. Phys. 45 (1966) 3161.
[9] S.P. Walch and C.W. Bauschlicher Jr., J. Chem. Phys., to be published.
[10] S.P. Walch and C.W. Bauschlicher Jr., Chem. Phys. Letters 94 (1983) 290.
[11] S.P. Walch, to be published.
[12] R.F. Stewart, J. Chem. Phys. 52 (1970) 431.
[13] W.A. Goddard III, T.H. Dunning Jr., W.J. Hunt and P.J. Hay, Accounts Chem. Res. 6 (1973) 368.
[14] A.D. McLean and B. Liu, Chem. Phys. Letters 101 (1983) 144.
[15] R.A. Kok and M.B. Hall, J. Phys. Chem. 87 (1983) 715.
[16] C.W. Bauschlicher Jr., S.P. Walch and P.E.M. Siegbahn, J. Chem. Phys. 78 (1983) 3347.

On the nature of the bonding in Cu_2

Charles W. Bauschlicher, Jr. and Stephen P. Walch

Polyatomics Research Institute,[a] Mountain View, California 94043

Per E. M. Siegbahn

Institute of Theoretical Physics, Vanadisvägen 9, S-113 46 Stockholm, Sweden

(Received 1 February 1982; accepted 26 February 1982)

The ground state of Cu_2 is found to arise from the $^2S(4s^1\,3d^{10}) + {}^2S(4s^1 3d^{10})$ limit and to involve a $4s$–$4s$ sigma bond pair. The dominant bond pair correlations are left–right and angular, with the former lengthening the bond and the latter contracting the bond, so that at the two-electron MCSCF level the R_e is slightly longer ($0.02a_0$) than at the SCF level. Correlation of the $3d$ electrons shortens the bond by $0.19a_0$, leading to a final bond length of $4.35a_0$, which is $0.15a_0$ longer than experiment. This error is of the same magnitude as twice the relativistic contraction of the 4s orbital of the ^2S state of the Cu atom ($0.13a_0$) and most of the remaining error in R_e is thought to be due to this relativistic contraction.

INTRODUCTION

Since the ground state of the Cu atom is ^2S ($4s^1 3d^{10}$), the bonding in Cu_2 is expected to involve a $4s$–$4s$ bond, giving rise to a $^1\Sigma_g^+$ ground state with all d orbitals fully occupied. This makes Cu_2 one of the simplest transition metal dimers. It is also one of the few transition metal dimers for which there is an accurate determination of the bond length (4.20 bohr).[1] For these reasons, Cu_2 serves as an important benchmark for theoretical calculations on transition metal bonding. There have been several previous calculations on Cu_2 (see Ref. 2 and references therein) and probably the best is that of Pelissier,[2] who used effective core potentials (ECP's), a reasonable valence basis, and a nonvariational CI treatment. One interesting feature of this work was the bond shortening at the CI level when the d electrons are correlated. Bagus and Björkman observed this for NiH,[3] and we have observed it for NiH, CoH, and CuH.[4] This bond shortening and its implications for the nature of the transition metal bond are discussed in this article.

COMPUTATIONAL DETAILS

The basis set is the $14s9p5d$ basis of Wachters,[5] optimized for the ^2S state, and augmented with the Hay[5] diffuse d and Wachters'[5] two diffuse $4p$ functions, optimized for ^2P, scaled by $\sqrt{1.25}$ to make them more suitable for a ground state. This basis is contracted in a segmented manner to [14s11p6d/8s6p4d]. The $3s$ combinations of the d's are excluded. In some of the calculations, an f polarization function is added. This is a 3 GTO fit to an STO with $\zeta = 5.0$. The f exponent was chosen by extrapolation of the optimum values for the Fe and Ni atoms. When the f function is used, only seven components are retained.

All calculations were performed with MOLECULE—noname–Siegbahn CI,[7] using either the NASA Ames 7600 or CRAY 1S.

Cu ATOM

In these calculations, symmetry and equivalence restricted SCF calculations were performed. These were followed by CI calculations including all single and double excitations from all valence configurations with the correct symmetry. The $3d$ and $4s$ valence orbitals are included in all calculations, while in the more extensive calculations, the $3s$ and $3p$ semicore electrons are also included. The calculations in which the $3s$ and the $3s$ and $3p$ are included are denoted as CI ($3p$) and CI ($3s3p$), respectively. The results of these calculations are summarized in Table I. CI + $3f$ denotes that the f function has been uncontracted.

From Table I, one sees that the SCF separation differs from numerical HF (NHF) by 0.07 eV, while at the CI ($3s3p$) + f level, the agreement with experiment is within 0.01 eV. However, when the f function is uncontracted, $3d^{10}4s^1$ is stabilized by ~0.1 eV with respect to $3d^9 4s^2$, thus worsening the agreement with experiment. This is consistent with our previous work,[8] which indicated that the $3d^{n+1}4s^1$ states of the transition metal atoms are stabilized relative to the $3d^n4s^2$ states upon uncontracting the f functions. Including relativistic effects stabilizes $4s^2 3d^9$ by 0.43 eV with respect to $4s^1 3d^{10}$.[9] Thus, it is not surprising that improvement in the calculation leads to $4s^2 3d^9$ too high with respect to $4s^1 3d^{10}$. However, we note here that the molecular calculations neglect relativistic effects, and a good description of the ^2S–^2D separation is obtained at the CI ($3s3p$) + f level. Thus, we chose to use this basis set for the molecular calculations.

TABLE I. Summary of Cu atom calculations. Davidson corrections are enclosed in parenthesis.

Calculation	$^2S(d^{10}4s^1)$	$^2D(d^9 4s^2)$	Δ
SCF	−1638.813 256	−1638.796 967	0.44
CI	−1639.064 659	−1639.015 096	1.35 (1.30)
CI + f	−1639.188 449	−1639.129 928	1.59 (1.55)
CI($3p$) + f	−1639.380 351	−1639.327 964	1.43 (1.41)
CI($3s3p$) + f	−1639.436 391	−1639.380 992	1.51 (1.50)
CI + $3f$	−1639.217 3[illegible]	−1639.155 872	1.67 (1.65)
CI($3p$) + $3f$	−1639.430 515	−1639.374 116	1.54 (1.53)
CI($3s3p$) + $3f$	−1639.494 822	−1639.435 222	1.62 (1.63)
EXP[a]			1.49
NHF			0.37

[a] C. E. Moore, Atomic Energy Levels, Natl. Bur. Stand. (US) Circ. 467, (1949).

[a] Mailing address: 1101 San Antonio Rd., Suite 420.

 0021-9606/82/126015-03$02.10

TABLE II. Summary of bond lengths for Cu_2 calculations (in bohrs). Davidson corrections are enclosed in parenthesis.

Calculation	Without f's	With f's
SCF	4.59	4.53
CI 2 electron	4.62	
2 el MCSCF ($\sigma_g^2 - \sigma_u^2$)	4.70	
2 el MCSCF ($\sigma_g^2 - \sigma_u^2$, $\sigma_g^2 - \pi_u^2$) (d frozen)	4.61	
(d's relaxed)	4.61	
6 el FVMCSCF ($d\sigma$, $4s$, $4p\pi_u$)	4.61	
6 el FVMCSCF ($d\sigma$, $4s4p$)	4.57	
6 σ CI (SCF reference)	4.54 (4.55)	4.53 (4.54)
6 σ CI (MC reference)	4.54	
14 el CI		4.42 (4.40)
22 el CI	4.42 (4.39)	4.38 (4.35)
34 el CI		4.39 (4.34)
Pelissier[a] SCF no f's	4.54	
Nonvariational CI 22 el	4.25	
Experiment[b]	4.20	

[a]Reference 2. [b]Reference 1.

Cu_2 CALCULATIONS

The calculated bond lengths for Cu_2 are summarized in Table II. The separation between computed points was 0.2 bohr, so the reported R_e values are expected to be within 0.02 bohr of the true minima of the model used.

The first calculation is a single configuration SCF ... $6\sigma_g^2(3d)7\sigma_g^2$(4S–4S bond) $6\sigma_u^2(3d)3\pi_g^4(3d)3\pi_u^4(3d)1\delta_g^4(3d)$ $\times 1\delta_u^4(3d)$.

Using these SCF orbitals, a series of CI calculations were carried out including single and double excitations from the SCF configuration with progressively more electrons being correlated. The CI's include a 2 el CI ($7\sigma_g$), a 6 σ el CI ($6\sigma_g$, $7\sigma_g$, and $6\sigma_u$), a 14 el CI ($6\sigma_g$, $7\sigma_g$, $6\sigma_u$, $3\pi_g$, and $3\pi_u$), a 22 el CI, which includes all $3d$ and $4s$ electrons, and a 34 el CI which includes the $3p$ as well as the $3d$ and $4s$ electrons. For each point, Davidson's correction[10] was computed, added to the computed energy, and the minima redetermined. These results are reported in parenthesis in Table II.

In addition to these CI calculations, a series of MCSCF calculations were performed. They included a two-configuration MCSCF, which included only $7\sigma_g^2 - 7\sigma_u^2$, which allows proper dissociation. A three-configuration MCSCF which, in addition to the $7\sigma_g^2 - 7\sigma_u^2$ configuration, includes $7\sigma_g^2 - 4\pi_u^2(4p)$. This MCSCF was performed first with the $1s$, $2s$, $3s$, $2p$, $3p$, and $3d$ orbitals frozen at the SCF level, and then with only the core ($1s$, $2s$, $3s$, $2p$, and $3p$) frozen, i.e., the $3d$ was relaxed at the MCSCF level. The $3d\sigma$ electrons ($6\sigma_g$ and $6\sigma_u$) were also included with the core frozen at the SCF level. In this calculation, a full valence MCSCF was performed with the 6 σ electrons in the $6\sigma_g$, $7\sigma_g$, $6\sigma_u$, $7\sigma_u$, and $4\pi_u$ orbitals. This is 36 CSF's in D_{2h}. This MCSCF was followed by a 6 el CI including all single and double excitations from all 36 references. The final FV-MCSCF distributes the 6 σ electrons into the $6\sigma_g$, $7\sigma_g$, $6\sigma_u$, $7\sigma_u$, and all components of the $4p$'s, i.e., $8\sigma_g$, $8\sigma_u$, $4\pi_g$, and $4\pi_u$.

DISCUSSION

At the SCF level, the R_e is more than 0.3 bohr longer than experiment even when f functions are included in the basis. Considering first correlations of the $4s$ and $4p$ electrons, inclusion of the $7\sigma_u$ orbital lengthens the bond. This is typical of an MCSCF which includes the bonding and antibonding orbitals. The inclusion of $7\sigma_g^2 - 4\pi_u^2$ shortens the bond into agreement with the 2 el CI, only slightly longer than the SCF. The importance of this angular correlation effect is a result of the near degeneracy of the $4s$ and $4p$ orbitals. Even though Cu is $3d^{10}4s^1$ and near degeneracy is not important for the Cu atom, the simultaneous excitation of $4s \rightarrow 4p$ on each atom is important for Cu_2 with a weight approximately equal to the importance of $7\sigma_g^2 - 7\sigma_u^2$. It is interesting to note that this effect was observed for Li_2 by Jönsson *et al.*,[11] in Cr_2 by Goodgame and Goddard,[12] and in our lab for Cs_2.[13] Goodgame and Goddard described this as a van der Waals term, and Jönsson *et al.* as a near degeneracy correlating with the united atom limit. We prefer to view this as a near degeneracy effect, allowing angular correlation of the σ bond. This excitation ($7\sigma_g^2 - 4\pi_u^2$) reduces the importance of $7\sigma_g^2 - 7\sigma_u^2$, which is a bond lengthening excitation, and moves a pair of electrons into the $4\pi_u$ bonding orbital.

Considering now correlation of the $3d$ electrons, the inclusion of only the $3d\sigma$ electrons has only a small effect, as is seen by the 6σ el CI. The inclusion of the 3π's ($3d$), the 14 el CI, shows a large bond shortening ~0.14 bohr, while inclusion of the 1δ orbitals (22 el CI) leads to an additional ~0.05 bohr shortening, or about 1/3 of the change of going from 6 to 14 el CI's. When the $3p$ electrons are also included (34 el CI), virtually no additional shortening occurs.

The large bond shortening due to correlation of the 3π electrons is thought to result from three effects: (i) the correlation resulting from the $4\pi_u$–3π interaction, due to the importance of the $7\sigma_g^2 - 4\pi_u^2$ excitation; (ii) orbital relaxation effects included in the CI (*vide infra*), and (iii) reduction of d–d repulsion between the centers.

Effects (ii) and (iii) are also present when the 1δ orbitals are correlated, while for $3d\sigma$ correlation only effect (ii) is present; thus, the smaller bond contraction due to correlation of these orbitals may be rationalized.

In Cu_2, the atoms are $3d^{10}4s^1$ like, and evaluating the SCF energy of the $3d^94s^2$ state using the $3d^{10}4s^1$ orbitals leads to an excitation energy of 4.70 or ~3.2 eV larger than experiment, whereas individual SCF calculations yield a separation of 0.37 eV. The inclusion of configuration interaction improves the separation through orbital relaxation and correlation, thus lowering the $3d^94s^2$ state relative to the $3d^{10}4s^1$ state. This is opposite to the effect if separate SCF calculations are carried out for each state. This reduction of the separation allows an increased $3d^94s^2$ interaction or some d–d bonding. We note here that Pelissier[2] stated that CI would not mix in more $3d^94s^2$ since CI increased the separation. This was based upon separate orbitals for each state and therefore does not apply in Cu_2. Similar effects have been observed for NiH.[4]

It is interesting to note that Pelissier's[2] nonvariation 22 el CI leads to an R_e 0.14 bohr shorter than our result. If the shortening we observe by including f functions at the 22 el CI level (~0.04 bohr) were subtracted from his result, he would be in excellent agreement with experiment. However, in our lab, we have found a useful estimate of the relativistic bond shortening is obtained from the relativistic contraction of the valence orbitals observed by Desclaux.[15] For Cu, this is 0.064 bohr or an expected bond shortening for Cu_2 of ~0.13 bohr. If this estimate is used, our 22 el CI with f's would be corrected from 4.35 to 4.22 bohrs. Considering the approximate nature of this relativistic shortening and the use of Davidson's correction to compute the bond length, this must be somewhat fortuitous. However, it does lead us to believe that there are potential problems with the ECP of Pelissier, which does not include relativistic effects. It is clear that to resolve this problem, 2 ECP's must be developed, one with and the other without relativistic effects included at the same level of treatment, i.e., basis set and correlation. The nonrelativistic ECP should be able to reproduce our all-electron result.

A final point is the mechanism by which $3d^9 4s^2$ allows d–d interactions. One might assume that a $4s^2$ atom would form a repulsive state; however, we have shown in ScH[14] that the $4s$–$4p$ near degeneracy allows a $4s^2 - 4p^2$ excitation which polarizes the $4s\sigma$ electrons into the π_u orbital, moving them out of the bonding region and allowing an increased $3d$ interaction.

CONCLUSION

The Cu atoms in Cu_2 are best described as $3d^{10}4s^1$ with a $4s$–$4s$ bond. The important correlation effects for the $4s$ electrons are the usual bonding to antibonding excitation and a bonding to $4\pi_u(4p)$ bonding orbital. We attribute this to the near degeneracy of the $4s$–$4p$ orbitals. This effect has been seen in other systems, such as Li_2, Cr_2, and Cs_2. We expect this to be a common feature of transition metal–transition metal bonds.

We see a large bond length contraction at the CI level when the $3d$ electrons are correlated. We attribute this in part to an improved description of the $3d^9 4s^2$–$3d^{10}4s^1$ separation, as a result of orbital relaxation and correlation overcoming the strong orbital bias in favor of $3d^{10}4s^1$. This allows an increased involvement of $3d^9 4s^2$ and the possibility of $3d$–$3d$ interactions. Our best bondlength is ~0.15 bohr longer than experiment and we attribute most of this to relativisitc effects, based upon atomic calculations of Desclaux. This is different from Pelissier's calculations, which appear to show little relativistic effect. The question of relativistic bond shortening is left as an unresolved problem.

[1] N. Aslund, R. F. Barrow, W. G. Richards, and D. N. Travis, Ark. Fys. 30, 171 (1965).
[2] M. Pelissier, J. Chem. Phys. 75, 775 (1981).
[3] P. S. Bagus and C. Bjorkman, Phys. Rev. A 23, 461 (1981).
[4] (a) S. P. Walch and C. W. Bauschlicher, Jr., Chem. Phys. Lett. 86, 66 (1982), (b) C. W. Bauschlicher, Jr. and B. H. Lengsfield (unpublished results).
[5] A. J. H. Wachters, J. Chem. Phys. 66, 4377 (1977).
[6] P. J. Hay, J. Chem. Phys. 66, 4377 (1977).
[7] Molecule is a Gaussian integral program written by J. Almlof. "Noname" is a general SCF MCSCF open-ended CI program written by C. W. Bauschlicher, Jr. and B. H. Lengsfield III. Siegbahn CI is the Unitary-Group CI of Per Siegbahn which was converted to CRAY and CDC by C. W. Bauschlicher.
[8] C. W. Bauschlicher, Jr., S. P. Walch, and H. Partridge, J. Chem. Phys. 76, 1033 (1982).
[9] R. L. Martin and P. J. Hay, J. Chem. Phys. 9, 4539 (1981).
[10] S. R. Langhoff and E. R. Davidson, Int. J. Quantum Chem. 8, 61 (1974).
[11] B. Jönsson, B. O. Roos, P. R. Taylor, and P. E. M. Siegbahn, J. Chem. Phys. 74, 4566 (1981).
[12] M. R. Goodgame and W. A. Goddard III, J. Phys. Chem. 85, 215 (1981).
[13] S. P. Walch, B. Laskowski, C. W. Bauschlicher, Jr., and S. R. Langhoff (unpublished work).
[14] C. W. Bauschlicher, Jr. and S. P. Walch, J. Chem. Phys. 76, 4560 (1982).
[15] J. P. Desclaux, At. Data Nucl. Data Tables 12, 311 (1973).

C-2